

PRECIPITATION EXTREMES OVER THE NETHERLANDS:
CHANGES DUE TO CLIMATE AND URBANIZATION

Vahid Rahimpour Golroudbary

Graduation committee:

Chairman/Secretary

Prof.dr.ir. A. Veldkamp

Supervisor(s)

Prof.dr. Z. Su

University of Twente

Co-supervisor(s)

Dr.ir. C.M.M. Mannaerts

University of Twente

Dr. Y. Zeng

University of Twente

Members

Prof.dr.ir. A.Stein

University of Twente

Prof.dr. G. van der Steenhoven

University of Twente/KNMI

Prof.dr. A.M.G. Klein Tank

WUR/MET Office Hadley

Centre for Climate Science and
Services

Dr.ir. G-J. Steeneveld

Wageningen University

Dr. M. Ek

National Center for

Atmospheric Research (NCAR)

ITC dissertation number 336

ITC, P.O. Box 217, 7500 AE Enschede, The Netherlands

ISBN 978-90-365-4680-5

DOI 10.3990/1.9789036546805

Cover designed by Benno Masselink

Printed by ITC Printing Department

Copyright © 2018 by Vahid Rahimpour Golroudbary



UNIVERSITY OF TWENTE.

ITC

FACULTY OF GEO-INFORMATION SCIENCE AND EARTH OBSERVATION

PRECIPITATION EXTREMES OVER THE NETHERLANDS:
CHANGES DUE TO CLIMATE AND URBANIZATION

DISSERTATION

to obtain
the degree of doctor at the University of Twente,
on the authority of the rector magnificus,
prof.dr. T.T.M. Palstra,
on account of the decision of the graduation committee,
to be publicly defended
on Thursday 29th of November 2018 at 14:45 hrs

by

Vahid Rahimpour Golroudbary

born on 7th July 1981

in Tehran, Iran

This thesis has been approved by
Prof. dr. Z. Su, supervisor
Dr. ir. C.M.M. Mannaerts, co-supervisor
Dr. Y. Zeng, co-supervisor

Acknowledgements

This thesis not only represents my work at the keyboard but is a milestone of approximately five years of work at the faculty of Geo- information Science and Earth Observation (ITC) at the University of Twente. I am earnestly grateful to all who have constantly supported me within my PhD programme. First, I wish to thank my main supervisor, professor Zhongbo (Bob) Su, head of the Water Resources Department (WRS) at ITC. I would like to express my sincere gratitude to Bob for his motivation, guidance and immense knowledge. He has been supportive since the beginning of my PhD research and has inspired me throughout the journey.

This study was also carried out under the supervision and guidance of Dr. Ir. C.M.M. (Chris) Mannaerts and Dr Yijian Zeng. I would like to thank them for their scientific advice, useful discussions, valuable comments and insightful contributions on my work. They helped me create the present thesis topic, and, during the most difficult moments in the writing of this thesis, they gave me the moral support and the freedom I needed to persist. Without their supervision and constant help, this dissertation would not have been possible. I am indebted to the European Commission's Erasmus Mundus programme for awarding me a full scholarship to do my PhD work at the ITC facility of the University of Twente.

I would like to thank the WRS staff members, particularly Anke, Tina, Murat, Benno, Job, Loes and Theresa, for their supportive and excellent services. I extend thanks to all my fellow doctoral students for their feedback, discussions, cooperation and friendship. I am sure that this research would not have been so fun without my officemates and friends, Bagher and Yasser, and other colleagues of the water cycle and climate group.

Most importantly, none of this could have happened without encouragement from my family. I have an amazing family, unique in many ways and the stereotype of a perfect family in many others. Their support has been unconditional over all these years; they have sacrificed many things for me to be here; they have cherished every great moment with me and have supported me whenever I need support. My parents and brothers have been with me through all phases of my life. Without their constant love and support in every possible way, I would never have reached this point. Thank you so much!

Finally, I must express my very profound gratitude to the love of my life "Khatereh" for accepting nothing less than excellence from me. You have made it possible for me to finish my PhD and gave me inspiration every second of every day. Your optimism and enthusiasm always kept me on track. This

dissertation stands as a testament to your unconditional love and encouragement. This thesis is dedicated to you.

Table of Contents

Acknowledgements.....	i
Table of Contents	iii
List of figures	v
List of tables.....	ix
Chapter 1 Introduction	1
1.1. Land surface characteristics of urbanisation	2
1.2. Precipitation	3
1.3. Urbanisation- precipitation feedback	5
1.4. Prior knowledge of precipitation extremes.....	7
1.5. Broader context	9
1.6. Objectives and research questions.....	14
Chapter 2 Attributing seasonal variation of daily extreme precipitation events across The Netherlands	17
ABSTRACT	18
2.1. Introduction	19
2.2. Materials and methods.....	20
2.2.1. Precipitation Dataset	20
2.2.2. Methodology.....	21
2.3. results	25
2.4. Discussion.....	35
2.5. conclusions	39
Chapter 3 Detecting the Effect of Urban Land Use on Extreme Precipitation in The Netherlands	41
ABSTRACT	42
3.1. Introduction	43
3.2. Materials and methods.....	44
3.2.1. Precipitation data	44
3.2.2. Definition of the precipitation indices.....	44
3.2.3. Statistical analysis.....	45
3.2.4. Classification of station types	48
3.3. Results	50
3.3.1. Changes in extreme precipitation indices	50
3.3.2. Assessing the monthly maxima of daily precipitation	54
3.3.3. Impact of urban land uses on extreme precipitation	55
3.3.4. Overall features of Urban-Impacted Extreme Indices	55
3.3.5. Monthly Features of Urban-Impacted Px1	56
3.4. Discussion.....	58
3.4.1. Extreme precipitation indices	58
3.4.2. Index changes in recent decades	59
3.4.3. Urban-impacted indices.....	60
3.5. conclusions	61

Chapter 4	Urban impacts on air temperature and precipitation over The Netherlands	63
	ABSTRACT	64
4.1.	Introduction	65
4.2.	Data and Methods	67
4.2.1.	Data quality control	67
4.2.2.	Selected stations	70
4.2.3.	Data analysis	71
4.3.	Results	74
4.3.1.	The UHI intensities	74
4.3.2.	UHI versus population density	75
4.3.3.	Precipitation	76
4.3.4.	Extreme value statistics	79
4.4.	Discussion	80
4.5.	conclusions	84
Chapter 5	Response of extreme precipitation over the Netherlands to urbanisation	85
	ABSTRACT	86
5.1.	Introduction	87
5.2.	Data and Methods	88
5.2.1.	Data	88
5.2.2.	Circulation conditions	89
5.2.3.	Urban land cover	89
5.2.4.	Analysis	89
5.3.	Results	92
5.4.	Discussion	102
5.5.	Conclusions	106
Chapter 6	Synthesis	109
6.1.	Precipitation facts	110
6.2.	Precipitation effects of land surface	111
6.3.	Seasonality of extreme precipitation	113
6.4.	Spatial precipitation pattern and trends	115
6.5.	Urbanisation effects	116
6.6.	Future research	119
	Bibliography	123
	Summary	143
	Samenvatting	147

List of figures

Figure 1.1. Water cycle.	4
Figure 1.2. Schematic representation of the probability distribution of daily precipitation, which has a skewed distribution (Zwiers et al., 2013).....	5
Figure 1.3. Urban land use map in the Netherlands in 2008 and a projection of urban land use for 2040 based on the global economy scenario by Dekkers et al. (2012).	6
Figure 1.4. Annual precipitation in the Netherlands from 1981 to 2010. Source: KNMI.....	9
Figure 1.5. Probability density function effects of the GEV parameter distributions. Panels (a) to (c) show two constant parameters with inconstant location, scale and shape parameters.	12
Figure 2.1. (a): Box-whisker plot for De-Bilt during 1961-2014. The inter-quartile range (IQR) extends whiskers to 1.5 times. The solid line shows the median of monthly maxima for maximum daily precipitation. The black dots indicate the data points which are exceeding the whiskers. The median (solid line), the 0.25 and 0.75 quantiles (dashed and dot-dashed lines) depicted with 95% confidence intervals (grey shaded). (b): Diagnostic plot from fitting the GEV model with NAO influences for maximum daily precipitation in De-Bilt during 1961-2014. The lines show NAO index (grey-dotted) annual maxima (black), 2 (red), 10 (green) and 50 (blue) year return level. 2 year return level analogous estimating to the median of the GEV distribution function.....	26
Figure 2.2. Diagnostic plots from fitting the non-stationary GEV model to one-month (upper panels) and two-month (lower panels) maximum precipitation in De-Bilt, The Netherlands. Plots in left show empirical data against fitted model that have been transformed to Gumbel scale. The plots in right indicate randomly generated data with the aid of the non-stationary GEV model against the quantiles of empirical data. The lines show regression (solid line), 1-1 line (red dashed line) and 95% confidence intervals (grey dashed line).....	27
Figure 2.3. The best non-stationary model distribution at each station	29
Figure 2.4. (a) Location parameter, (b) relative amplitude of location parameter, (c) the phase of maximum location parameter, (d) scale parameter, (e) the relative amplitude of scale parameter with circles that show scale value at each station, (f) the phase of maximum scale parameter, the values of location and scale parameter at each station denoted by RGB circles in (c and f) respectively, (g) shape parameter.....	31
Figure 2.5. 10-year return levels derived from non-stationary models for individual months during the year at 231 rain gauge stations (circles) and the background indicate their spatial pattern over the Netherlands. Panels (a) to panel (l) show the months January to December.....	33
Figure 2.6. 10-year return level from (a) annual maxima block, (b) stationary models, (c) non-stationary models; 50 year return level from (d) annual maxima block, (e) stationary models, (f) non-stationary models. The stationary	

and non-stationary GEV models fitted for the individual monthly blocks to estimate the yearly return level.....	35
Figure 3.1. Distribution of urban (asterisk) and rural (circles) stations in the Netherlands. The regions A, B, C and D are represented by symbols coloured blue, red, green, and yellow, respectively.....	49
Figure 3.2 Spatial distributions of extreme precipitation changes (%) during two multi-decadal periods from 1961 to 2014. The ordinary Kriging interpolated changes for the indices are shown. The maps from top to bottom, right to left (a-j) represent Px1, Px5, Ptot, SDII, P10 mm, P20 mm, P30 mm, CWD, P95Ptot, and P99Ptot, respectively.....	52
Figure 3.3 The panels from (a) to (j) show the analysis of time series of extreme indices during two multi-decadal periods over the last 54 years for Px1, Px5, Ptot, SDII, CWD, P10 mm, P20 mm, P30 mm, P95Ptot, and P99Ptot respectively. The solid and dotted lines show the indices and the least square fit weighted by linear regression analysis for 1961-2014. The difference between the average of each extreme index from 1961 to 2014 and the average from 1961 to 1990 supports the pattern of index changes shown in Figure 3.2.....	53
Figure 3.4. Px1 monthly variation for amount (a) and trend (b) during the period II (green line) and period III (blue line) in 95% confidence intervals (dashed lines).	54
Figure 3.5. The slope of extreme precipitation index changes from the 1961-1990 average across the regions A to D (from (a) to (d)) and whole country (e) for urban (blue filled columns) and rural (red filled columns) stations. The slopes were calculated using the Theil–Sen’s slope, and the statistical significance was estimated by the Mann-Kendall test. The estimated changes are statistically significant at $\alpha=0.05$ for all indices with some exception (CWD for all regions, P20 mm for rural in region B, Px1 for rural in region B and D, Px5 in urban region B).	56
Figure 3.6. Panels (a-d) show the mean of Px1 amounts (mm) for the urban stations (blue line) and rural stations (dashed line) across the regions (A, B, C, and D) between 1961 and 2014.	57
Figure 3.7. The slope of PI changes relative to the 1961-1990 average for the urban (blue filled columns) and rural (red filled columns) stations in different regions (A, B, C, and D) between 1961-2014. The slopes were calculated using the Theil–Sen’s slope.....	58
Figure 4.1. The criteria for selecting reliable Amateur weather stations (PWS) in this study	68
Figure 4.2. Urban (PWS) and rural (AWS) stations that were used in this study. The urban stations with more than 1000 addresses per square kilometre marked with asterisk and their labels correspond to the rows in Table 4.3. Gray-shading display urban areas in the Netherlands (EEA, 2014).	70

Figure 4.3. Hourly variation of mean observed urban heat island values from 2011 to 2015. The UHI at night-time decreases near sunrise74

Figure 4.4. Box-Whisker plot for the PWS hourly UHI from 2011 to 2015. UHI is plotted conditional on their occurrence during spring (a), summer (b), autumn (c) winter (d). The whiskers are set to 1.5 times the inter-quartile range (IQR). The lines show the 0.25 (dotted), 0.5 (solid), and 0.75 (dashed) quantiles. The red crossed dots indicate the maximum data points for outliers.....75

Figure 4.5. (a): A time series plot of the hourly-accumulated precipitation that averaged for urban stations (red line) and rural stations (blue line). (b): Mean (solid line) and 95% confidence interval of hourly precipitation between January 2011 and December 2015. The rural stations (blue) and the differences of hourly precipitation between cities (PWS) and rural station (AWS) (black). (c): The rural hourly precipitation (blue line) and the differences of hourly precipitation between cities (PWS) and rural station (AWS) (black line) between January 2011 and December 2015 for summer (upper panel) and winter (lower panel). The shaded areas show 95% confidence intervals.77

Figure 4.6. Relationship between mean hourly temperature ($^{\circ}\text{C}$) in each bin and wet time fraction (WTF) as well as precipitation fractional (PF) of extreme precipitation (greater than 90th percentile) for urban stations (upper panels) and rural stations (bottom panels) for night-time during 2011-2015.78

Figure 4.7. Estimated location parameter for the hourly maximum UHI against hourly temperature (a) and estimated location parameter for the maximum hourly precipitation (b) averaged for cities (red solid line) and rural (blue dashed line) for the individual months.79

Figure 5.1. Regression slopes ($\delta P_{95th} \delta T(\%)$) for 231 rain gauge stations (red circles) obtained from quantile regression (QR) and binning method (BT). Panel (a) to panel (d) show precipitation relationship with mean, maximum, dew point and atmospheric temperatures, respectively. The one-one line is shown by grey solid line.92

Figure 5.2. Estimated regression slopes ($\delta P_{95th} \delta T(\%)$) for the 231 rain gauge stations in the Netherlands obtained from the mean surface temperature (T_{mean}), maximum surface temperature (T_{max}), atmospheric temperature at 850 hPa pressure level (T_a) and dew point temperature (T_d).94

Figure 5.3. (a) Variations in precipitation among the nine weather types during 1985- 2014. (b) Locations of rain gauge stations (blue closed circles) and areas of urban land cover (grey shading) in the Netherlands (EEA, 2014). The eighth of a circle with a radius of 20 km radius for the southwesterly geostrophic wind direction (W8) is for the De Bilt station.....95

Figure 5.4. (a): Box-and-whisker plot of the maximum daily precipitation and the extended inter-quartile range (i.e., the whiskers extend to 1.5 times the inter-quartile range) for the De Bilt station during 1985-2014. The outlying data points are indicated by black dots. The median of the daily maximum

precipitation is displayed by the black solid line shaded in the 95% confidence interval. The dashed and dot-dashed lines show the 0.25 and 0.75 quantiles. (b): The GEV model is fitted to determine the influences of T_a , T_d and the NAO index on annual maximum daily precipitation in De Bilt from 1985 to 2014. The dotted green, dotted blue, dashed black, dotted red, solid red, solid green, and solid blue lines depict T_a , T_d , the annual maxima, the NAO index, and the 2-, 10- and 30-year return level. This diagnostic plot shows that the 2-year return level approximates the median of the GEV distribution.

.....97

Figure 5.5. Monthly return level for the maximum daily precipitation (median of all rain gauge stations) vs. the return period from the stationary models (dotted lines) and the non-stationary models (solid lines) in the Netherlands from 1985 to 2014.....99

Figure 5.6. Two-, 5-,10- and 30-year return levels derived using non-stationary models averaged over urban (red lines) and non-urban (blue lines) rain gauge stations in the Netherlands from January to December. Panels (a) to (i) reflect the stations classified as W1 to W9 due to the land use types upwind of the stations. 100

Figure 5.7. Precipitation intensity return levels for 2-, 5- and 10-year return periods for nine stations classified as urban and non-urban within the Netherlands. The estimates are obtained using the non-stationary assumption at each station and averaged over the urban and non-urban stations. The regression lines for the urban (red) and non-urban (blue) stations are indicated by power-law trend lines. 101

List of tables

Table 2-1. Percentage of stations (%) present the non-stationary model parameters (location, scale and shape) located within the parameters CI which derived from the stationary models.....	30
Table 3-1. Definition of the extreme indices for precipitation (P)	45
Table 3-2. Number of stations in the urban and rural subsets in different regions. The annual maxima of daily precipitation (mm) averaged for the urban and rural stations in each region during the 54-year period (I) and two multi-decadal periods (II and III) are also listed.....	48
Table 4-1. Measurement accuracy defined by manufactures for each type of stations	68
Table 4-2. Quality control for the temperature and precipitation parameters (Jarraud, 2008)	69
Table 4.3 describes more of the details of the selected stations for further analysis. These stations have similar designs and are classified as urban stations by the Dutch amateur website (http://www.hetweeractueel.nl). The local climate zone (LCZ) around each PWS (buffer with 0.3 km radius) is Table 4-3. Information of selected urban stations extracted for a 5 km radius around the station. Row: the numbers correspond to labels in Figure 4.2. Type: see details in Table 4.1; LCZ: local climate zone for 0.3 km radius around the personal amateur weather stations (PWS) (OMR: open mid-rise, OLR: open low-rise); OAD: address density per km ² ; STED: urbanity degree (1: very strong urban ≥ 2500 addresses per km ² ; 2: strong urban 1500–2500 addresses per km ² ; 3: moderate urban 1000–1500 addresses per km ²); POP: population; PD: population density per km ² ; D: distance between urban (PWS) and paired rural (AWS) (km); AWS: corresponding KNMI stations..	70
Table 4-4. The linear relationship properties between UHI (°C) and population density (10 ³ per km ²) during the night-time cycle for the individual months between 2011 and 2015. R ² : coefficient of determination, a: slope and b: intercept values of the regression line.	76
Table 5-1. Percent goodness of fit for the stationary (S) and non-stationary (NS) models.....	98

Chapter 1
Introduction

Urbanisation is one way by which humans intervene and change their surrounding land cover. The impacts of human activities and (consequently) their surroundings on weather and climate (e.g., temperature and precipitation) are receiving increasing attention from society. The main objective of this research is to investigate extreme precipitation occurrences in the Netherlands and the differences in these occurrences between urban and non-urban areas and to understand these variations in relation to internal climate variabilities. Climate signals can be described using weather statistics (i.e., mean values, spatiotemporal variability and extremes) (Stull, 2017), provided that there are available long-term (e.g., over 30 years) observed data. This chapter gives a short general introduction of the land surface characteristics of urbanisation and precipitation, as well as their potential interactions and the statistical approaches used to investigate these interactions.

1.1. Land surface characteristics of urbanisation

Detailed knowledge of land-atmosphere interactions is of great importance for many applications, such as agricultural management, water resource modelling and the detection of climate change impacts. The land surface is affected by various human activities (e.g., land use changes, deforestation, and expansion of agriculture or urban areas). Water, energy and other exchanges, such as the exchange of anthropogenic greenhouse gas emissions, are occurring in the lower part of the atmosphere (i.e., the atmospheric boundary layer (ABL)). The ABL, also known as the planetary boundary layer (PBL), is directly affected by contact with the land surface (Stull, 2011). Indirectly, land surface forcing, e.g., transpiration, evaporation and heat transfer responses to surface characteristics, can change the whole troposphere with a slow response towards the upper atmosphere. As such, it is crucial to understand the effects of land use (i.e., urban/non-urban) on atmospheric variables to study the interactions of the land surface (cover) with the atmosphere.

Land cover, e.g., vegetation cover types or other particular surface covers, is transformed by land use changes, which modify or convert one type of land surface into another (e.g., forest to agriculture land). These modifications of natural land surface areas have been well known for nearly two centuries across the globe, but their impacts on the atmosphere and climate have been detailed only in recent decades (Mills, 2014). Land cover changes in the form of urbanisation are modifications of surface covers in a roughly geometrical configuration (urban form) and a composite of urban settlements, buildings and impervious materials. Urbanisation leads to greater heat capacities and surface energy modifications in urban areas than in natural surrounding areas (Oke, 1982). Compared to the surrounding non-urban areas, urban areas are expected to experience i) lower evapotranspiration due to the decrease in vegetated areas ii) higher sensible heat fluxes than latent heat fluxes; iii) more

anthropogenic heat generation from fuel use, transportation, industry and other urban residence activities; iv) a reduction in the effective albedo because of tall buildings and the reflection of shortwave radiation by multiple walls; v) greater reabsorption of emitted radiation. All these changes in urban surface energy (e.g., the enhancement of heat capacity and release of stored heat to the atmosphere) influence temperature, wind flow and turbulent mixing. The phenomenon by which temperatures are higher in urban areas than in surrounding rural or vegetated areas is known as the urban heat island (UHI) effect, which is particularly predominant in clear, calm weather conditions. Similar to sea breezes, urban circulation can be generated during calm-wind and fair-weather conditions, during which the surrounding non-urban blows towards the warm urban region. This circulation causes air to rise and can create clouds and precipitation (i.e., the warm and moist air rises in the atmosphere, colliding with the overlying cooler layer of air) over or downwind of the urban area.

1.2. Precipitation

The water cycle is actually related to the atmosphere, oceans and land and is composed of 6 components: precipitation, condensation, evaporation, transpiration, surface runoff, infiltration and groundwater flow (Figure 1.1). Plant-related water processes and liquid exchanges from the land surface to the atmosphere occur in vapour form (transpiration and evaporation). Subsequently, the atmospheric moisture and water vapour with a sufficiently low-temperature change to liquid and form clouds (around condensation nuclei) and precipitation. Precipitation can be rainfall, snowfall and other forms of solid or liquid water that descend from the clouds. Precipitation falls to the land (rain, snow and ice) and flows over the ground (runoff) or moves from the ground into the soil (infiltration and groundwater). Precipitation is the most significant component of the water cycle on land (Flato et al., 2000). Precipitation alterations have a direct impact on water availability, which affects runoff generation and surface water storage. Changes in peak flow attributes, total runoff, water quality, and hydrological amenities could have four separate effects on area hydrology due to land use changes, such as urbanisation (Leopold, 1968). In this study, rainfall is the sole term for precipitation.

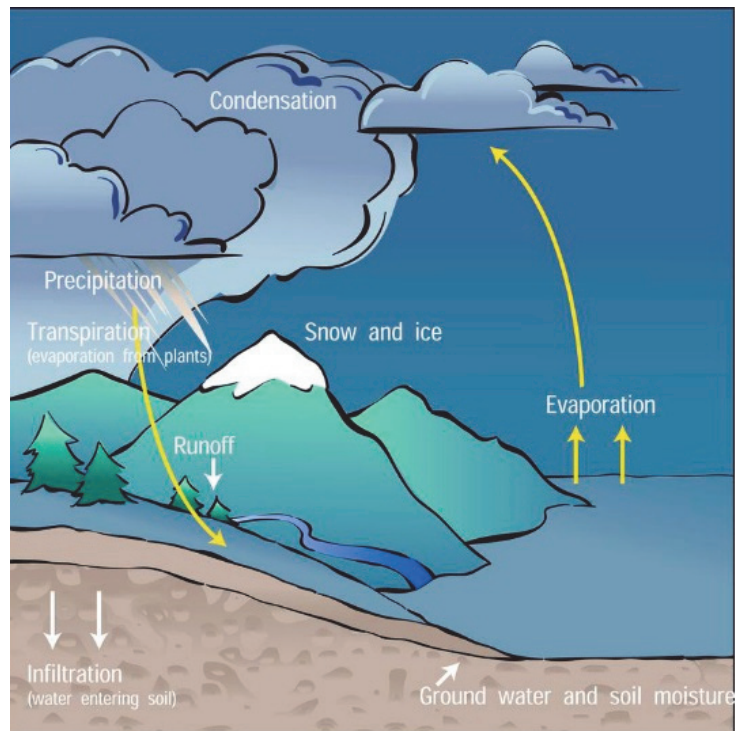


Figure 1.1. Water cycle.
Source: https://www.windows2universe.org/earth/Water/water_cycle.html

Knowledge about precipitation, one of the essential parameters of the water cycle, is imperative for weather forecasting and hydrological research in terms of the intensity and frequency of rainfall for operational water management and acceptable risks (floods and landslides) to infrastructure designs. High temporal and spatial variations in precipitation and changes in the amount and distribution of precipitation indicate changes in the intensity and frequency of extreme precipitation events (Zwiers et al., 2013). Extreme precipitation typically occurs due to a specific weather situation that requires significant atmospheric moisture and strong vertical motion associated with orographic and dynamical forcing and convective instability (Kunkel et al., 2013; Westra et al., 2014). Extreme precipitation occurrences result from complex climate systems altered by human influences, natural variability or other forcing factors. Therefore, climate system changes are expected to alter the distribution of precipitation and extreme events in the coming years (Figure 1.2).

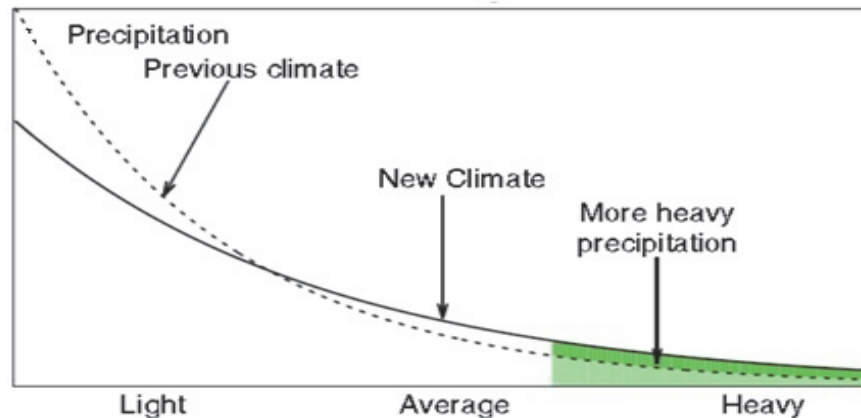


Figure 1.2. Schematic representation of the probability distribution of daily precipitation, which has a skewed distribution (Zwiers et al., 2013).

1.3. Urbanisation- precipitation feedback

The distribution of the global population shows that people do not live uniformly across the world; higher fractions of populations are moving to cities, and more people will live in urban areas in the future. The forecasted population in developed countries will increase from 75% in 2000 to 83% in 2030 (Cohen, 2003). Over the last century, only 14% of people lived in urban centres, while in 1950, approximately 30% of people lived in urban centres. Over 50% of the world's population had moved into an urban area by the end of 2008 (Satterthwaite 2008), and if the predicted trend continues, this percentage will increase to 66% by the end of 2050 (United Nations, 2015). For the Netherlands, approximately 90% of the population in 2014 was concentrated in urban regions, which contained at least 90,000 inhabitants (United Nations, 2015). The average annual rates of urban and rural population changes (1.05% and -5.90%, respectively) and the average annual rates of urban and rural area changes (0.77% and -6.17%, respectively) between 2010 and 2015 indicate a fairly rapid urbanisation in the Netherlands (Un, 2015). Previous studies have reported continuous urbanisation in the Netherlands, with an increase from 2% to 13% from 1900 to 2000 (Daniels et al., 2015b; Dekkers et al., 2012; Hazeu et al., 2011), and this trend has continued in recent years. Dekkers et al. (2012) assumed economic growth will increase in the coming years and projected an urbanisation growth of approximately 41% by 2040 in the Netherlands (Figure 1.3). This increase in urbanisation is important because it might have a local influence on climate. Therefore, the interaction between land cover changes (e.g., urban form) and climate is one of the most investigated issues to understand the expected threats of climate change on human society. Since the 1920s, researchers have observed that urban areas

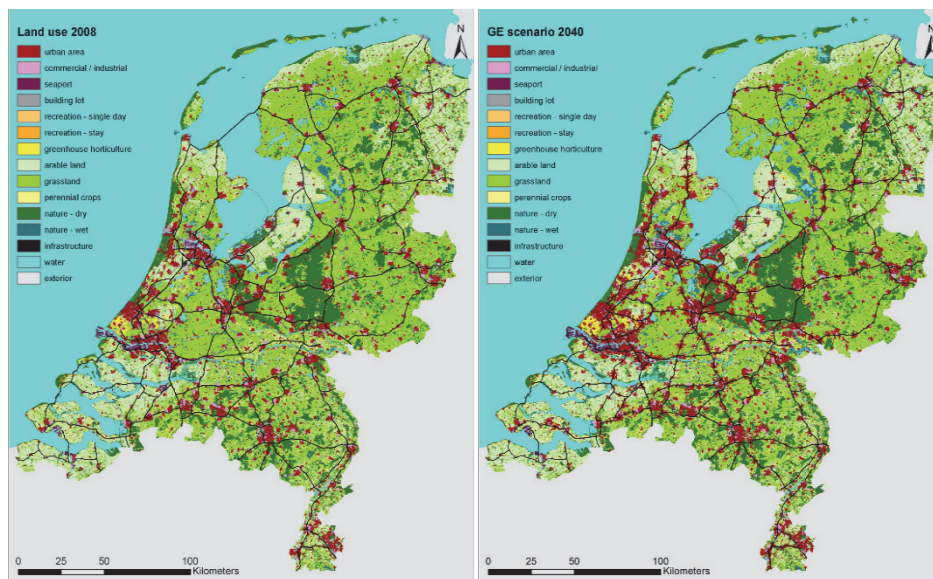


Figure 1.3. Urban land use map in the Netherlands in 2008 and a projection of urban land use for 2040 based on the global economy scenario by Dekkers et al. (2012).

impact the distribution of precipitation. For instance, Horton (1921) reported that a number of urban centres in the northeastern United States spawn thunderstorm growth. Atmospheric researchers have designed experiments to monitor such changes. For example, urban effects on precipitation patterns in the 1970s were observed to increase precipitation in urban areas by the Metropolitan Meteorological Experiment (METROMEX) (Ackerman et al., 1978). In particular, the impacts of urbanisation on precipitation occurrences have been discussed in several studies, which have concluded that the urban influence on precipitation changes could be caused by UHI, surface roughness and increases in aerosol concentrations (Han et al., 2014; Shepherd, 2005). Destabilization caused by UHI perturbation on the PBL plays a crucial role in convection and mesoscale circulation and therefore in precipitation occurrences (Lin and Chen, 2011; Shem and Shepherd, 2009). Thermal perturbations (i.e., a large sensible heat flux) were identified as among the physical mechanisms for extreme precipitation events downwind of urban areas, especially under calm atmospheric conditions (Han et al., 2014). The influence of urbanisation on precipitation and convection could also be induced by the enhancement of convergence as a result of expanded urban surface roughness. Greater surface roughness in urban areas than in the countryside causes the air approaching an urban area to slow near the upwind boundary and be diverted around the urban area. Subsequently, the diverted air could move upward at the downwind side of the urban area (Rozoff et al., 2003). Understanding the impacts of roughness on precipitation requires systematic studies in disrupted or bifurcated convective systems. There are no conclusive studies on the

initiation of moist convection due to the diverted airflow downwind of urban areas (Steenefeld et al., 2011). In addition, surface roughness enhancement alone (i.e., without the strong upward motion necessary for moist convection) is likely insufficient to increase precipitation (Miao et al., 2011; Rozoff et al., 2003; Thielen et al., 2000). Furthermore, various factors must be considered to understand the mechanisms and roles of urban-induced aerosols in increasing or decreasing precipitation. The interactions between aerosols (urban air pollution) and clouds, depending on the aerosol type (aerosol size and concentration) and environmental conditions, can affect precipitation evolution (Khain, 2009; Tao et al., 2012). Rosenfeld et al. (2007) reported that aerosols and pollutant emissions can alter the radiation process via direct and indirect impacts on intake and changes in the precipitation pattern. Based on previous studies, reductions in precipitation could be likely under low aerosol concentrations (Junkermann et al., 2011), while precipitation enhancement could be likely under high aerosol concentrations, high humidity and strong convection (Altaratz et al., 2014; Han et al., 2012). However, the importance of aerosols and surface roughness in precipitation (inhibiting or enhancing the precipitation amount) is very complex, and it is questionable whether any conclusions can be made about the physical processes responsible for precipitation changes over urban areas.

1.4. Prior knowledge of precipitation extremes

Since 1951, the increase in extreme precipitation events has been greater than the increase in mean precipitation over several mid-latitude areas (IPCC, 2014). This disproportionately high trend in extreme precipitation can be explained by increases in the moisture holding capacity of the atmosphere due to global warming, while mean precipitation is dependent on the atmospheric energy budget (Barbero et al., 2017; Lenderink and van Meijgaard, 2010; Pall et al., 2007). Significant enhancements in the frequency and intensity of extreme precipitation have been reported by many studies for different areas in the world (Buishand et al., 2013; Easterling et al., 2000; Hardwick Jones et al., 2010; Westra et al., 2013) and have been projected under the global warming context (Hartmann et al., 2013; Hirsch and Archfield, 2015). Christensen et al. (2007) concluded that extreme events are more likely to occur under the current warming climate than under an unchanging climate.

Significant changes in precipitation extremes with positive trends have been demonstrated by a growing number of studies in Europe (Casanueva et al., 2014; Feyen et al., 2012; Karagiannidis et al., 2012; Klein Tank and Können, 2003; Madsen et al., 2014; Santos and Fragoso, 2013; van den Besselaar et al., 2012). For example, van den Besselaar et al. (2012) found a median reduction of approximately 21% between the first and last 20 years of the return period from 1951-2010 over European regions. An increasing change in

extreme precipitation was found for Germany (Hundecha and Bárdossy, 2005; Zolina et al., 2008) and Belgium (De Jongh et al., 2006; Schmith, 2001), which are neighbouring countries of the Netherlands. Significant increases have been found for winter, and less significant increases have been found for autumn and spring. Lenderink et al. (2009) demonstrated that the coastal regions in the Netherlands have had more precipitation than the inland areas, especially in summer, since the middle of the last century. A significant increase in the annual upper percentile precipitation (i.e., 90th, 95th, and 99th percentiles) was illustrated by Burauskaite-Harju et al. (2012) using a limited number of long-term series from ground stations in the Netherlands. An increase in rare precipitation events was found by (Roth et al., 2012), with an average increase of 22% for daily gridded E-OBS data from 1950 to 2010 over the Netherlands. Buishand et al. (2013) found significant increases in extreme precipitation for six investigated indices from 1910 to 2009 in the Netherlands, where the mean winter precipitation enhancements were statistically significant at most stations. Buishand et al. also found a relatively strong enhancement in summer precipitation in the 1980s.

The North Sea induces airflow to the Netherlands (by the prevailing south or southwest wind) containing sufficient water vapour for precipitation (Sisternans and Nieuwenhuis, 2004; Stolk, 1989). Moreover, the annual cycle of precipitation illustrates a discrepancy between the west coast and inland areas, which is mainly driven by circulation changes and increases in the sea surface temperature (SST), particularly during the summer half-year (van Haren et al., 2013). There are other factors (e.g., land cover and land uses) contributing to the regional and seasonal patterns of precipitation in the Netherlands. Figure 1.4 shows the spatial variability of annual precipitation during the last few decades over the Netherlands. It is clear that the annual precipitation in some regions is greater than that in other regions. The highest annual precipitation amount, for example, in the middle of the country has

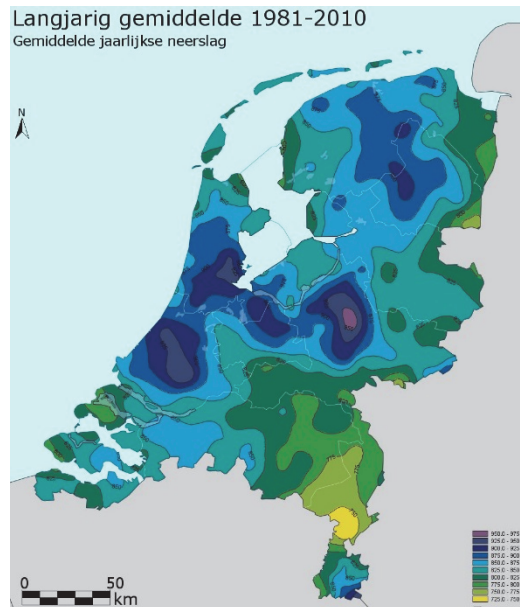


Figure 1.4. Annual precipitation in the Netherlands from 1981 to 2010. Source: KNMI

been influenced by the elevated forest area (i.e., a combination of topography and land cover) (Ter Maat et al., 2013).

This study uses the extreme value theory (EVT) to investigate the distribution of precipitation extremes, especially for Dutch urban areas. This approach has been the subject of many studies in hydrology and climatology and makes it possible to estimate the return levels of extreme events. In the following section, a short overview of the data and some basic concepts of the applied method in this study are given. Then, the research questions and outline of the thesis are presented.

1.5. Broader context

The Netherlands can be defined as an urbanised area inside a river delta (i.e., the Rhine, Meuse and Scheldt Rivers), and many parts of the Netherlands are situated below the sea level. Topographically, the Netherlands contain flatland in the north and west and higher lands in the south and east. The region has a temperate climate and small climatological differences due to the lack of significant orography. The reliable estimation of the precipitation distribution in the Netherlands is strongly related to long timeseries of rainfall data and the sequences of these timeseries. The Royal Netherlands Meteorological Institute (KNMI) operates two rain gauge networks: a network of automatic gauges that consists of 35 stations with 1000 square kilometres coverage per station and a network of manual gauges with 325 stations with 100 square kilometres

coverage per station. Recorded data from manual rain gauges are typically used in this study. Observed meteorological variables from limited amateur weather stations are also used in this study (more details on the station locations and data quality are presented in Chapter 3 and Chapter 4), since there is a lack of long-term recorded observations in Dutch cities. Radar data at a 2.4 km spatial resolution are available after 1998 in the Netherlands. These radar data, which have a temporal resolution of 5 minutes or more, are used in Chapter 5. Although there are other sources of data (such as satellites, disdrometers, and microwave links), the length, substantial biases and uncertainties, and spatiotemporal resolution of these records are not sufficient to be used for the type of analysis in this study. The importance of data quality for analysing extreme events has already been discussed in many studies.

An extreme precipitation event could be quantified as precipitation exceeding some percentile and/or absolute threshold based on the precipitation distribution at a location (i.e., at a point or throughout a spatial region) over a specified time (which can vary from hourly to monthly). Extreme precipitation events can be further defined by a block maxima approach (e.g., annual, seasonal or monthly), which could also be applied to develop intensity-duration-frequency (IDF) curves for practical design criteria. Empirical and theoretical statistical approaches can quantify variations in extreme precipitation. The empirically based method introduces metrics as trends in the frequency of threshold exceedance that is applicable to moderate precipitation extremes. For the theoretical method, the EVT distribution is applied to quantify the return levels and trends in the distribution parameters of precipitation extremes (Coles, 2001).

Statistical analysis is needed to investigate recent historical changes in precipitation observations and the probability of certain precipitation intensities. The probability distribution of precipitation is important for quantifying the frequency and intensity of extreme precipitation events. Temporal changes (or trends) in observations can typically be checked visually or by statistical hypothesis tests. Different parametric and nonparametric statistical trend analyses can be applied to test changes in observed precipitation extremes. Linear regression is the most common parametric trend test that assumes a normal distribution for the targeted variable (Dobson and Barnett, 2008; Einfalt et al., 2011; Frei and Schär, 2001; Neter et al., 1996; Seber and Lee, 2012). Alternatively, the most widely used classical nonparametric trend test is the Mann-Kendall test (Kendall, 1948; Mann, 1945), which can be modified for auto-correlated data. In this case, the trends are estimated by the nonparametric Theil-Sen's slope (Sen, 1968; Theil, 1950), and the pre-whitening procedure is applied for auto-correlated data to effectively remove or reduce the impact of autocorrelation (Yue et al., 2002). More details on this statistical analysis are presented in Chapter 3.

The statistical methods for rarely recorded events are evaluated using EVT, which was developed by Gumbel (1958), who published the book "Statistics of extremes" that covers this subject. The statistical theory of extremes originated from studying the observed extreme distribution with the Gaussian (Dodd, 1923) and the normal distribution (Tippett, 1925). Then, Fréchet (1928) identified a continuous probability distribution called Weibull distribution. Furthermore, Fisher and Tippett (1928) demonstrated that the limiting distribution is possible for only three types of distributions. Regarding the EVT assumptions, let n be the random variable sequence (X_1, X_2, \dots, X_n) , which are independent and identically distributed (iid). A physical process for n time units, $M_n = \max(X_1, X_2, \dots, X_n)$, conforms to a common probability distribution. If considering normalizing constants as $b_n > 0$, $a_n \in \mathbb{R}$ and some non-degenerate distribution (i.e., $\frac{M_n - a_n}{b_n} \xrightarrow{d} H$), then based on the Fisher-Tippett theorem, H belongs to one of three following types (Embrechts et al., 1997):

Type I: Gumbel distribution:

$$\Lambda(x) = \exp\{-\exp(-x)\}, \quad x \in \mathbb{R} \quad (1.1)$$

Type II: Fréchet type:

$$\Phi_\alpha(x) = \begin{cases} 0, & x \leq 0 \\ \exp(-x^{-\alpha}), & x > 0 \end{cases} \quad \alpha > 0. \quad (1.2)$$

Type III: Weibull type:

$$\Psi_\alpha(x) = \begin{cases} \exp(-(-x)^{-\alpha}), & x \leq 0 \\ 0, & x > 0 \end{cases} \quad \alpha < 0. \quad (1.3)$$

Among the several probability distributions (e.g., Gumbel, generalized extreme value (GEV), log-normal, and log-Pearson type 3) to describe the distribution of extreme precipitation, GEV distribution with a three parameter and a simple estimation method can be applied to represent extreme precipitation distribution in a sufficient flexible way (Wilks, 1993). The GEV is the usual distribution from EVT for the block maxima approach. The cumulative distribution function (CDF) of the GEV distribution follows as:

$$F(x; \mu, \sigma, \varepsilon) = \begin{cases} \exp\left(-\left[1 + \varepsilon \frac{x - \mu}{\sigma}\right]^{-\frac{1}{\varepsilon}}\right), & \& \quad \varepsilon \neq 0 \\ \exp\left(-\exp\left(-\frac{x - \mu}{\sigma}\right)\right), & \& \quad \varepsilon = 0 \end{cases} \quad (1.4)$$

$$\text{where: } \left[x: 1 + \varepsilon \frac{x - \mu}{\sigma} > 0 \right], \quad \begin{cases} \mu \in \mathbb{R} \\ \sigma > 0 \\ \varepsilon \in \mathbb{R} \end{cases}$$

The distribution's maximum position is defined by the location parameter (μ), which does not have an impact on the standard deviation (Figure 1.5(a)). The spread of the distribution is defined by the scale parameter ($\sigma > 0$), which is straightforwardly linked to the standard deviation (Figure 1.5(b)). The shape parameter (ϵ) covers the tail behaviour of the distribution (Figure 1.5(c)), where $\epsilon=0$, $\epsilon > 0$, and $\epsilon < 0$, respectively, define the exponential reduction of the infinite upper tail (Gumbel distribution), a slow reduction of the longer infinite upper tail (Fréchet type), and a shorter finite upper tail at $x=\mu-\frac{\sigma}{\epsilon}$

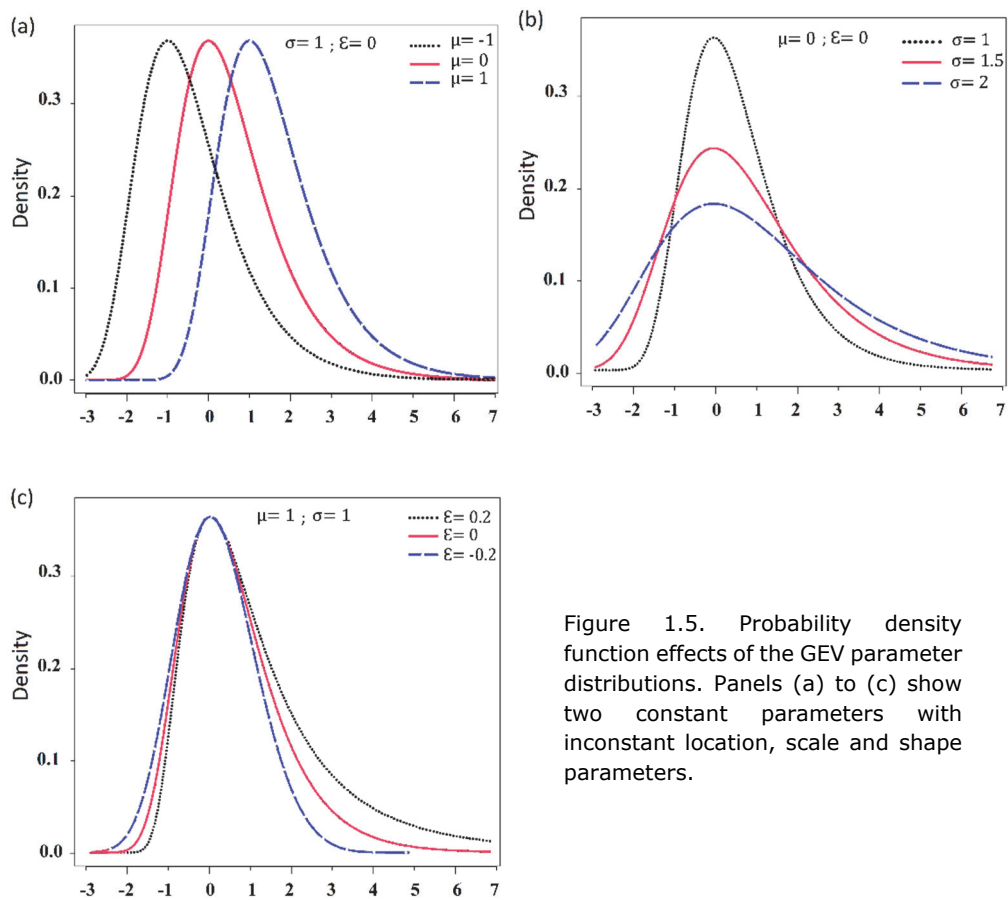


Figure 1.5. Probability density function effects of the GEV parameter distributions. Panels (a) to (c) show two constant parameters with inconstant location, scale and shape parameters.

(Weibull type). For estimating the distribution parameters, the L-moment method (Hosking, 1990) and maximum likelihood (Jenkinson, 1955) can be used. When there is a sufficiently large body of data for extreme events, the maximum likelihood is the preferable approach, as the climate introduces nonstationary properties that suggest the covariates to identify their impacts on extreme events.

The statistical frequency of an extreme precipitation event, e.g., whether an event occurs once in a decade or once in a century, presents an interesting question that can be answered by GEV analysis, which considers events to have a return period of "T" years, where "P=1/T" shows the probability that an event will occur in T years. The related return level is defined by the value of rainfall that at least overpasses the mean for the defined T years. Therefore, the return level coherency in the GEV distribution is demonstrated by (1-P)th, which means that the return level can be described by inverting the GEV equation as follows:

$$G^{-1}(1-p; \mu, \sigma, \varepsilon) = \begin{cases} \mu - \frac{\sigma}{\varepsilon} (1 - [-\ln(1-p)]^{-\varepsilon}), & \varepsilon \neq 0 \\ \mu - \sigma \ln[-\ln(1-p)], & \varepsilon = 0 \end{cases} \quad (1.5)$$

The estimated return levels and periods are debatable for updating design norms and protection measures against hazards. Furthermore, rainfall observations (i.e., the amount and temporal profile of occurrences) are often used for understanding and assessing regional water systems due to the lack of discharge data (Overeem et al., 2009). The example of precipitation return levels and period usage in the Netherlands shows the dependences of these factors on land use, and different types of land use have different criteria for surface water flooding (e.g., once every 100 years and once every 10 years for urbanised areas and grassland, respectively). Dutch sewer systems are vulnerable to heavy convective precipitation (Zondervan, 1978) and are designed to be capable of the discharge of 2-year return levels; therefore, inundated streets might be observed for 10-year or larger extreme events (Rioned, 2006). These return levels and period estimations are based on the constant distribution of a given variable during a certain time period (i.e., one-year period), called stationary assumptions (Rootzén and Katz, 2013). However, evidence on the dependence of the extreme event frequency on time and/or other factors shows that extreme precipitation events might have nonstationary behaviour. For the Netherlands, since 1950, precipitation thresholds have been enhanced by 10% for those events with an occurrence rate exceeding once per year (Klein Tank and Lenderink, 2009). Buishand et al. (2013) reported that the mean precipitation increased approximately 25% during the last century over the Netherlands. Moreover, increases in the number of days of heavy (more than 10 mm) and very heavy (more than 20 mm) precipitation were found for winter and summer, respectively (Sluijter et al., 2011; van den Hurk et al., 2014). The evidence of variations in extreme precipitation as a consequence of climate change or other forcing factors violates the stationary assumptions, which may lead to underestimation with undesirable outcomes. Theoretical aspects of nonstationary in the context of EVT and covariate modelling were reported in the 1980s (Leadbetter and Lindgren, 1983; Moore, 1987). The nonstationary approach was developed in many types of environmental research and applications based on time or other

covariates. Comparisons of different covariates and understanding inter-annual variations are further possible with nonstationary models. Therefore, this approach more reliably represents the behaviour of extreme events than the stationary approach. More details on statistics and nonstationary modelling were described by (Coles, 2001), who considered external forces in the statistical analysis of extreme events. The occurrences of return values and the return period could be provided by this method to appraise extreme distributions. This study presents the seasonal cycle of extreme precipitation by developing the nonstationary GEV model for the Netherlands in Chapter 2.

1.6. Objectives and research questions

The ongoing urban land use development and increase in the concentration of the population in urban areas further contributes to the increase in the vulnerability of urban areas to extreme precipitation variations. Despite the fact that international reports on urban climate consist of useful information, their particular outcomes are not easily extrapolated to Dutch circumstances. Although rainfall intensity projections at larger scales may be relevant, due to the coarse resolution of regional climate models, a substantial evaluation for specific urban areas is needed (Willems et al., 2012). Furthermore, variations in climatic conditions, air quality, geometry, urban landscape, and building types and components render such an extrapolation challenging. In addition, the emphasis in the majority of international studies has been on information for rainfall intensity at the local level, especially for the upcoming years, which is not reliable enough to be applied as an indicator for evaluating extreme rainfall events in many cities of the Netherlands (Buishand et al., 2010; Tank, 2009).

Changes in precipitation extremes in the context of climatology are of particular interest since little quantitative knowledge is available about the direct and indirect effects of climate change and urbanisation on precipitation extremes in the Netherlands. Furthermore, without a proper estimate of the extreme precipitation events caused by changes in climate and land use (e.g., urbanisation), water systems might fail in response to high precipitation rates and extreme hydrological events, putting communities at risk. This thesis will focus on analysing the statistics and spatial and temporal variability of extreme precipitation. The statistics and their links to peak extreme events are important to engineers, hydrologists, water managers, urban and regional organizers, and climate researchers who rely on water system infrastructures to protect cities from the hydrological risks of extreme events. Extreme precipitation statistics are regularly determined by a block maxima approach (e.g., annual maxima) or a certain threshold when there are enough data for the convenient convergence of probability distribution functions. Next, the extreme precipitation return levels can be estimated for a given return period.

Moreover, an assessment of extreme precipitation changes with respect to urban climate enables the extreme precipitation discrepancy between urban and non-urban areas to be distinguished, which improves the knowledge of the interaction between the land and atmosphere. In this study, we analyse different aspects of precipitation extremes (e.g., due to changes in climate and urbanisation) by answering the following research questions:

- ✓ What is the seasonal variation of daily extreme precipitation in the Netherlands? (Chapter 2)
- ✓ Are observed trends in precipitation patterns significant for recent decades? Moreover, is there evidence of more extreme precipitation increases in urban areas than in rural areas? (Chapter 3)
- ✓ Is there any relationship between temperature changes and population? What is the impact of temperature on extreme precipitation? (Chapter 4)
- ✓ How does the extreme precipitation response to dew points and atmospheric temperatures in precipitation return levels vary between urban and non-urban areas? (Chapter 5)

To answer the first two questions, we used the daily data from KNMI (231 rain gauge stations) from 1961 to 2014. For the first question, we analysed daily extreme precipitation with stationary and nonstationary models, as described in Chapter 2. The daily precipitation statistics were studied for individual months throughout the year. The regional variability of extreme precipitation was considered to characterize and attribute the seasonal variations of daily extreme precipitation events in the Netherlands. The significance of the models was investigated by Akaike's information criterion (AIC) and the log-likelihood ratio test (LRT). We studied the spatial patterns of the precipitation annual means and amplitudes, the phase of the GEV parameters, and the daily extreme precipitation return levels in the Netherlands. The second question is answered in Chapter 3, which focuses on the behaviour and trends of daily extreme precipitation. The extreme precipitation indices were defined by absolute and percentile thresholds. A methodology was presented to estimate trends considering the non-Gaussian distribution of the observations. After removing the autocorrelation noise from the time series, the time series trends were estimated for one 54-year period and two 30-year periods. For the second half of the second question, the precipitation differences between the urban and rural stations, which were classified based on land surface characteristics, were investigated with respect to distance from the sea. The impacts of urbanisation on the Dutch local climate were further investigated by answering the third question. The study proceeds in Chapter 4 using the hourly meteorological data observed in the city by amateur stations and observed in rural areas by KNMI automatic stations. The recorded meteorological data from local amateur and automatic stations provided new opportunities to analyse more details of urban climate variation. Possible relationships were extracted

for the investigated parameters. The temperature dependence of extreme precipitation was detected, and the extreme precipitation in urban areas was found to be higher than that in the paired rural stations. Although the extreme precipitation discrepancies between urban and rural areas are reported in Chapters 3 and 4, the answer to the last question of this study is analysed in detail in Chapter 5. A methodology for scaling extreme precipitation by binning and quantile regression methods is explained in this chapter. Likewise, a nonstationary model to derive return levels for given return periods is presented. The extreme precipitation was scaled by the surface air, dew point and atmospheric temperature values of 1985 and 2014. The urban and non-urban areas were categorized individually for different wind directions based on their upwind land characteristics. Radar data were further used to investigate short-duration precipitation over the land surface of the Netherlands. The discrepancy between urban and non-urban areas for extreme precipitation return levels was obtained by deriving precipitation intensity and frequency as a function of duration.

Chapter 2

Attributing seasonal variation of daily extreme precipitation events across The Netherlands *

* This chapter has been published as:
Rahimpour, V., Zeng, Y., Mannaerts, C.M., Su, Z., 2016a. Attributing seasonal variation of daily extreme precipitation events across The Netherlands. *Weather Clim. Extrem.* 14, 56–66. doi:10.1016/j.wace.2016.11.003

ABSTRACT

A recent study showed a rise in total and extreme precipitation in the Netherlands over the past century. The present study attempts to characterize and attribute the seasonal variation of daily extreme precipitation events in the Netherlands. Statistical models for extreme values were used to fit daily rainfall maxima for all months during the period 1961–2014, using data from the 231 rain gauges distributed across the country. A generalized extreme value (GEV) approach was used to determine the probability distribution of extreme values and their dependency on time and the monthly North Atlantic Oscillation (NAO) index. The non-stationary models used to represent the annual cycle of the GEV parameters assumed an invariant shape parameter and harmonic functions as location and scale parameters. The best non-stationary model was selected using Akaike's information criterion (AIC) and the loglikelihood ratio test (LRT). The results indicated that the estimates derived from the non-stationary model differed from those obtained with the aid of the stationary model, and had lower uncertainties. These non-stationary estimates were within the confidence intervals (CI) of the stationary estimates at most rain gauge stations. The nonstationary model estimated parameters with less uncertainty and with smaller CI, thus permitting more accurate representation of extreme precipitation in the Netherlands. The spatial pattern of annual mean location and scale GEV parameters was compatible with coastal, land cover (such as the wooded and heathland areas of the Veluwe region of the province of Gelderland) and orography (in the southeast of the country). The location parameter peaked over the west coast, especially on the central west coast during the summer half-year, while the centre and east of the country had the highest values during the winter half-year. The scale parameter peaked in the centre of the country during the summer, in the east in the early summer and along the west coast in the spring. The 10-year and 50-year return levels were calculated with the aid of the non-stationary model for all months. The spatial distribution of these extreme event probability clearly reflects the regional differences in the Netherlands.

2.1. Introduction

Precipitation is the most significant component of the water cycle for human life. Knowledge of changes in precipitation is therefore urgently needed as a basis for the planning and management of water resources in a rapidly changing world. Previous studies have reported a rise in overall precipitation and in the frequency of extreme precipitation events at higher latitudes (Anagnostopoulou and Tolika, 2012; IPCC, 2012; Karagiannidis et al., 2012; Trenberth et al., 2007). Zwiers et al. (2013) demonstrated that variations in mean precipitation can change the intensity and frequency of extreme precipitation.

Buishand et al. (2013) showed that the incidence of precipitation and extreme events has been increasing throughout the Netherlands, except in some regions in the southeast of the country, during the past years. Most analyses of precipitation events use the approach presented by Buishand and Velds (1980). This involves simulation of extreme precipitation using the Gumbel distribution for the weather station of the Royal Netherlands Meteorological Institute KNMI at De Bilt at intervals of from 5 minutes to 10 days during the period 1906-1977. Van Montfort and Witter (1986) used hourly data from De Bilt between 1906 and 1982, and daily data from 32 other Dutch weather stations from 1932 to 1979, to model the particular exceedances of rainfall, using the peak over threshold (POT) approach. In the last decade, Smits et al. (2004) used the long time series of rainfall data from De Bilt for the period 1906 to 2004 to model extreme rainfall throughout the Netherlands at intervals of from 4 hours to 9 days, with the aid of the POT approach and a generalized extreme value (GEV) distribution. They concluded that the rain gauge information from De Bilt can be representative of the other regions in the Netherlands if adjusted by a correction factor (which varies from 0.93 to 1.14, depending on the area concerned).

Most previous studies (such as Wijngaard et al. 2005; Buishand et al. 2009; Overeem et al. 2009; Hanel and Buishand, 2010; Overeem and Buishand, 2012) applied the GEV model to climatological statistics for the Netherlands to describe the monthly and annual distribution of precipitation maxima. Regional differences in precipitation throughout the Netherlands are currently calculated on the basis of annual rainfall at De Bilt, though Diermans et al. (2005) showed that this was not appropriate for investigation of regional variability in extreme rainfall. Mudersbach and Jensen (2011) and Rust *et al.* (2009) calculated the seasonal dependence of precipitation on the modified location and scale parameters of the GEV distribution for explicit modelling of monthly variation. This approach explained the possible external influences on extreme precipitation events.

The North Atlantic Oscillation (NAO) is one of the major source of variability in North Atlantic region and significantly affects meteorological parameters in the Northern Hemisphere (Wakelin et al., 2003; Sienz et al., 2010). The NAO is specified by NAO index in the difference of normalized sea level pressures between the Azores and Iceland (Hurrell, 1995; Jones et al., 1997).

The GEV distribution model can be used to represent the annual precipitation cycle, while NAO index influences extreme precipitation events. Furthermore, the monthly variation generated by the GEV distribution model contains information about return levels (Maraun et al., 2009; Rust et al., 2009). In the present study, the variation in extreme precipitation will be assessed by the best non-stationary model for each weather station in the Netherlands, taking the impact of NAO into account. The seasonally dependent impacts of 1-day precipitation can be used for risk assessment and risk management relating to flooding, irrigation and soil erosion in the Netherlands.

This paper examines three statistical approaches (the use of block maxima, a stationary model and a non-stationary model) to the modelling of the annual cycle. The non-stationary models for monthly maxima were determined separately for each of the 231 rain gauges in the Netherlands. The non-stationary GEV models used harmonic functions for the location and scale parameter, together with an invariant shape parameter. Section 2 describes how daily precipitation data records are obtained, and explains the methodology for determining the best non-stationary model for estimation of the statistical parameters. Section 3 presents details of the estimated parameters, the pattern of monthly return levels and the return levels of annual maxima determined with their aid. The results obtained with the optimal non-stationary model, the various spatial patterns and the physical interpretation of the discrepancies between them are discussed in section 4. Finally, conclusions are presented in section 5.

2.2. Materials and methods

2.2.1. Precipitation Dataset

Rain gauges cover the Netherlands with a spatial resolution of 10 km. The precipitation is recorded daily, and datasets are quality-controlled and validated by KNMI. These long-term data with less than 1% missing data were reviewed and the gaps in them filled by use of the ECAD (European Climate Assessment & Dataset) datasets (Klein Tank et al., 2002). There is only a negligible difference between the corrected dataset and the original quality-controlled and homogenized dataset as far as the detection and attribution of extreme precipitation in the Netherlands is concerned (Buishand et al., 2013). Further information about the operations of KNMI

(largely in Dutch, with an English summary) is available at <http://www.knmi.nl/nederland-nu/klimatologie/monv/reeksen>. In the present study, the index of a monthly maximum of 1-day precipitation (P1) was calculated for all 231 stations during the 54-year period 1961- 2014. This index has been selected as it has a significant impact on human life and is often used to estimate the probability of rare extreme precipitation events, and for the purposes of infrastructure design (Min et al., 2011; Sillmann et al., 2013).

2.2.2. Methodology

Extreme value theory (EVT) was used to evaluate data on rare precipitation events. In accordance with the block maxima method in EVT, the sample under study is divided into consecutive non-overlapping blocks, and the maximum value in each block is identified. Monthly and annual blocks were defined in the present study. The block maxima are used to determine the probability distribution of the precipitation. The standard GEV model is then employed to fit the parameters and hence to determine the frequency and intensity of extreme precipitation events.

Regarding the EVT assumptions, we consider n random variable sequence (X_1, X_2, \dots, X_n) , which are independent and identically distributed (iid). A physical process for n time unit $M_n = \max (X_1, X_2, \dots, X_n)$, conform to a common probability distribution. In this study the M_n represent the annual maxima or monthly maxima for the n number of monthly or annual blocks of daily precipitation (X_i) , respectively. The block size needs to be chosen carefully, as the reliability of the estimate of the distribution factor is strongly related to the length of the precipitation series and their sequences. Equation (2.1) regarding the Fisher-Tippett theorem can be used to estimate the distribution of M_n for a given precipitation dataset:

$$F(x; \mu, \sigma, \varepsilon) = \begin{cases} \exp\left(-\left[1 + \varepsilon \frac{x-\mu}{\sigma}\right]^{-\frac{1}{\varepsilon}}\right), & \& \varepsilon \neq 0 \\ \exp\left(-\exp\left(-\frac{x-\mu}{\sigma}\right)\right), & \& \varepsilon = 0 \end{cases} \quad (2.1)$$

$$\text{where: } \left[x: 1 + \varepsilon \frac{x-\mu}{\sigma} > 0 \right], \quad \begin{cases} \mu \in R \\ \sigma > 0 \\ \varepsilon \in R \end{cases}$$

The location parameter (μ) defines the position of maximum precipitation, and the spread of the distribution is represented by the scale parameter ($\sigma > 0$). The shape parameter (ε) is important to represent the very rare occurrences which termed with return period more than 100 years, and can define the extreme value distribution types as follows:

$\varepsilon = 0$ (Gumbel distribution) an exponential reduction of the infinite upper tail

$\varepsilon > 0$ (Fréchet-type) a slow reduction of the longer infinite upper tail

$\varepsilon < 0$ (Weibull-type) a shorter finite upper tail, depicting the occurrence of very rare events.

The Gumbel distribution is equal to $F(x) = e^{-1} \approx 0.37$ if $x = \mu$ in the above equation.

The L-moment method (Hosking, 1990) and maximum likelihood (MLL) estimation (Jenkinson, 1955) can be used to estimate the distribution parameters when there is a sufficiently large body of data on extreme events. The MLL method is the preferable approach in the present study (Klein Tank et al., 2009), especially when the climate is non-stationary.

The non-stationary properties of extreme precipitation could be calculated by considering the dependence of the GEV distribution on a covariate or time. The non-stationary extreme value in Equation (2.2) described by Coles (2001) includes the independent variable (such as precipitation) and the time-dependent parameters (such as location, scale and shape):

$$F(x; \mu(t), \sigma(t), \varepsilon(t)) = \exp\left(-\left[1 + \varepsilon(t) \frac{x - \mu(t)}{\sigma(t)}\right]^{-\frac{1}{\varepsilon(t)}}\right) \quad (2.2)$$

Consequently, the constant GEV parameters μ (or σ or ξ) are replaced by the new parameters, μ_0 and μ_1 (or the corresponding parameters for σ and ξ) (Maraun et al., 2009). For instance, the parameter dependence for location is derived from the primary analysis of observed time series in Equation (2.3). The μ_0 presents a constant offset and μ_1 represents a linear dependence on a time-dependent function $C(t)$.

$$\mu = \mu(t) = \mu_0 + \mu_1 \cdot C(t) \quad t = (1, 2, \dots, n) \quad (2.3)$$

In Equation (2.3), $C(t)$ can denote a time function that reflects a parametric trend or influence of an observed time series of extreme events that called a covariate (Katz et al., 2002). The component in Equation (2.3) can be used to reflect the sinusoidal occurrence of maxima which leads to the Equation (2.4).

$$\mu_i = \mu_0 + A_\mu \cdot \sin(\Psi C_i + \Phi_\mu) \quad \Psi = \frac{2\pi}{12} \quad (2.4)$$

where 12 means 12 months in a year, A_μ represents the amplitude of the sinusoidal oscillation component, Φ_μ the phase, and the angular frequency is represented by Ψ .

The expression for the location parameter can be written in a convenient linear form by introducing the parameters A_μ and Φ_μ .

$$\mu_i = \mu_0 + \mu_1 \cdot \sin(\Psi C_i) + \mu_2 \cdot \cos(\Psi C_i) \quad i = (1, 2, \dots, 12) \quad (2.5)$$

$$A_\mu = \sqrt{\mu_1^2 + \mu_2^2} \quad \Phi_\mu = \arctan2\left(\frac{\mu_2}{\mu_1}\right) \quad (2.6)$$

It follows that the desired seasonal model is a Fourier series:

$$f(t) = \frac{a_0}{2} + \sum_{k=1}^k (a_k \sin(k\Psi t) + b_k \cos(k\Psi t)) \quad k (0, 1, \dots, \infty) \quad (2.7)$$

The seasonal model considered here can be represented by a Fourier series limited to $k = (0, 1, 2)$ harmonics because inclusion of higher harmonics complicates the statistic model by adding extra underdetermined parameters. The optimal model is therefore defined for each time series separately. The parametric model with $k = 2$ describes each parameter as shown in Equations (2.8) and (2.9).

$$\mu(t) = \mu_0 + \mu_1 \cdot \sin(\Psi t) + \mu_2 \cdot \cos(\Psi t) + \mu_3 \cdot \sin(2\Psi t) + \mu_4 \cdot \cos(2\Psi t) \quad (2.8)$$

$$\sigma(t) = \sigma_0 + \sigma_1 \cdot \sin(\Psi t) + \sigma_2 \cdot \cos(\Psi t) + \sigma_3 \cdot \sin(2\Psi t) + \sigma_4 \cdot \cos(2\Psi t) \quad (2.9)$$

Previous studies concluded that there was no systematic difference between the values of the shape parameter in the Netherlands and in the neighbouring country Belgium (Buishand, 1991; Gellens, 2003). Accordingly, the shape parameter was assumed to be spatiotemporally independent at each station. Therefore, particularly in our study $\varepsilon(t) = \varepsilon_0$. The sinusoidal models used in this study were developed by considering the impact of the NAO on the location and scale parameters. The NAO is the dominant teleconnection pattern for seasonal climatic variations in the Netherlands. The monthly NAO index for the period 1961 - 2014, provided by the US National Weather Service's Climate Prediction Center (CPC) (see further details at <http://www.cpc.ncep.noaa.gov>), was used in this study. The non-stationarity models for the monthly precipitation maxima were determined by fitting the GEV models with the monthly NAO. The monthly NAO was incorporated as an additional linear covariate for $\mu(t)$ and $\sigma(t)$ in the Equations (2.8) and (2.9), respectively.

Thirty-three combinations of non-stationary models (9 parametric sinusoidal models and 24 combinations of parametric sinusoidal models and NAO) have been considered to describe time-dependent variations and the impact of the NAO on estimates. The models name denoted by $MDL_{k_\mu N, k_\sigma N}$ that shows the harmonic level (k) for Fourier series on location and scale parameters and NAO influences by the subscripts $k_\mu N$ and $k_\sigma N$ respectively. The simplest model ($MDL_{0,0}$) described time-independent GEV parameters as a stationary GEV. The most complex model estimated 13 parameters, while the simplest model estimated three parameters. The time series $x(t_i)$ for parameter estimation was fitted by maximizing the log-likelihood function as follows:

$$l \equiv \log L = \sum_{i=1}^n \left(-\log(\sigma(t_i)) - \left(1 + \frac{1}{\varepsilon}\right) \log \left(1 + \varepsilon \frac{x(t_i) - \mu(t_i)}{\sigma(t_i)}\right) - \left[1 + \varepsilon \frac{x(t_i) - \mu(t_i)}{\sigma(t_i)}\right]^{\frac{1}{\varepsilon}} \right) \quad (2.10)$$

The goodness of fit and the significance of the models were tested with the aid of Akaike's information criterion (AIC) (Akaike, 1974) and the log-likelihood ratio test (LRT) (Sienz et al., 2010). Both methods (AIC and LRT) are used to choose the best model at each station. The corrected AIC (AIC_c) (see Equation

(2.12)) (Burnham and Anderson, 2002) is used to select the best model for a small sample ($\frac{n}{k} < 40$).

$$AIC = -2l(\hat{\theta}|MDL_j) + 2k \quad (2.11)$$

$$AIC_c = -2l(\hat{\theta}|MDL_j) + 2k \left(\frac{n}{n-k-1}\right) \quad \theta = (\mu, \sigma, \varepsilon)^T \quad \theta = \hat{\theta} \quad (2.12)$$

where $\hat{\theta}$ is the maximum likelihood estimator and $l(\hat{\theta}|MDL_j)$ is the log-likelihood estimated at $\hat{\theta}$ (more information detailed by Burnham and Anderson (2004)). The various models may be ranked by considering the difference between the value of AIC_c for each model and the minimum value of AIC_c at each station:

$$\Delta AIC_c = AIC_{c,j} - AIC_{c,min} \quad (2.13)$$

The Akaike weight was used to find the probability of each model in the universe of models investigated:

$$W_j = \frac{e^{-0.5\Delta AIC_{c,j}}}{\sum_{j=1}^j e^{-0.5\Delta AIC_{c,j}}} \quad (2.14)$$

In our study, the AIC_c emerges the candidates for the best non-stationary models. Only those models falling in the range $0 < \Delta AIC_c < 2$ (suggested by Sienz et al. 2010), will be further investigated with the LRT, for selecting a conclusive best model (Claeskens and and Hjort, 2008). If the LRT was not possible, we would rely on the appropriate model which was selected by AIC_c . If the models have the same AIC_c and the LRT was not possible, the model with the least parameters was selected as an appropriate nonstationary model. Where MDL_j with fewer parameters is a submodel of MDL_i , the LRT selects the best model with the aid of Equation (2.15):

$$D = 2[l_j(\hat{\theta}|MDL_j) - l_i(\hat{\theta}|MDL_i)] \quad (2.15)$$

The probability P of the occurrence of extreme events is defined as the chance of the event occurring at least once on average in T years; hence, " $P = \frac{1}{T}$ ". The long-term return level (r_T) of extreme precipitation events for the same period T can be estimated by considering annual maxima (for further details, see Coles (2001)).

$$P(x > r_T) = 1 - F(r_T; \mu, \sigma, \varepsilon) = \frac{1}{T} \quad (2.16)$$

The return level is derived numerically from monthly stationary and non-stationary GEV models. $F_i(x)$ is the probability of the occurrence of an extreme event smaller than x (i.e. monthly maxima) in month i and can be found by solving the equation:

$$\prod_{i=1}^{12} F_i(r_T) = 1 - \frac{1}{T} \quad (2.17)$$

Both normal and bootstrap procedures are appropriate for the estimation of MLL parameters. In the present study, the parametric bootstrap procedure was used to obtain the confidence intervals (CI) of estimates. In fact, the parametric bootstrap procedure was found to give better estimates and more realistic intervals than the normal approximation, particularly for long return periods. Enough replicate sample sizes of 10^4 observations were available for running the parametric bootstrap method. In order to validate the non-stationary models, the estimated GEV parameters (location, scale, shape and also return levels) were compared with the estimated parameters obtained by monthly stationary analysis.

2.3. results

Precipitation for the Netherlands was investigated at the 231 weather stations during the period from 1961 to 2014. The occurrence and distribution of the heavy precipitation (more than 10 mm) shows the summer half-year (between June and November) included a higher percentage of heavy rainfall, especially in July and August, during the past 54 years. This is accordant to Buishand et al. (2013)'s results, which indicated the non-stationary nature of extreme precipitation over the Netherlands by showing more intensive extreme precipitation occurrence during the heavy rainfall seasons. Figure 2.1(a) demonstrates the box- whisker plot for monthly maxima of maximum daily precipitation for De-Bilt station (as a representative station) in the Netherlands, between 1961 and 2014. It shows some data points are upper the whiskers while the lower whiskers are closer to the boxes. The sinusoidal pattern could be seen from the median data points. The maximum of the median is pronounced between June and August with larger boxes against the other months. Therefore, the distribution of extreme precipitation and the seasonal variation of their occurrence during last 54 years indicate that it is unreasonable to assume that extreme precipitation is stationary in the Netherlands.

Extremes analysis differs mainly due to the estimated return levels. In this respect, the return level for each station was reconstructed by considering NAO impacts on GEV parameters. Although the diagnostic plots are similar for GEV models with/without NAO impacts, the important differences were revealed from the return level plot. Figure 2.1(b) shows the plot of block maxima with effective return levels with NAO influences for De Bilt station. The variation of

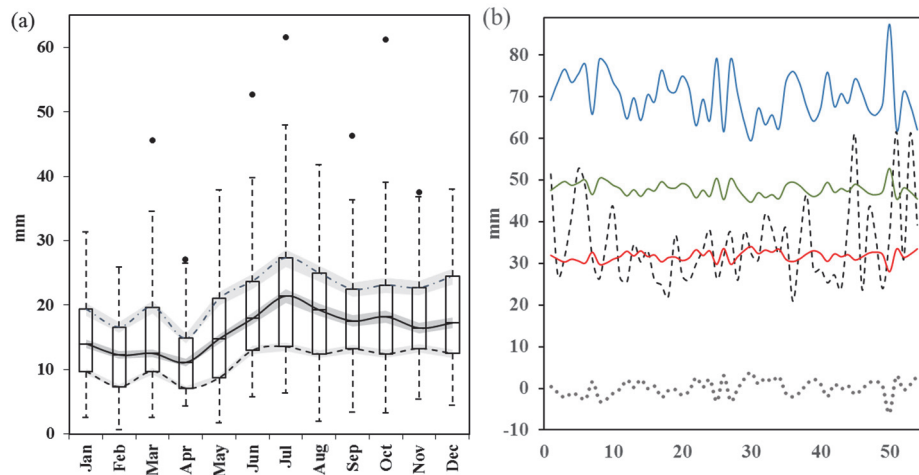


Figure 2.1. (a): Box-whisker plot for De-Bilt during 1961-2014. The inter-quartile range (IQR) extends whiskers to 1.5 times. The solid line shows the median of monthly maxima for maximum daily precipitation. The black dots indicate the data points which are exceeding the whiskers. The median (solid line), the 0.25 and 0.75 quantiles (dashed and dot-dashed lines) depicted with 95% confidence intervals (grey shaded). (b): Diagnostic plot from fitting the GEV model with NAO influences for maximum daily precipitation in De-Bilt during 1961-2014. The lines show NAO index (grey-dotted) annual maxima (black), 2 (red), 10 (green) and 50 (blue) year return level. 2 year return level analogous estimating to the median of the GEV distribution function.

GEV distribution in Figure 2.1(b) suggests the assumption of NAO impacts for the developed non-stationary models are reasonable. It shows the fluctuations in return levels for different return periods vary accordingly (e.g. inversely) with those represented by the NAO index.

The annual block, with a large block length (e.g. 365 days), leads to a convenient convergence of the PDF of maximum daily precipitation towards the GEV distribution. For resolving the seasonal evolution, the monthly blocks (sub-annual blocks) should enable large block length to obtain a good approximation as well. In this respect, the diagnostic plots (e.g. Figure 2.2) for De-Bilt station were demonstrated for the one-month blocks and the two-month blocks. The two-month blocks were created by combining the observations of two adjacent months from two successive years (e.g. Jan 1961

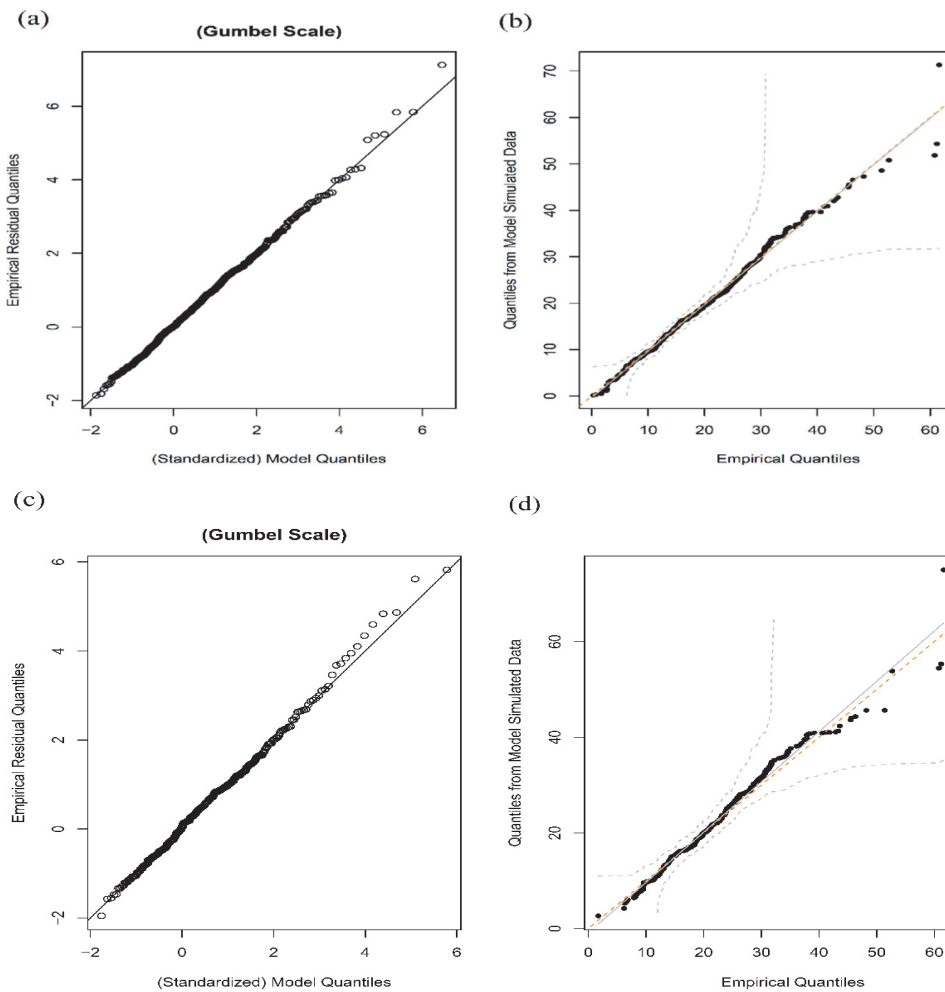


Figure 2.2. Diagnostic plots from fitting the non-stationary GEV model to one-month (upper panels) and two-month (lower panels) maximum precipitation in De-Bilt, The Netherlands. Plots in left show empirical data against fitted model that have been transformed to Gumbel scale. The plots in right indicate randomly generated data with the aid of the non-stationary GEV model against the quantiles of empirical data. The lines show regression (solid line), 1-1 line (red dashed line) and 95% confidence intervals (grey dashed line).

and Jan 1962, a block length of 62 days). Therefore, the created two-month blocks preserve the seasonal cycle. The one-month and two-month data were rescaled by Gumbel (time-independent) distribution to depict the diagnostic plots (Rust et al., 2009).

The qq-plot in Figures 2.2(a) and 2.2(c) show the empirical quantiles versus derived quantiles with the aid of the fitted model. The probability plots in Figures 2.2(b) and 2.2(d) respectively depict the empirical frequency distribution of one-month and two-month against their fitted GEV distribution. The plots are almost similar for one-month and two-month blocks. Figure 2.2 demonstrates reasonable assumptions for the model and good agreement between the empirical and fitted GEV model. The similar plots for both one-month and two-month blocks show there is no significant improvement by doubling the length of blocks (e.g. using two-month blocks). The suitability of the block length was verified for other stations with the same results. Consequently, the one-month block length was chosen in our study.

Our initial aim was to use parametric non-stationary GEV models to estimate the seasonal variation of extreme precipitation and to compare the approximations obtained in this way with stationary estimates. Since Hurrell (1995) found a significant relation between NAO and precipitation throughout Europe, the impact of NAO will also be considered in this study. The various combinations of non-stationary models mentioned in section 2.2 were examined in order to select the optimal seasonal model. The non-stationary models selected at each station were then ranked in order of AICc. Since this approach tends to include more complicated models, the LRT was also used whenever possible to choose the optimal model. Comparison of the results obtained with the AICc and the LRT approaches showed that the selected models are similar in almost all stations.

Assessment of the non-stationary models identified all the best non-stationary models, taking the monthly impact of NAO on the scale parameter into account. Figure 2.3 shows the best non-stationary models found in this way for all weather stations in the Netherlands. Analysis of these data indicated that model $MDL_{0,2N}$ was best at 52.4 % of the stations and $MDL_{1,0N}$ at 37.6% of the stations. $MDL_{1,2N}$ gave the best fit with the data at 4.8% of the other stations, $MDL_{2,0N}$ at 4.3% and $MDL_{0,1N}$ at 0.9 %. Readers may be reminded that the best non-stationary model at most stations located in the eastern part of the country (e.g. red dots in Figure 2.3) indicates that it only considers the scale parameter and the influence of the NAO index on it. More

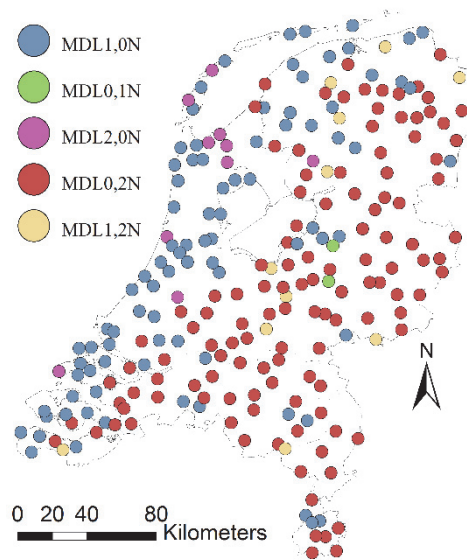


Figure 2.3. The best non-stationary model distribution at each station

complicated models such as $MDL_{2N,2N}$, and the models where NAO influences both the location and scale parameters do not come into consideration for selection as the best non-stationary model. Another point is that the best non-stationary model for the western part of the country, $MDL_{1,0N}$, indicates that there are no NAO effects on both location and scale parameters. As such, one cannot find NAO effects on location parameter at all for the Netherlands (see Figure 2.3), while only NAO effects on scale parameter for all stations. The combination of the simplest ($k=0$) and complicated ($k=2$) sinusoidal variation for location and scale parameters show the dominant non-stationary models in the eastern part of the country.

The stationary model and the best non-stationary GEV model were used to estimate parameter distributions and return levels at each station. The results show reasonable estimates of the parameters by the non-stationary models at most stations, since most of the parameters estimated by the non-stationary models are located within the CI of the estimates obtained by the stationary models (Table 2.1). The non-stationary model estimated narrower CI for location and scale parameters for all stations between March and November, than the stationary ones. The narrower CI can be found for shape parameter at all station for all months.

Table 2-1. Percentage of stations (%) present the non-stationary model parameters (location, scale and shape) located within the parameters CI which derived from the stationary models.

	Jan	Feb	Mar	Apr	May	Jun	Jul	Aug	Sep	Oct	Nov	Dec
location	95%	44%	77%	38%	96%	44%	41%	71%	87%	77%	87%	76%
scale	75%	64%	46%	16%	42%	91%	75%	66%	63%	87%	90%	87%
shape	88%	94%	95%	60%	94%	96%	95%	96%	97%	93%	85%	87%

The best non-stationary GEV model was used to estimate parameter distributions for all available 231 rain gauges in the Netherlands. Kriging has been found to be the best method for interpolating precipitation data in the Netherlands (for further details, see Sluiter (2014, 2012, 2009)). This method has therefore been used here to represent the spatial structure of estimated GEV parameters for all areas in the Netherlands, as shown in Figure 2.4.

Figure 2.4(a) presents the spatial distribution of μ_0 , (i.e. the annual mean of the location parameter), Figure 2.4(b) gives the relative amplitude of the location parameter, $(\sqrt{\mu_1^2 + \mu_2^2 + \mu_3^2 + \mu_4^2 + \mu_{NAO}^2} / \mu_0)$, and Figure 2.4(c) shows the monthly distribution of the maximum location parameter.

The location parameters are highest in the west and middle of the country (Figure 2.4(a)). Relatively high values of μ_0 are found in the west of the Netherlands (especially along the central west coast, which includes areas of high population) as well as in the middle of the country (the Veluwe area, including forestland with a maximum elevation of 100 m). The southwest and the southeastern corner of the country (the province of Limburg) also have higher values of μ_0 than other parts of the country.

Figure 2.4(b-c) shows the relative amplitude and phase of the location parameter, with a gradient from the east to the west of the country. The relative amplitude falls off from the west toward the east. Maximum values are found in the west in the summer half-year (between June and November), but in the east in the winter half- year (between December and May).

Figure 2.4(d-f) shows a similar spatial distribution for the scale parameter (σ_0 , the relative amplitude of the scale parameter, $(\sqrt{\sigma_1^2 + \sigma_2^2 + \sigma_3^2 + \sigma_4^2 + \sigma_{NAO}^2} / \sigma_0)$, and the month in which the scale parameter is maximum. Figure 2.4(d) shows that σ_0 is highest in the west, southwest and middle of the country, and lowest in the north and south. The relative amplitude in Figure 2.4(e) shows a gradient from west to east that is weaker along the west coast areas than in other parts of the country. Figure 2.4(f) presents the overall pattern of the

occurrence dates of the highest scale parameter. The maximum scale parameter occurs in spring (March, April and May) in the west of the country, and early in summer in the east. The highest values are found in the middle and east, and the lowest values in the north and northwest.

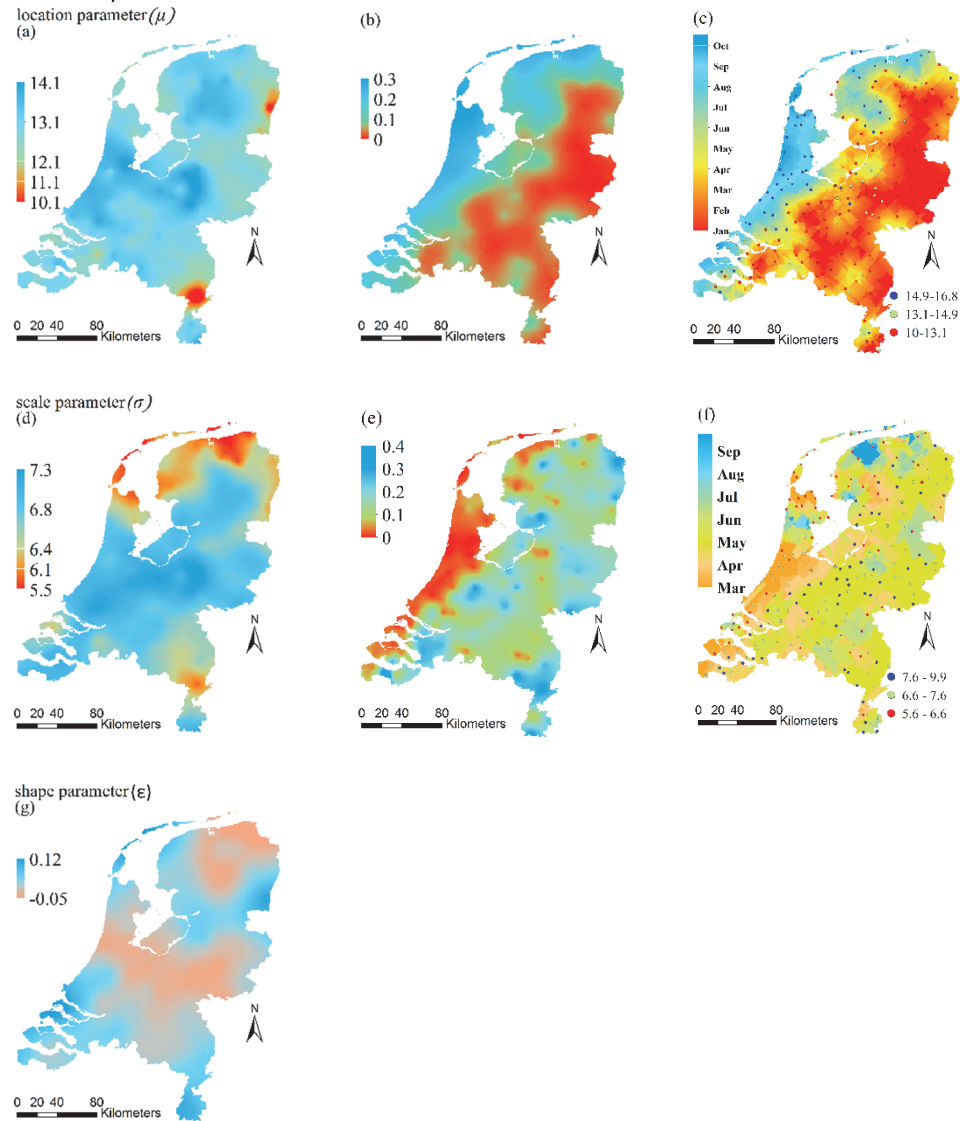


Figure 2.4. (a) Location parameter, (b) relative amplitude of location parameter, (c) the phase of maximum location parameter, (d) scale parameter, (e) the relative amplitude of scale parameter with circles that show scale value at each station, (f) the phase of maximum scale parameter, the values of location and scale parameter at each station denoted by RGB circles in (c and f) respectively, (g) shape parameter.

Figure 2.4(g) presents the spatial distribution of the shape parameter estimated from non-stationary models without any annual cycle (fixed shape parameter), which differs from the distribution of the location and scale parameters. The maximum values of the shape parameter occur in the southwest and far southeast of the country. The value of this parameter is minimum along a west-east axis in the middle of the country, and increases toward the south and north.

The parameters estimated from non-stationary models at each station were used to derive return levels for individual months throughout the year. The variation of the spatial pattern of the 10-year return level from January to December is shown in Figure 2.5(a) to (l). As mentioned above, Kriging was used to interpolate the estimates of the 10-year return level across the country. Use of the actual values determined for each station might yield better approximations, but interpolation was only used in this study to represent the overall regional variation of return levels.

It may be seen from Figure 2.5 that the 10-year return level of extreme precipitation varies from about 20 mm in winter (DJF) across the north of the country to nearly 33 mm in summer (JJA) in western areas. In another words, the 10-year return level is highest in the summer half-year (between June and November). Moreover, the 50-year return levels of extreme precipitation vary between 28 mm and 50 mm with a spatial distribution similar to that for the 10-year return levels (results not shown). Apart from estimating the return level for each month of the year as indicated above, annual return levels are also useful for many hydrological applications. These can be determined by considering the maximum value for each year without taking the details of the annual cycle into account.

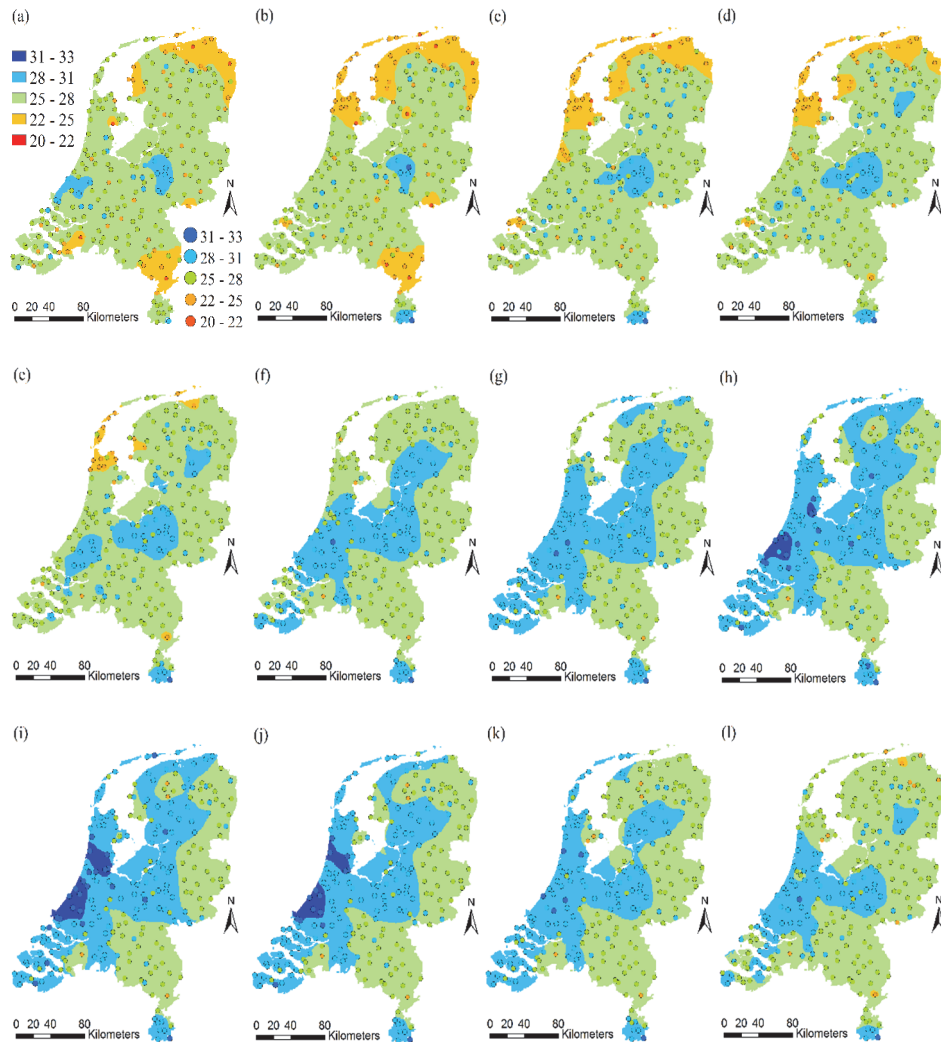


Figure 2.5. 10-year return levels derived from non-stationary models for individual months during the year at 231 rain gauge stations (circles) and the background indicate their spatial pattern over the Netherlands. Panels (a) to panel (l) show the months January to December.

The block maxima approach assumes that the variable to be estimated is time independent. It follows that this approach is not suitable for estimation of non-stationary return levels. As shown above, the spatial distribution and the level of extreme precipitation vary throughout the year. We have nevertheless compared estimates of the return level obtained with the aid of annual block maxima, stationary GEV models and non-stationary GEV models in order to see what effect this has on the results obtained. Return levels were estimated

at each station for return periods of both 10 and 50 years. Interpolation was then used to show the overall distribution of the return levels throughout the country.

Figure 2.6(a-c) shows the 10-year return levels estimated with the aid of annual block maxima, the stationary GEV model and the non-stationary GEV model respectively. The non-stationary model gives lower estimates than the other two approaches. The difference between the non-stationary estimates and two others, especially the stationary estimates, is particularly clear in the southeast and west of the country.

Figure 2.6(d-f) shows the 50-year return levels estimated with the aid of annual block maxima, the stationary GEV model and the non-stationary GEV model respectively. The stationary and the non-stationary GEV models were fitted for the individual months and were used to estimate return levels for each month. Then, the yearly return level was obtained by solving the equation (2.17). The difference between the non-stationary and stationary estimates is particularly marked in Figure 2.6. The stationary approach gives the largest estimates of extreme precipitation at the 50-year return level when compared with the other two approaches. This may be because the shape parameter is estimated separately for each month in the stationary model. The months with several extreme events could lead to a larger positive shape parameter and hence to higher return levels. However, the available knowledge of time-independent shape parameters in the Netherlands (Buishand, 1991; Gellens, 2003) indicates that the shape parameter is invariant in the non-stationary model. The non-stationary models used for this purpose have smaller error intervals due to the use of a fixed shape parameter and sinusoidal location and scale parameters to model the annual cycle. It follows that return level estimates from non-stationary models are more realistic than those from stationary models.

The interpolated return levels derived from non-stationary models show a clear rise from the east to the west of the country, with the exception of the elevated areas in the southeast, which have higher return levels than neighboring parts of the Netherlands. High return levels prevail in the centre of the country (the

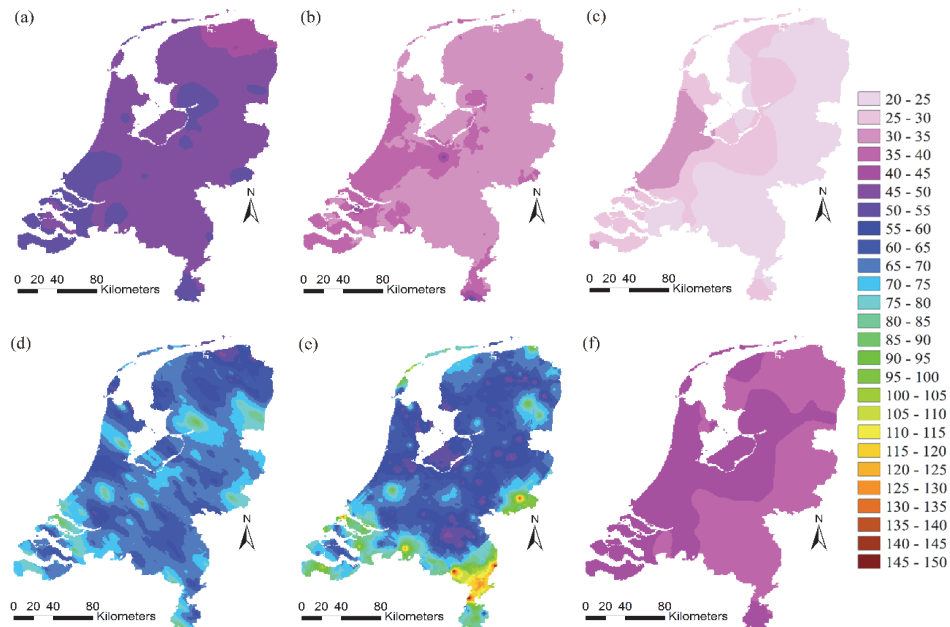


Figure 2.6. 10-year return level from (a) annual maxima block, (b) stationary models, (c) non-stationary models; 50 year return level from (d) annual maxima block, (e) stationary models, (f) non-stationary models. The stationary and non-stationary GEV models fitted for the individual monthly blocks to estimate the yearly return level.

Veluwe) with its elevated forestlands, the southwest and the west coast, which includes densely populated areas along the coast (especially the central west coast). On average, the 10-year and 50-year return levels are higher along the west coast than in eastern parts of the Netherlands, for all the three approaches.

2.4. Discussion

One-day monthly maximum precipitation estimated with the aid of the GEV distribution model was calculated to investigate the regional differences in extreme precipitation across the Netherlands. These calculations were based on the high-quantile precipitation data taken from rain gauge stations throughout the Netherlands. Previous studies estimated the extreme precipitation characteristics on the assumption that precipitation patterns in the Netherlands are stationary. The present study considers the precipitation to be non-stationary, varying according to the latitude of the stations, which are located between 50° and 53° N, and with a marked seasonal cycle.

The non-stationary models used in this study incorporated unfixed location and scale parameters and a constant shape parameter at each station. The influence of NAO and time-dependent GEV parameters was taken into account with the aid of appropriate Fourier series. The best non-stationary model was chosen for each station with the aid of statistical criteria (AIC and LRT) from a total of 33 time-dependent models that take the monthly impact of NAO on the location and scale parameters into account. It was found that the simple models MDL_{0,2N} and MDL_{1,0N} were best for most stations, as shown in Figure 2.3.

The selected non-stationary models explain that observed variation in extreme precipitation is linked to the NAO. The larger scale parameter leads to more spread out of the extreme precipitation distribution. The NAO index enhancements are on average associated with the extreme precipitation intensification in the Netherlands. This link between the NAO and extreme precipitation not only undermines the basic assumption of stationary data for precipitation but also reveals the fluctuations of precipitation intensity in the Netherlands connected with the NAO pattern. In particular, the extreme precipitation will be aggravated over the country by the higher NAO index values. Therefore, the historical observed extreme precipitation, considering stationarity, is not a reliable predictor of return levels for long return periods. The estimation of future extreme precipitation needs to consider the time dependency of probability distributions and fluctuations of North Atlantic Oscillation.

Our findings confirm that non-stationary models with a harmonic structure give a better estimate of the relevant parameters and lower uncertainty, as previously reported by Maraun et al. (2009) and Rust et al. (2009). The seasonal estimates were found to be appropriate and less uncertain, since the estimates obtained with the best non-stationary model at most stations are well within the CI of the estimates obtained with the stationary model. Moreover, the parameters estimated with the aid of the non-stationary model and their CI are lower than those estimated by the stationary model. It may thus be concluded that the non-stationary models give reasonable estimates of the GEV parameters. In other words, they give a better estimate regarding the impact of the NAO and the annual seasonal cycle on the parameters.

The spatial distribution of the parameters shown in Figure 2.4 reveals differences in the spatial patterns of the location and scale parameters. There are marked divergences between the location and scale parameters regarding the phases of the maximum values (Figures 2.4(c) and 2.4(f)). However, the spatial patterns of the annual mean in Figures 2.4(a) and 2.4(d) reflect strong correlation between the two parameters in this respect.

Figures 2.4(b) and 2.4(e) show further details of the relative amplitude of the annual cycle of the location and scale parameters. The amplitude of the annual mean in the location parameter falls from 30% in the west to less than 1% in the east of the Netherlands, while the amplitude of the annual mean scale parameter rises from less than 1% in the west to almost 40% in the southwest and middle of the country. Nevertheless, the seasonal variation of the location parameter in the west of the country is stronger than that of the scale parameter.

Figures 4(c) and 4(f) show that the location and scale parameters have their highest values during the summer in the west and middle of the Netherlands. On the other hand, the heavier precipitation in the east of the country occurs during the winter.

Dominant extreme precipitation, with high values of the location and scale parameters, was detected along the west coast of the Netherlands (where densely populated regions are to be found) during the summer half-year. In the east of the country, location parameters were low and the annual cycle was correspondingly weaker while the scale parameter showed a strong annual variation. Thus, extreme precipitation values are low in the east of the country, especially during the winter half-year. This result can be useful for risk assessment and water management in the Netherlands.

As Figure 2.5 shows, clear 10-year return level patterns may be seen with higher values in spring over the middle of the country, in particular the Veluwe area. This higher extreme precipitation could be related to the orography and the presence of forestlands in this part of the country. The 10-year return level is low in the north of the country during the winter half-year, while increasing during the summer half-year. Similarly, the west coast shows increases during the summer half-year. This pattern arises from temperature variations in the North Sea (low in the winter half-year and higher in the summer half-year) together with unstable atmospheric conditions (Attema and Lenderink, 2014). The west coast has the highest values, which fall off however with increasing distance from the coast. This gradient could be due to the westerly circulation that is largely responsible for precipitation in the Netherlands (Lenderink et al., 2007). To sum up, therefore, there are two dominant patterns of 10-year return levels in the Netherlands: one over the forestlands in the middle of the country in the spring and another over the entire west of the country with higher extreme precipitation during the summer half-year, especially in August and September.

Figure 2.5 also reveals constant high values during all months in the southeastern corner of the country. This could be due to the relatively high altitude of this part of the Netherlands. In addition, the spatial pattern of the

10-year return level indicates that the return levels in the east of the country, which peak in August, are still lower than the values found in the west of the country during the same period. The prevailing westerly winds and distance to the coast could also be the reason for this difference.

Although large quantities of moisture are transferred from the North Sea to the Netherlands by the prevailing south or southwest wind (Sisternans and Nieuwenhuis, 2004; Stolk, 1989), precipitation is probably reduced by the lower water temperature of the North Sea off the west of the Netherlands. The changes in circulation (van Haren et al., 2013) and the increases in sea surface temperature (SST) in the Netherlands (Lenderink et al., 2009) could lead to higher extreme precipitation along the west coast during the summer half-year. As shown in Figure 2.5, the west coast has lower extreme precipitation than the inland areas in the late winter and spring combined with higher extreme precipitation in the summer and autumn.

The estimates of the 10-year and 50-year return levels shown in Figure 2.6 were derived by three approaches, involving the use of annual maxima, monthly stationary models and non-stationary harmonic models. The 10-year and 50-year return levels estimated with the aid of the non-stationary models show marked regional differences, unlike those derived from annual maxima and stationary models. The extreme variation of the distributions obtained by the latter two approaches arises from the overestimation of the parameters concerned. The estimation errors produced when using the stationary model (with invariant parameters) are reduced by taking the annual cycles into account when determining the extreme precipitation.

The main pattern shown by the inspection of Figure 2.6 is of higher return levels over the central west coast where the populated areas are located and a drop in return levels from the west toward the east of the Netherlands. It might be thought at first sight that the increasing distance from the coast is the reason for this decrease. However, a closer look at Figure 2.6 shows that the return levels are actually higher in populated areas on the central west coast, in the Veluwe area, the southwest and the southeastern corner of the Netherlands. These high values could perhaps be explained by greater transfer of moisture from the sea along the west coast, the land cover in the middle of the country and the orography in the southeast. The observed positive gradient of return levels from the east to the west of the country could be helpful in hydrological applications, as a basis for recognition of regions that are exposed to a high risk of extreme precipitation.

This study only considered GEV parameters as a harmonic function dependency on time and influence of NAO index. It might be interesting to develop more sophisticated non-stationary models with other relevant covariates. Future

studies could investigate the plausible covariates in terms of climate variability and the influences of a linear trend or quadratic function of parameters variation, which is beyond the scope of current manuscript.

2.5. Conclusions

Quantitative knowledge of extreme precipitation events (such as return level or return period) is needed to describe what can be expected in the future due to climate change. Building on the knowledge gained from previous studies in the Netherlands, the present study is an initial attempt to use non-stationary models to reflect the impact of the NAO and the annual climatic cycle on extreme precipitation in the Netherlands. The non-stationary models developed to confirm that extreme precipitation can vary in different ways under the influence of the annual and seasonal cycles, depending on regional characteristics. The parameters and return levels estimated with the aid of non-stationary models showed lower uncertainty than those derived from the stationary model. In other words, the non-stationary models gave more reasonable estimates of the seasonal variation of the model parameters and the impact of the NAO on extreme 1-day precipitation within narrow confidence intervals at most of the 231 rain gauge stations in the Netherlands.

The approach adopted in this study uses a harmonic function model for all monthly maxima during the year with seasonal variations instead of individual models for every month. The spatial patterns of parameters and return levels obtained in this way reflect the regional differences in extreme precipitation across the Netherlands. In addition to the high extreme precipitation in the southeastern corner of the country, the prevailing pattern is one of high extreme precipitation in the Veluwe area in the spring and along the central west coast in the summer half-year.

The estimates of time-dependent model parameters, phase and relative amplitude together with return level patterns could be extended to include the evaluation of further meteorological aspects and regional characteristics of extreme precipitation in the Netherlands. Future investigation of non-stationary extreme events should lead to more reliable and exhaustive knowledge of such phenomena. Use of other possible covariates or non-parametric models might permit more reliable prediction of the variation and distribution of extreme precipitation in the Netherlands.

Chapter 3

Detecting the Effect of Urban Land Use on Extreme Precipitation in The Netherlands *

* This chapter has been published as:
Rahimpour, V., Zeng, Y., Mannaerts, C.M., Su, Z., 2017. Detecting the effect of urban land use on extreme precipitation in the Netherlands. *Weather Clim. Extrem.* 17, 36–46.
doi:10.1016/j.wace.2017.07.003

ABSTRACT

A notable increase in heavy precipitation has been observed over the Netherlands in recent decades. The aim of this study was to assess the influences of urban land use on these extreme precipitation patterns. Significant differences between an earlier multi-decadal period and a recent period were found in the Netherlands between 1961 and 2014. The significant changes in different indices indicate that severe precipitation events were not distributed homogeneously across the study area. The precipitation probability and distribution were assessed using the block maxima approach by comparing observations from urban and rural areas at different timescales. The possible effects of land use on extreme precipitation were assessed by quantifying the differences between urban and rural rain gauge stations according to the spatial gridding method. This study shows that urban land use may have affected the extreme precipitation patterns across the Netherlands. The data from all the categorized stations show that urban areas receive more intense extreme precipitation than do rural areas. Relative to other areas in the Netherlands, the urban areas in the western populated regions of the country exhibit prominent urban land use influences on the extreme precipitation patterns.

3.1. Introduction

Human life is more directly affected by precipitation than any other atmospheric phenomenon (Levizzani et al., 2002); thus, detecting changes in precipitation has become a critical research focus in recent decades (Hanel and Buishand, 2010). Extensive work has been dedicated to studying extreme precipitation events (Aguilar et al., 2009; Chen et al., 2012; Griffiths et al., 2005; Gutowski et al., 2010; Trenberth et al., 2007; van den Besselaar et al., 2012; Wang and Zhang, 2008; Westra et al., 2013; Patrick Willems, 2013). Studies above have shown that precipitation and extreme events have increased at higher latitudes and that the intensity and frequency of extreme precipitation events have intensified. Physically, changes in the North Atlantic Oscillation (NAO) and the sea surface temperature (SST) are the major sources of precipitation changes in the Northern Hemisphere (Hurrell, 1995; Jones et al., 1997; Lenderink et al., 2009). In addition, several studies have shown that land use and topography can affect regional climates. Thus, extreme precipitation patterns can be influenced by the type of land use in high-latitude regions.

The Netherlands is located along the North Sea. Recent studies have revealed that the total precipitation and frequency of extreme events have increased over a large part of the Netherlands (Burauskaite-Harju et al., 2012; van Haren et al., 2013; Daniels et al., 2014; Rahimpour Golroudbary et al., 2016). Buishand et al. (2013) concluded that precipitation over the Netherlands increased by approximately 26% during the period from 1910 to 2013. Furthermore, Ter Maat et al. (2013) investigated the combined effects of forestation and topography on the maximum rainfall in the Netherlands and found that elevated forest areas (with a maximum elevation of 100 m) in the middle of the country received more precipitation than did the surrounding areas. Hurk et al. (2014) reported that the intensity of extreme precipitation in the western regions (including the most urbanised areas) was greater than that in the other regions of the Netherlands. The various physical and chemical processes (such as the Bowen ratio, heat storage capacity, and surface roughness) could be responsible for the effects of urban areas on precipitation (Oke, 1982; Shepherd, 2006; Mitra et al., 2012). Further studies also concluded that urbanisation effects on precipitation should be considered in the Netherlands (Daniels et al., 2015).

This study investigates the variability in extreme daily precipitation and its spatial patterns across the Netherlands. The main objective is to analyse variations in extreme precipitation in three climatological periods and identify the likely discrepancy in extreme precipitation between urban and non-urban (rural) areas in the Netherlands. The link between the land use types and the monthly daily precipitation maxima was found by categorising stations in the

Netherlands as urban or rural according to their local environmental characteristics (land use and surface features). This method is based on high-quality, historically observed precipitation data and the calculation of extreme precipitation indices and individual time series of the monthly daily precipitation maximum across the country.

In the following section, the precipitation data, precipitation indices, methods used in statistical analysis, and urban and rural stations are introduced. In section 3.3, the results and analysis of the trends in the observed indices are presented; the monthly amounts and trends during the different climatological periods are compared, and the regional differences in extreme precipitation are investigated. In section 3.4, the discussion is presented, and the conclusions are in section 3.5.

3.2. Materials and methods

3.2.1. Precipitation data

Long-term precipitation data from manual rain gauges in the Netherlands were quality controlled and validated (Buishand et al., 2013). These rain gauges reported daily precipitation (more details are provided at <http://www.knmi.nl>). The homogenised dataset was statistically tested and described by Buishand et al. (2013), and only a negligible difference in the detection of trends in extreme indices was observed between the homogenised dataset and the original quality-controlled dataset. A total of 231 rain gauges were used in this study, and the record length was 54 years (1961-2014). Complete data were available for 80% of the gauges, and missing data represented less than 1% of the data from the remaining gauges for this period. The missing data were replaced by values from ECAD (European Climate Assessment & Dataset) datasets (Klein Tank et al., 2002). The rain gauges have reasonable spatial coverage (with a spacing of approximately 10 km), and ordinary kriging was used to grid the precipitation data at a 1 km resolution (for a more detailed discussion, see Sluiter (2009, 2012, 2014)).

3.2.2. Definition of the precipitation indices

Extreme precipitation indices were defined to provide a true perspective of the observed changes based on the characteristics of the extreme events, including their frequency, amplitude, and persistence (Klein Tank et al., 2009). Extreme precipitation indices have been comprehensively described and classified into two groups (Zhang and Yang, 2004; Zhang et al., 2005; De Lima et al., 2010; Tian et al., 2011; Maragatham, 2012). The first group defines absolute thresholds and enumerates the number of days exceeding a certain absolute precipitation value, whereas the second group is based on

percentile thresholds. The number of days exceeding a certain percentile threshold (representing the frequency of threshold crossing) is fixed for the World Meteorological Organization (WMO) base period (1961-1990). The specific indices used for this study are shown in Table 3.1. The details of the index definitions and calculations are described in Klein Tank et al. (2009). The extreme precipitation indices were calculated by using RCLimDex (Zhang and Yang, 2004) software package in the R environment (R Foundation for Statistical Computing, Vienna, 2011).

Table 3-1. Definition of the extreme indices for precipitation (P)

Indices	Indicator description (units)
Px1	Monthly maximum 1-day precipitation (mm)
Px5	Monthly maximum consecutive 5-day precipitation (mm)
Ptot	Annual total precipitation in wet days $P \geq 1$ mm (mm)
SDII	Average daily precipitation amount on wet days (mm/day)
P10 mm	Annual count of days when $P \geq 10$ mm (days)
P20 mm	Annual count of days when $P \geq 20$ mm (days)
P30 mm	Annual count of days when $P \geq 30$ mm (days)
CWD	Maximum number of consecutive wet days with $P \geq 1$ mm (days)
P95Ptot	Annual total P (between 1961 and 2014) when $P >$ 95th percentile of precipitation for the 1961-1990 period (%)
P99Ptot	Annual total P (between 1961 and 2014) when $P >$ 99th percentile of precipitation for the 1961-1990 period (%)

3.2.3. Statistical analysis

This study investigated long-term time series data (period I: from year 1961 to 2014):

$$\bar{X}_k = x_i, x_{i+1}, \dots, x_p \quad (3.1)$$

where $i = 1961$, $p = 2014$, and $k=1, 2, \dots, 231$.

The time series of extreme values for each station (X_k) was divided into two multi-decadal periods as follows:

$$\bar{X}_{k,A} = x_i, x_{i+1}, \dots, x_m \quad \text{and} \quad \bar{X}_{k,B} = x_{m+1}, x_{m+2}, \dots, x_p \quad (3.2)$$

where $m = \left(\frac{p+i}{2}\right)$, and the two multi-decadal periods in this study are defined as period II (from 1961 to 1987) and period III (from 1988 to 2014). The calculated value for m is rounded down to the nearest integer (i.e. 1987.5 rounded down to 1987).

The time series anomalies (D_{ki}) are calculated by considering the climatological average (\bar{X}_k) relative to the WMO base period (1961-1990) ($\bar{X}_{k,WMO}$) for each station (k) as follows:

$$\bar{X}_k = \frac{\sum_{i=1961}^{2014} (x_i)}{54} \quad , \quad \bar{X}_{k,WMO} = \frac{\sum_{i=1961}^{1990} (x_i)}{30} \quad (3.3)$$

$$D_{ki} = \left(\frac{x_i - \bar{x}_{k,WMO}}{\bar{x}_k} \right) * 100 \quad (3.4)$$

where x_i is defined as in Equation (1) and PD_{ki} is the percentage anomaly for each station (k) and year (1961 ≤ i ≤ 2014). The overall percentage anomaly (PD_i) over the country (i.e. 231 stations) for each year i is defined as follows:

$$PD_i = \frac{\sum_{k=1}^{231} D_{ki}}{231} \quad (3.5)$$

The variation in precipitation could be observed visually or investigated using statistical methods (i.e. the hypothesis test). A broad range of parametric and non-parametric methods have been used to investigate trends in extreme precipitation in previous studies (Arnbjerg-Nielsen et al., 2013). In this study, the variations in precipitation observations were investigated using the Mann-Kendall test (Kendall, 1948; Mann, 1945) because of the non-Gaussian distributions of the observations.

In the Mann–Kendall test, the null and alternate hypotheses (H0 and H1) of the trend test are that no trend exists and that a monotonic trend exists in the time series, respectively. The Mann-Kendall statistical test is expressed as follows:

$$S = \sum_{i=1961}^{p-1} \sum_{j=i+1}^p \text{sgn}(X_j - X_i) \quad (3.6)$$

where X_j and X_i are sequential data. The term $\text{sgn}(X_j - X_i)$ is defined as follows:

$$\text{sgn}(X_j - X_i) = \begin{cases} +1 & \text{if } (X_j - X_i) > 0 \\ 0 & \text{if } (X_j - X_i) = 0 \\ -1 & \text{if } (X_j - X_i) < 0 \end{cases} \quad (3.7)$$

When $n \geq 8$, the mean of S ($E(s) = 0$) and variance is normally distributed:

$$\text{VAR}(S) = \frac{1}{18} [n(n-1)(2n+5) - \sum_{q=1}^n t_q(t_q-1)(2t_q+5)] \quad (3.8)$$

Where n is the length of the time series and t_q is the number of occurrences of the qth value, ($q=1, 2, \dots, 54$). The normalized statistic test Z_S can be expressed as follows:

$$Z_S = \begin{cases} \frac{S-1}{\sqrt{\text{VAR}(S)}} & \text{if } S > 0 \\ 0 & \text{if } S = 0 \\ \frac{S+1}{\sqrt{\text{VAR}(S)}} & \text{if } S < 0 \end{cases} \quad (3.9)$$

In a two-tailed test, when $|Z_S| > Z_{1-\alpha/2}$, the H0 hypothesis (no trend) can be rejected because the $|Z_S|$ value is larger than the critical value at the chosen significance level of the test (for this study $\alpha=0.05$ and $Z_{1-\alpha/2}=\pm 1.96$).

The strength of the trend was calculated based on the Theil–Sen's slope (Theil, 1950; Sen, 1968), which is known as a nonparametric linear regression slope (β). This method calculates the overall slope using the

median of the slopes of all the pairs of sequential data (X_j and X_i). The nonparametric estimate is expressed as following:

$$\beta = \text{Median} \left[\frac{X_j - X_i}{j - i} \right] \quad \text{for all } j > i \quad (3.10)$$

The autocorrelation in time series can affect the result of the Mann–Kendall test (von Storch, 1995). The Yue et al. (2002) approach (FTPW) proposed a modified pre-whitening for the Mann–Kendall trend to reduce effectively the impact of autocorrelation. In the FTPW approach, if the slope (estimated with the Theil–Sen’s slope) differs from 0, the data are detrended by the slope as follows:

$$X_{\text{detrend}_n} = X_{\text{original}_n} - \beta \cdot n \quad (3.11)$$

where X_{original_n} and X_{detrend_n} are the original and detrended time series at time n , respectively. Subsequently, the noise from the detrended time series is removed by a lag 1 autoregressive (AR (1)) coefficient:

$$X'_{\text{detrend}_n} = X_{\text{detrend}_n} - r_1 \cdot X_{\text{detrend}_{n-1}} \quad (3.12)$$

where X'_{detrend_n} is the residual and r_1 is the autocorrelation coefficient. The trend is then added back to the time series values. The X''_{detrend_n} demonstrates the linear trend without the autocorrelation noise.

$$X''_{\text{detrend}_n} = X'_{\text{detrend}_n} + \beta \cdot n \quad (3.13)$$

Finally, the Mann-Kendall test is applied to the adjusted time series to measure the significance of the trend (Yue et al., 2003).

The magnitude of daily precipitation varies from one station to another. Therefore, the temporal variability of spatial averages of Px1 may be dominated by the stations with large Px1 variations. To reduce this effect we used the standardized data for Px1 at each station by transforming the data to the probability-based index (PI). To detect the monthly maximum daily precipitation (Px1) differences between urban and rural areas, the observed values are normalized to the PI index between zero to one by the fitting of a generalized extreme value (GEV) (Min et al., 2009). The study assumes that the Px1 for an individual month follows the GEV distribution function as follows:

$$PI = F(P_i; \mu, \sigma, \varepsilon) \quad (3.14)$$

$$F(x; \mu, \sigma, \varepsilon) = \begin{cases} \exp\left(-\left[1 + \varepsilon \frac{x - \mu}{\sigma}\right]^{-\frac{1}{\varepsilon}}\right), & \& \varepsilon \neq 0 \\ \exp\left(-\exp\left(-\frac{x - \mu}{\sigma}\right)\right), & \& \varepsilon = 0 \end{cases} \quad \begin{cases} \mu \in \mathbb{R} \\ \sigma > 0 \\ \varepsilon \in \mathbb{R} \end{cases} \quad (3.15)$$

where the monthly maximum precipitation in year i (P_i) is defined by location (μ), scale (σ) and shape parameters (ε). The GEV parameters were estimated via the maximum likelihood estimation (Jenkinson, 1955) and bootstrap method (104 replicate sample sizes).

3.2.4. Classification of station types

A clear, unified definition is not available for determining the land use extents. Specifically, for mapping the urban extent, different approaches are available based on population density, satellite images and other maps (Schneider et al., 2009). Different datasets can lead to different boundaries between urban and rural areas, resulting in different station classifications. Therefore, we used the Co-ORdination of INformation on the Environment (CORINE) database, which was used in the previous studies of Chrysanthou et al. (2014) and Daniels et al. (2014) to distinguish between urban and rural areas in the Netherlands. In this study, the CORINE land cover at 100*100-m resolution for the year 2012 (EEA, 2014) was applied to classify the stations into urban and rural subsets. The urban extent was defined by six land cover categories, i.e. i) discontinuous urban fabric; ii) industrial or commercial units and public facilities; iii) road and rail networks and associated land; iv) port areas and airports; v) mineral extraction sites, dump sites, and construction sites; and vi) green urban areas and sport and leisure facilities. Suomi et al. (2012) concluded the footprint of the urban heat island (UHI) effect is approximately 5 km. Therefore, the area within a 5 km radius of the rain gauge stations was extracted to identify the land cover types. The stations where the six urban land cover categories represented more than a quarter of the surrounding area were classified as urban stations, and the others were defined as rural stations (Daniels et al., 2014). The urban and rural station subsets were created via spatial gridding, which is also employed in climate monitoring by NOAA/NCDC (Hausfather et al., 2013).

Table 3-2. Number of stations in the urban and rural subsets in different regions. The annual maxima of daily precipitation (mm) averaged for the urban and rural stations in each region during the 54-year period (I) and two multi-decadal periods (II and III) are also listed.

Region	Dominant soil types	subset	Number of stations	I (mm)	II (mm)	III (mm)	Mean Population	Mean Elevation (m)
A	Clay and peat	Urban	15	36.3	34.2	38.5	127710	0
		Rural	46	35.3	32.8	37.8	17059	1
B	Clay	Urban	5	35.6	34.4	36.1	102672	0
		Rural	46	34.5	32.6	36.3	39349	1
C	Sand and loam	Urban	10	35	32.8	37.4	57900	10
		Rural	62	34.7	33.1	36.2	27342	9
D	Sand	Urban	12	33.3	32.2	34.4	75205	38
		Rural	35	34.4	32.9	35.8	22797	35
Countrywide		Urban	42	35	33.3	36.7	93106	13
		Rural	189	34.7	32.9	36.5	26920	10

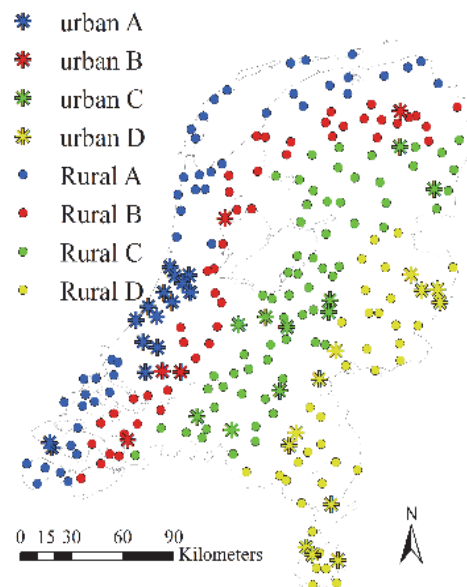


Figure 3.1. Distribution of urban (asterisk) and rural (circles) stations in the Netherlands. The regions A, B, C and D are represented by symbols coloured blue, red, green, and yellow, respectively.

Daniels et al. (2014) found that the distance from the coast had a greater effect on precipitation changes than did other surface characteristics in the Netherlands. They concluded that the SST influence on extreme summer precipitation in the Netherlands is confined to within 25 km of the coast. Lenderink et al. (2009) showed that SSTs have a strong influence on regions within 50 km of the coast. To account for the effect of distance from the coast on precipitation, four regions were classified to investigate the differences among the subsets of urban and rural stations. The stations were considered in four regions: A, B, C, and D, which are located 0-25 km, 25-50 km, 50-100 km, and 100-200 km from the coast, respectively (Daniels et al., 2014). Each defined region contained a sizeable fraction (between 20% and 30%) of the total stations in the Netherlands. Accordingly, the four regions were used to classify the individual urban and rural station subsets for each region (Table 3.2). Figure 3.1 shows the distributions of urban and rural stations with respect to the defined regions.

As shown in Table 3.2, the mean elevations of the rain gauges in the defined urban and rural subsets are similar. Therefore, similar topographic effects on precipitation are expected for the urban and rural subsets in a given region.

The population of each subset was averaged based on the extracted population within 5 km of each station on 1 January 2015 (available at the Dutch national statistical institution website) (CBS, 2015). The average population in the vicinity of the urban stations in region A is greater than those of the other regions. Moreover, the largest difference in the average population between the urban and rural stations exists in regions A and B in the western Netherlands.

3.3. Results

In this section, the results of the analysis of the extreme precipitation indices across the Netherlands are presented, and the 1-day maximum precipitation values (Px1) in different individual months are investigated. The influence of urban land use on extreme precipitation is assessed based on the results for extreme indices and the categorised stations across the country. The regional features of urban land use effects on extreme precipitation were assessed via the analysis of urban-impacted Px1 in the four defined regions (section 3.3).

3.3.1. Changes in extreme precipitation indices

The results in Figure 3.2 show that almost all of the indices have increased throughout the Netherlands during the last 54 years and the recent multi-decadal period (except for CWD). The changes in the indices in period II (i.e. from 1961 to 1987) were smaller than those in period III (i.e. from 1988 to 2014), indicating that most of the index changes occurred during the recent multi-decadal period.

Figure 3.2 presents the spatial pattern of the index changes between the two multi-decadal averages (e.g. Period III – Period II) over the Netherlands. Figures 3.2(a) and 3.2(b) show the changes in the monthly maxima of 1-day and 5-day precipitation (Px1 and Px5), respectively, thereby illustrating the variations in extreme precipitation. The Px1 changes are positive in the recent multi-decadal period (period III) throughout the Netherlands except in the southeast of the country. The Px5 changes are positive for most stations, especially in the east of the country.

Buishand et al. (2013) claimed that the mean annual rainfall amount on the western side of the Netherlands increased over the last century. The overall increase in the Ptot data (Figure 3.2(c)) confirms this result, and positive changes have been observed, especially for stations in the western part of the country. Moreover, in Figure 3.2(d), the simple precipitation intensity index (SDII) shows positive changes for a large part of the country in the recent multi-decadal period. The long tail of the frequency distribution of extreme precipitation may be strongly affected by a slight increase in the average (Groisman et al., 1999). Therefore, the positive changes in the total

annual precipitation are associated with an upward slope for changes in heavy precipitation events (such as the P10 mm, P20 mm and P30 mm indices). The changes in heavy precipitation events between the two multi-decadal averages are mostly positive throughout the country (Figures 3.2(e-g)).

Significant changes are not observed in the consecutive wet day indices (i.e. CWD) across the Netherlands (Figure 3.2(h)). The CWD shows positive changes clearly larger in the western and southwestern regions than the rest of the country. P95Ptot and P99Ptot represent the 95th and 99th percentiles of wet days, respectively.

Figures 3.2(i) and 3.2(j) demonstrate the changes between two multi-decadal averages in percentile exceedance for the very wet days (P95Ptot) and extremely wet days (P99Ptot). These indices show that the increasing change in extreme precipitation is more rapid and disproportionate compared with that of the annual total precipitation across the Netherlands.

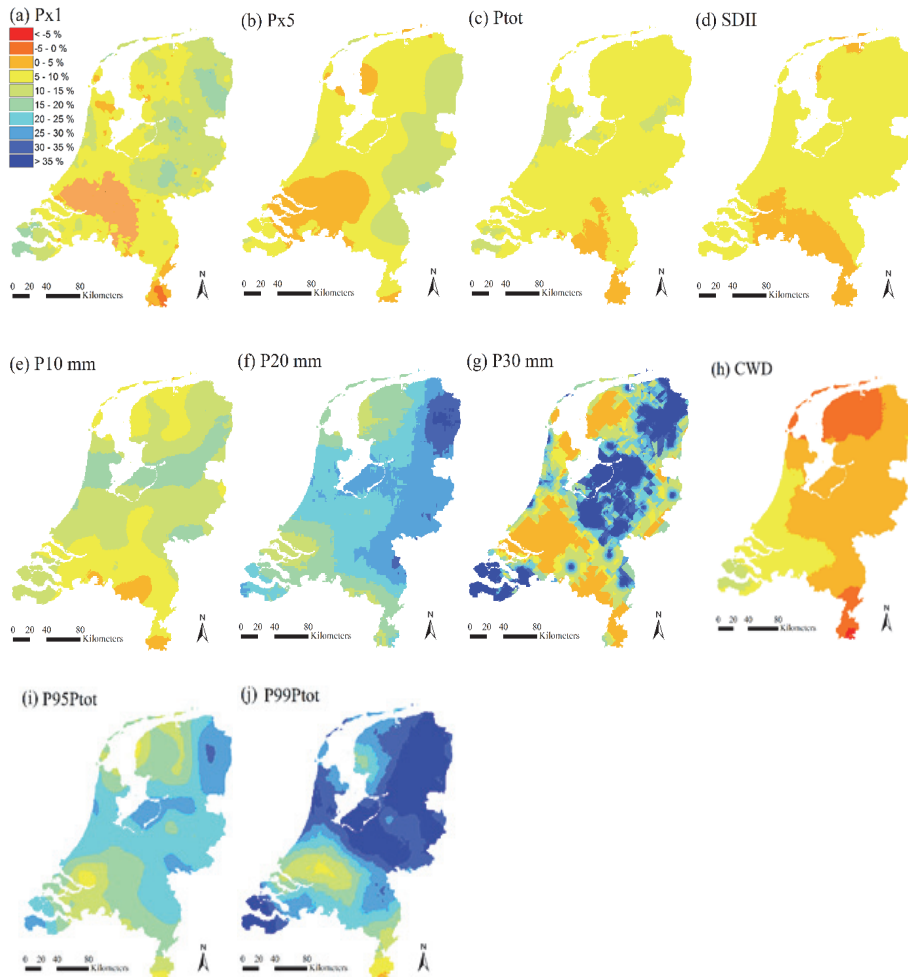


Figure 3.2 Spatial distributions of extreme precipitation changes (%) during two multi-decadal periods from 1961 to 2014. The ordinary Kriging interpolated changes for the indices are shown. The maps from top to bottom, right to left (a-j) represent Px1, Px5, Ptot, SDII, P10 mm, P20 mm, P30 mm, CWD, P95Ptot, and P99Ptot, respectively.

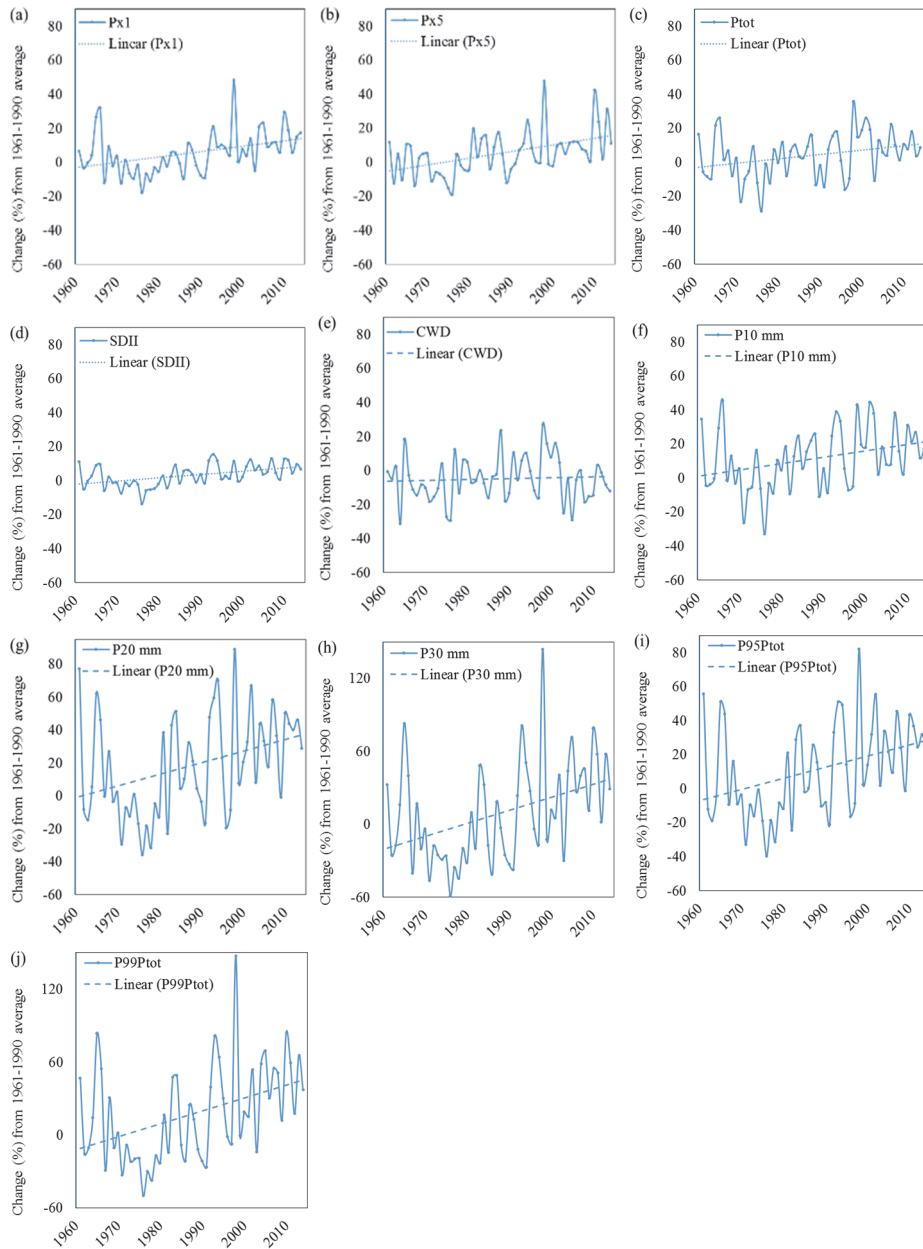


Figure 3.3 The panels from (a) to (j) show the analysis of time series of extreme indices during two multi-decadal periods over the last 54 years for Px1, Px5, Ptot, SDII, CWD, P10 mm, P20 mm, P30 mm, P95Ptot, and P99Ptot respectively. The solid and dotted lines show the indices and the least square fit weighted by linear regression analysis for 1961-2014. The difference between the average of each extreme index from 1961 to 2014 and the average from 1961 to 1990 supports the pattern of index changes shown in Figure 3.2.

In addition to the estimated changes in the indices between the averages of the two multi-decadal periods, the data were assessed to identify long-term changes in recent years in the Netherlands. The index time series were averaged spatially over all stations in order to calculate the differences between each year of the index time series and the WMO base period (1961-1990). Figure 3.3 shows the result of this analysis for each index. Most of the plots related to extreme precipitation show positive, statistically significant annual changes. The observed changes in the wet indices (P10 mm, P20 mm, P30 mm, P95Ptot and P95Ptot) represent significant positive trends, resulting in larger annual values.

3.3.2. Assessing the monthly maxima of daily precipitation

The maximum daily precipitation (Px1) index is the most widely used extreme precipitation index for hydrological applications. The analysis of Px1 could provide a better understanding of the impacts of extreme precipitation on human life, infrastructure, agriculture, and socioeconomic systems (Nicholls and Alexander, 2007; Min et al., 2011). In the following, the Px1 index, which was considered to be representative of the extreme precipitation indices, was used to assess the extreme precipitation variations for individual months (from January to December).

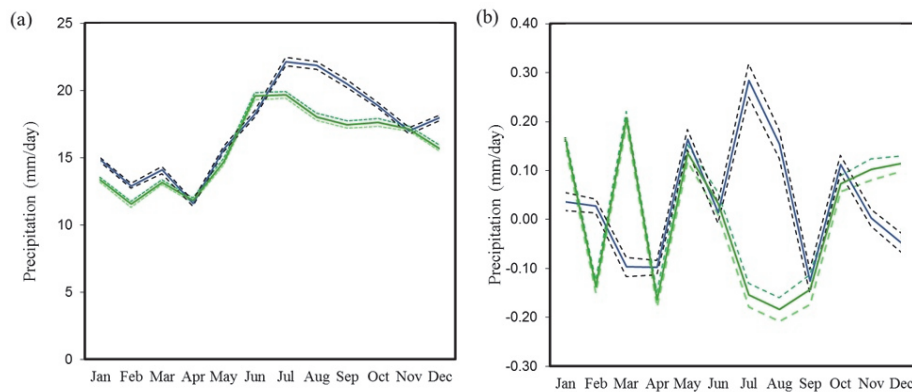


Figure 3.4. Px1 monthly variation for amount (a) and trend (b) during the period II (green line) and period III (blue line) in 95% confidence intervals (dashed lines).

The rain gauge data were separated into monthly blocks of data, and the maximum daily precipitation values and the associated trend were determined for each block. The Px1 amount for the periods III and II and the trends are shown in Figure 3.4. It shows that the monthly Px1 amounts are greater in period III than in period II. The presented differences between periods III and II based on Px1 (hereafter as $\Delta_{III-IIPx1}$) indicate that the largest monthly $\Delta_{III-IIPx1}$ amounts occur in July and August. Moreover, the smallest (negative) $\Delta_{III-IIPx1}$ amounts occur in June. For the trend, the

smallest difference (negative) occurs in March, and the largest $\Delta III-IIPx1$ trends occur in July and August. The $\Delta III-IIPx1$ trends have increased more in the summer half-year (May-October) than in the winter half-year (November-April).

3.3.3. Impact of urban land uses on extreme precipitation

This section investigates the extreme indices for the urban areas in the Netherlands with respect to the defined regions (i.e. regions A, B, C and D). This investigation is then followed by a detailed analysis of the effects of urban land use on the $Px1$ index on a monthly basis. Then, the regional features of the differences in the $Px1$ index between the urban and rural areas are investigated.

3.3.4. Overall features of Urban-Impacted Extreme Indices

The slopes of indices changes relative to the 1960-1990 average were estimated for the urban and rural stations between 1961 and 2014 throughout the Netherlands (Figure 3.5). The stations across the country were divided into two groups, urban stations and rural stations (see section 2.3). The investigated indices exhibited positive trends with respect to the 1961-1990 average at the urban and rural stations during period I. The pattern of index changes for the urban stations was similar to that for the rural stations. The positive changes in the extreme indices of the urban stations are relatively higher than those of the rural stations throughout 54-year period. In Figure 3.5, the overall slopes of the index changes with respect to the 1961-1990 average were steeper for the urban stations than for the rural stations during the recent multi-decadal period.

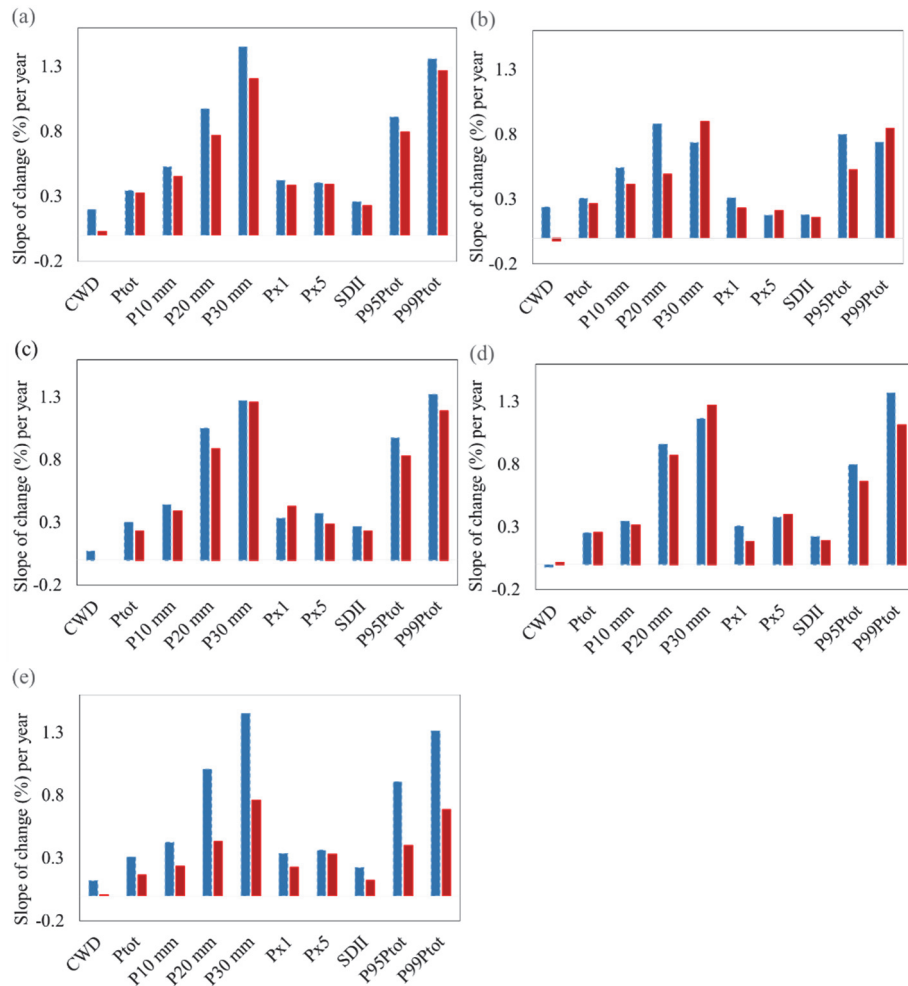


Figure 3.5. The slope of extreme precipitation index changes from the 1961-1990 average across the regions A to D (from (a) to (d)) and whole country (e) for urban (blue filled columns) and rural (red filled columns) stations. The slopes were calculated using the Theil-Sen’s slope, and the statistical significance was estimated by the Mann-Kendall test. The estimated changes are statistically significant at $\alpha=0.05$ for all indices with some exception (CWD for all regions, P20 mm for rural in region B, Px1 for rural in region B and D, Px5 in urban region B).

3.3.5. Monthly Features of Urban-Impacted Px1

The results in Figure 3.6 show that the regions A and B show similar patterns of Px1 variations and exhibit relatively high values in August. In contrast, the Px1 values are higher in June and July in the regions C and D. The Px1 mean for region A is slightly higher in the urban areas than in the rural areas between 1961 and 2014. These differences in Figure 3.6 are easier to

distinguish for regions A and B due to the greater variation rather than the rest regions. Between August and November, the Px1 values are higher in the urban areas in region A than in other regions. The Px1 values are also higher in the urban areas than in the rural areas in region B between July and November. The urban Px1 is higher than the rural one in region C for all months but July, and in region D for 7 months other than January, March, May, July, and December.

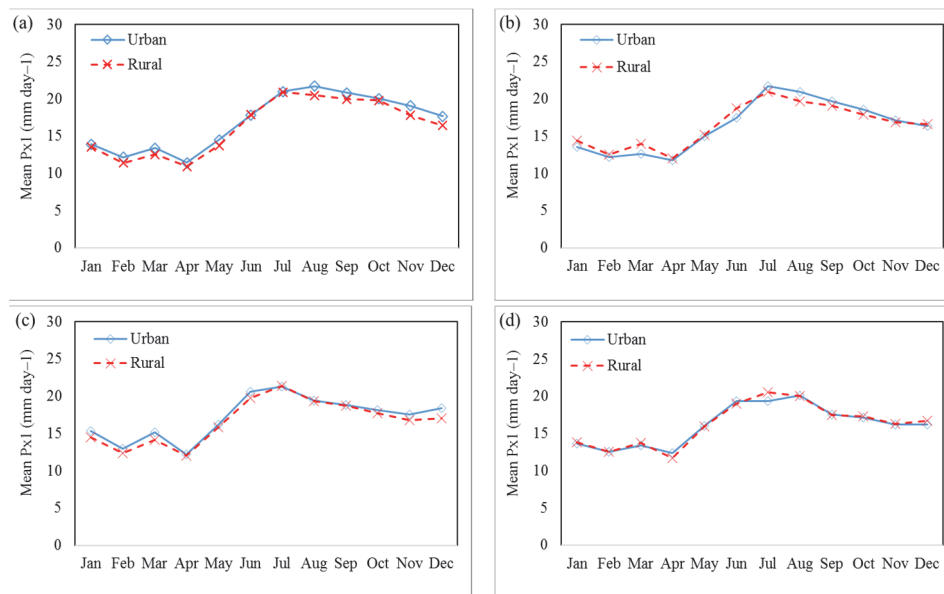


Figure 3.6. Panels (a-d) show the mean of Px1 amounts (mm) for the urban stations (blue line) and rural stations (dashed line) across the regions (A, B, C, and D) between 1961 and 2014.

The Px1 index trends were further analysed across the urban and rural areas in the Netherlands for the individual months. Owing to the uncertain estimated means of the monthly Px1 time series and the inhomogeneity in the Px1 time series for the urban and rural areas, the values of the monthly Px1 index from each station are standardized before estimating the urban and rural averages (Min et al., 2011). The standardized monthly maximum precipitation (PI) values were spatially averaged for the urban and rural areas in each region. The trend in the PI changes relative to the WMO base period (1961-1990) mean was estimated for each month over the 54-year time series (Figure 3.7).

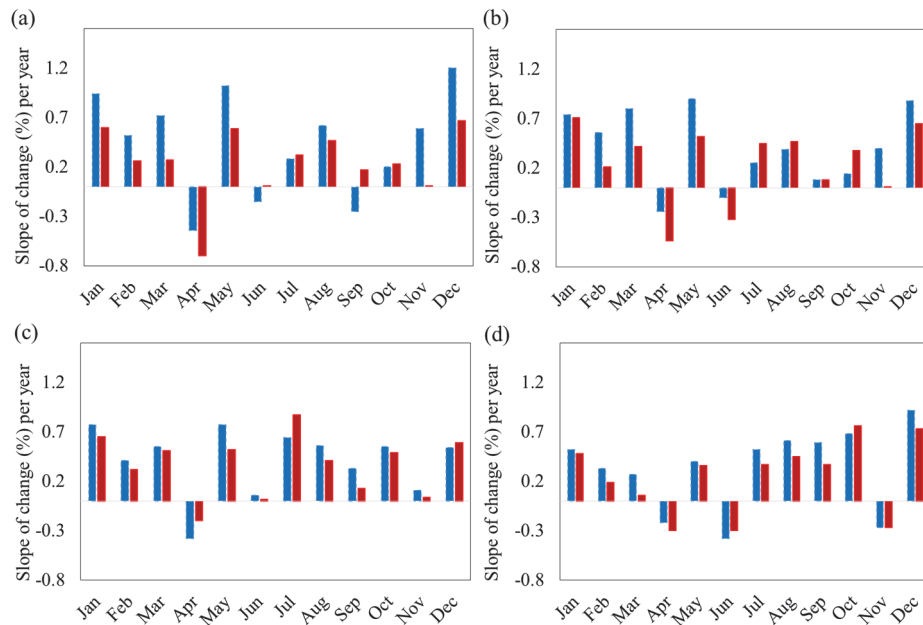


Figure 3.7. The slope of PI changes relative to the 1961-1990 average for the urban (blue filled columns) and rural (red filled columns) stations in different regions (A, B, C, and D) between 1961-2014. The slopes were calculated using the Theil–Sen’s slope.

All regions are characterized by overall greater trends for urban areas than for rural areas, although there are some exceptions depending on the selected region and month. The estimated trends in the urban areas exhibit larger increases than do those in the rural areas during the recent multi-decadal period.

3.4. Discussion

3.4.1. Extreme precipitation indices

This study investigates extreme precipitation events in the Netherlands over the past 54 years using extreme precipitation indices. The trends in these indices over the 54-year period are not significant for all the stations throughout the country. However, certain indices show statistically significant changes in local areas where heavy precipitation amounts and intensity have increased over the past 54 years. All of the extreme precipitation indices indicate that conditions became wetter in the Netherlands from 1961 to 2014, especially during the recent years. The changes in indices are probably related to the changes in the atmospheric circulation (such as NAO) and the sea surface temperature (van Haren et al., 2013). In addition, urban land use can lead to greater precipitation (Daniels et al., 2015).

3.4.2. Index changes in recent decades

The calculated changes in the indices during the two multi-decadal periods (i.e. III and II) can be used to investigate coherent changes in extreme precipitation. The comparison of the two periods shows that the recent multi-decadal period generally has relatively stronger trends and larger values than the earlier period. A prevailing pattern of significant positive changes in the indices is present in the recent multi-decadal period in the Netherlands (Figure 3.3).

Among the indices, Px1 was used to analyse the details of the extreme precipitation changes in each month (Figure 3.4). The Px1 values revealed that a greater number of extreme precipitation events occurred in period III than in period II. Additionally, extreme precipitation events in the Netherlands occurred most frequently in the summer half-year (especially July and August) during the recent multi-decadal period (period III). The monthly Px1 amounts and trends increased more dramatically over the recent multi-decadal period than over the previous one. Therefore, period II was relatively dry, whereas period III was relatively wet. In other words, the observed discrepancy between the two multi-decadal periods in this study could be driven by the available low frequency of extreme precipitation in Europe from 1970-1980 and the high frequency of extreme precipitation from 1990-2000 (P. Willems, 2013).

The estimated trend during period III are larger than that in period II in particular for the summer half-year. Similar decadal changes in the Netherlands have been studied by Lenderink et al. (2009). Their results showed that the precipitation trends have been closely related to SSTs since the 1950s. As a natural source of variability, atmospheric circulation could influence the decadal precipitation patterns. Therefore, the greater increase in index trends during period III may be due to variations in atmospheric circulation. The link between cyclonic westerly circulation and precipitation found by Attema and Lenderink (2014) represents a possible physical mechanism for the mentioned periods (August to November). The smaller change in monthly Px1 in the winter half-year during the recent multi-decadal period (III), relative to the previous one (II) may be related to the effects of NAO. The NAO index increased notably before the early 1990s and decreased strongly in recent decades.

3.4.3. Urban-impacted indices

The well-known causes behind the precipitation changes and possible physical mechanisms (such as circulation, sea and land surface temperatures) were investigated in previous studies (such as Attema et al., 2014; Daniels et al., 2014). In this study, the effects of different land use types on the variability of the indices are quantified based on the differences between the urban and rural areas in the Netherlands according to the CORINE land cover classification. More specifically, Daniels et al. (2014) found that precipitation changes are more greatly affected by the distance from the coast than by other surface characteristics in the Netherlands. To separate this “distance from the coast” effect from the investigation of the impact of urban land use on extreme precipitation, the urban and rural stations were divided into the four regions in terms of their location and distance from the coast. Consequently, the urban and rural areas in each region are affected by approximately similar external influences (such as the NAO (Hurrell, 1995), SSTs (Lenderink et al., 2009), and circulation variability (van Haren et al., 2013)). The changes in the trends of the extreme precipitation indices relative to the 1961-1990 average are larger in the urban areas than in the rural areas over the last 54 years (see section 3.3). The four defined regions were used to disentangle the coast-inland precipitation gradient from the differences in urban and rural stations. The results demonstrate that the urban influence might have contributed to the observed increase in extreme precipitation. The larger significant changes in most indices and the larger monthly Px1 amounts in the urban areas relative to the rural areas in the same regions can be attributed to the urban impacts on precipitation.

Urban area development occurred in the Netherlands during the recent multi-decadal period (Feranec et al., 2007), and Hazeu and Wit (2004) detected a 4.76% change in the land surface between 1986 and 2000. Additionally, Daniels et al. (2015) found that the urban land use along the west coast of the Netherlands increased from 14% in 1960 to 33% in 2010. This increase in urban land use might have contributed to influences on the local climate. The patterns of index changes in the urban and rural areas differ among the four investigated regions. In the populated western part of the Netherlands, the urban areas were found to have received more intense extreme precipitation than the rural areas. The areas with the largest populations lie along the western coast of the Netherlands (CBS, 2015). This part of the country (region A) exhibits a large discrepancy between the index changes in urban areas and those in rural areas.

This discrepancy between urban and rural areas highlights the influence of urban areas on the extreme precipitation. Previous studies also observed

urban influences on the atmosphere and local climate, such as temperature (Brandsma and Wolters, 2012) and precipitation (Daniels et al., 2015, 2016), in the Netherlands. Therefore, in addition to other external factors, the land use type should be treated as an external signal that affects extreme precipitation patterns. Future work using high spatial and temporal resolution data could be performed to determine the urban influences on extreme precipitation and the possible physical mechanisms associated with this process.

3.5. Conclusions

The extreme precipitation analysis shows that frequency and magnitude of extreme events significantly increased in certain parts of the country, especially in the western urbanised areas of the country. This study shows that the slopes of the index changes relative to the 1961-1990 average in the Netherlands were positive. For both urban and rural areas, the indices follow the same pattern of changes during the two multi-decadal periods. However, the indices in the urban areas have changed to a greater degree than have those in the rural areas during the recent multi-decadal period. The monthly maxima of daily precipitation indicate that the greatest increases occurred in August. The monthly Px1 events increased more during the recent multi-decadal period than during the earlier one for the entire country. In addition, the differences in the monthly Px1 amounts and trends between the two multi-decadal periods are higher in the late summer and autumn.

Overall, larger trends are present in the extreme precipitation indices in urban areas than in those in rural areas. The monthly maxima of daily precipitation were greater in the urban areas than in the rural areas in the Netherlands. This study investigated the impacts of urban land use on Px1 in terms of different regions. The extreme precipitation differences between the urban and rural areas were persistent but varied from region to region. In all the regions, the urban areas received more intense extreme precipitation than did the rural areas, but the observed discrepancy was rarely significant and depended on the region. The Px1 data indicate that a relatively larger discrepancy between urban and rural areas was present in the western densely urbanised region relative to the other regions. The patterns and changes in extreme precipitation, which are strongly dependent on the selected periods and regions, were clearly affected by urban land use in the Netherlands.

Chapter 4

Urban impacts on air temperature and precipitation over The Netherlands ³

³ This chapter has been published as:
Rahimpour, V., Zeng, Y., Mannaerts, C.M., Su, Z., 2018. Urban impact on air temperature and precipitation over the Netherlands, *Clim. Res.* 75, 95–109.
doi:<https://doi.org/10.3354/cr01512>

ABSTRACT

The detection of changes in the weather of urban areas is an important issue for understanding the impact of weather on human lives. Five years of basic weather observations (2011–2015) from automatic and amateur networks across The Netherlands were used to investigate the urban effects on meteorological parameters with a focus on temperature (e.g. urban heat island [UHI]) and precipitation. Representative stations were selected based on metadata and a set of criteria for data quality control. An hourly analysis indicates that UHIs are a nocturnal phenomenon in The Netherlands and are more prominent after sunset, when they exceed 2°C. A seasonal analysis shows that UHIs occur in all seasons during the year, with the most significant UHI occurring in the summer. Furthermore, the differences in the precipitation of urban and rural areas were shown to be greatest after sunrise during the day. The maximum hourly UHI and hourly precipitation distributions were analyzed using a generalized extreme value model. The occurrences of maximum precipitation are likely to be more frequent at urban stations than at the nearby rural stations. Additionally, the distinct seasonal cycle of precipitation that is dependent on the UHI demonstrates that the maximum UHI and precipitation occurred in the summer. Our results indicate that the UHI and precipitation enhancements in Dutch urban residential areas, as obtained from the data of weather amateurs, are in agreement with the results presented in the literature, and that 7% more precipitation occurs in cities than in rural areas.

4.1. Introduction

Urbanization is increasing dramatically and, consequently, the surface characteristics and local climates of urban areas will be considerably affected (Han et al., 2014). Urbanization modifies the radiation, thermal and dynamic characteristics of the underlying surface and makes the land cover in urban areas quite different from that of the surrounding areas. These differences caused a horizontal gradient of energy and moisture in the surrounding environment, impacting the boundary layer characteristics as well as the heat and water exchanges between the land surface and atmosphere, which may lead to alterations of temperature and precipitation patterns (Mills, 2014; Sailor, 2011).

The physical properties of city buildings are known to modify the energy budget and the exchanges of fluxes between the land surface and atmosphere (e.g. heat, water, and momentum between the land surface and overlying atmosphere), which cause alterations of the atmospheric composition and meteorology over urban areas (Kaufmann et al., 2007; Lin and Chen, 2011; Pall et al., 2007; Peterson, 2003; Stone et al., 2012; Trusilova et al., 2008; Zhang et al., 2009).

Studies over the past decades have focused on the urban surface energy balance and urban heat island (UHI). UHI can be generated by changes in the climate system due to land-use changes associated with urbanization (Oke, 1982). These changes could be induced by well-known factors, such as urban geometry, air pollution, anthropogenic heat or impervious surfaces (Ryu and Baik, 2012). Building densities and reduced vegetation inhibit urban albedo and enhance the heat stored in urban areas (Erell et al., 2011). The UHI effects on mesoscale circulation can be observed in convective precipitation (Shepherd, 2005). In the past decade, numerous studies have reported that urban morphological parameters can considerably influence precipitation variability (Chen et al., 2015; Hu et al., 2012; Ikebuchi et al., 2007; Niyogi et al., 2011; Shem and Shepherd, 2009; P. Willems et al., 2012). The possible mechanism leading to the discrepancy in the precipitation of urban areas and that of their surrounding areas has been discussed by Shepherd (2005) as being i) an increased convergence due to extended surface roughness, ii) destabilization caused by UHI perturbations of the planetary boundary layer, or iii) enhanced aerosols in an urban environment for cloud condensation nuclei sources.

The Netherlands can be defined as the urbanized area (comprising mid-sized cities with less than 10 km radii) inside the Meuse and Rhine river delta, with many sections situated below sea level (Steeneveld et al., 2011). Despite the vast number of international reports on urban climates, particular outcomes

cannot be clearly extrapolated to the Dutch circumstances. The existing studies (e.g. the UHI and their effects on rainfall intensities at the local level, especially in the coming years) are not reliable enough to serve as indicators of UHI and extreme rainfall events for many of the cities in the Netherlands (Schlünzen et al., 2010; Van Hove et al., 2011). The variations of climatic conditions, air quality, urban landscapes and geometries, and building types and components render such extrapolations challenging. It becomes imperative to understand the interactions between Dutch urbanization and meteorological observations, especially those of extreme weather conditions that could threaten citizens and vital infrastructures (Rovers et al., 2014). Very few studies have delineated the Dutch urbanization effects on the relationship between temperature and precipitation (e.g. Brandsma et al., 2003; Haines et al., 2006,).

Approximately 90% of the Dutch population in 2014 were concentrated in urban regions with at least 90,000 inhabitants (*World Urbanization Prospects The 2014 Revision*, n.d.). The urbanization and population average growth rates (0.77% and 1.05%, respectively) between 2010 and 2015 indicate a fairly rapid urbanization in the Netherlands (*World Urbanization Prospects The 2014 Revision*, n.d.). Although there has been a continuous urbanization in the Netherlands (Daniels et al., 2015b; Hazeu et al., 2011), long-term meteorological observations are scarce for Dutch cities (for more details, see Van Hove et al. (2011)). The study presented here attempts to investigate the temperature and precipitation variations using citizen's personal amateur weather stations (PWS) to understand the urban environments of a number of Dutch cities (Jiang et al., 2016). The lack of long-term urban meteorological data in Dutch cities motivates the use of observations from PWS. Observations from PWS in the Netherlands have previously been used by Steeneveld et al. (2011) and (Wolters and Brandsma, (2012). These studies investigated the UHI effects on human comfort and factors influencing UHIs, whereas the present study concentrates more on urban-rural temperature and precipitation differences and on the urbanization effects on the relationship of temperature and precipitation. In contrast to the aforementioned studies, the urbanization effects in this study mainly focus on the hourly UHI and precipitation values of a 5-year period (2011-2015). The temperature and precipitation hourly data on local time (LT) obtained by averaging available sub-hourly values for temperature and accumulated precipitation amount for each hour, respectively. The most populated areas in the western and northern regions of the Netherlands (approximately 60 km from the North Sea) were considered in this study (Rahimpour et al., 2017). A dedicated process based on the city size and data availability (section 2) was used to select the stations.

This study quantifies the gradients of meteorological variables between the urban and surrounding rural areas. The records from PWS were used, and the data were investigated separately for days and nights. The generalized extreme value (GEV) approach and bootstrap method were used to determine the distributions of the maximum hourly UHI and precipitation in the cities for 2011-2015. This study is divided into 5 sections. Section 2 introduces the data and methods. Section 3 presents the analysis results of the UHI, their relation with population densities and the GEV parameter distribution of maximum UHI and precipitation. The findings are discussed in section 4, and the study is augmented by the conclusions in section 5.

4.2. Data and Methods

A large number of automatic weather stations (AWS) that are in accordance with the WMO standards exist in the Netherlands (every 1000 km²) have been installed in very open areas without any obstacles around the temperature and precipitation instruments (Wolters and Brandsma, 2012). Due to their nature, AWSs stations are mainly located in rural areas. In the absence of WMO stations in Dutch cities, amateur weather stations (PWS) were studied for their use as urban stations. The rural stations (AWSs) were selected based on their distances to the selected PWSs. The investigated PWS have their data published on two weather websites (<http://www.wunderground.com> and <http://www.hetweeractueel.nl>). This study considered all available PWS in the Netherlands to select appropriate stations within Dutch cities. The lack of archived data in most PWS inside Dutch cities limits the study period as from 2011 to 2015. The 11 PWS stations were selected based on their locations, instrument types and accuracies, the available record lengths and the data quality (see section 2.2).

4.2.1. Data quality control

Although the quality of the AWS data is controlled by the Koninklijk Nederlands Meteorologisch Instituut (KNMI), there is a lack of professional quality control (QC) for the PWS archived data. The PWS requires data QC to obtain reliable observations (Figure 4.1).

The PWS QC includes instrument issues and setup issues (adverse effects of local installations). The instrument assessment was limited to the defined uncertainties of PWS manufacturers because an inter-comparison of all PWSs is virtually impossible (Steenefeld et al., 2011).

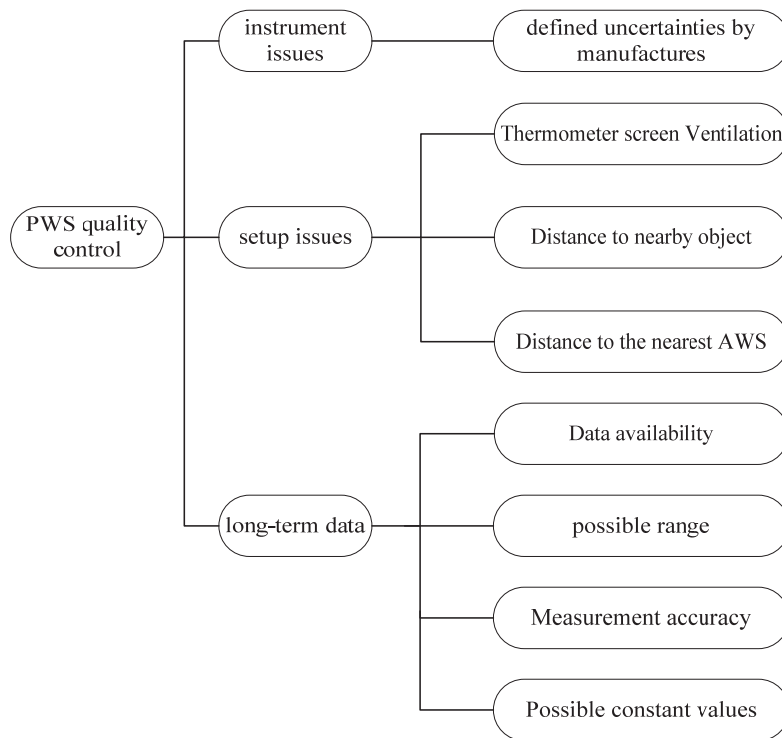


Figure 4.1. The criteria for selecting reliable Amateur weather stations (PWS) in this study

The typical uncertainties for the deduced parameters from PWS are listed in Table 4.1 (and are similar to each other with only small differences). On the other hand, the AWS accuracies reported by KNMI are 0.1°C, 3% and 0.5 m/s for temperature, humidity and wind speed, respectively (Van Hove et al., 2015).

Table 4-1. Measurement accuracy defined by manufactures for each type of stations

Station type	Temperature (°C)	Humidity (%)	wind speed (m/s)	precipitation (mm)	pressure (hPa)
Alecto WS-4000 (I)	0.1	1	-	0.1	0.1
Davis Vantage Pro 2 or 2+ (II)	0.5	3	1	1	1
Davis Vantage VUE (III)	0.5	3	1	1	1
Oregon Scientific WMRS200 (IV)	3	7	3	1	0.1
Oregon Scientific WMR928n (V)	0.5	3	0.9	0.2	0.1
CRESTA WXR 815 (VI)	1	5	0.9	0.8	5
TFA Nexus Pro (VII)	1	5	0.5	-	3

The selected PWSs are similar to (most of them are Vantage Pro series) those amateur stations used by previous studies (e.g. McLaren et al., 2005; Steeneveld et al., 2011; Wiacek et al., 2007). The Wolters and Brandsma

(2012) approach (which is based on the established ideas about in situ urban meteorological observations, as summarized in Oke (2004)) was applied to select representative stations from the available PWS in cities. The selection approach considered a number of criteria regarding a station's detailed metadata and sufficient information concerning the observational circumstances (see Figure 4.1). In this respect, the selected PWS for this study have shielded temperature sensors and active ventilation to avoid direct sunlight. In addition, the distance to the surface of the temperature sensor (height of sensor) is set to be greater than 1.5 m for the selected sheltered stations (without radiation exposure (Oke, 2004)). For a rural background climate, the meteorological observations were explored using the AWSs. Other external forces have been proven to have potential effects on local climate observations (such as the coastal breezes, regional circulations, annual cycles in the observation, open water influences, and soil types) (Van Hove et al., 2015, 2011). To separate these forcing effects from the investigations of urban impacts on temperature and precipitation, the PWSs and nearest AWSs were paired off by their similar influences from the aforementioned external forces. Although this approach cannot totally remove all external forces, it helps diminish their impacts on the analysis of the overall features of the temperature and precipitation discrepancies between the urban and rural, which is focused on in this study. Consequently, this study assumes that the paired urban and rural areas are affected by approximately the same external influences.

Table 4-2. Quality control for the temperature and precipitation parameters (Jarraud, 2008)

Parameter	Precipitation amount (R)	Air temperature (T)
Possible range	$0 \leq R \leq 40$ mm/min and $0 \leq R \leq 300$ mm/day	$-80 \leq T \leq 60$ °C
Required measurement uncertainty	0.1 mm for $R < 5$ mm and 2% for $R > 5$ mm	0.1 K for $-40 < T \leq 40$ °C and 0.3 K for $T > 40$ °C or $T \leq -40$ °C
Possible constant values quantified based on daily	For 10 d if $R \geq 1.0$ mm and for 5 d if $R > 5$ mm	For 5 day

To achieve more reliable results with data analysis, the QC of long-term hourly data from PWS are required. The basic quality requirements follow those of their respective WMO guidelines, as followed by Klein Tank (2007) for the European Climate Assessment & Dataset (ECA&D) meteorological measurements (see more details in Table 4.2 and the WMO (2007) guideline). The last column in Table 4.2 shows the condition for detecting constant values (the repetitive same values) that might be recorded due to digitization error. In practice, these constant values, the improbable zero measurements, and the unusually low or high values (or physically impossible data) were

detected as suspicious values at each station. Then, the suspect values at each station were compared with the values of the nearest stations. If the neighbouring stations recorded significantly higher or lower values than the suspect value, those values were flagged within the data series.

4.2.2. Selected stations

Figure 4.2 shows the locations of the favourable stations for investigating possible urban climate effects. The appropriate PWS observations are lacking for the urban areas in the east, middle and south of the country during the investigated 5-year period (e.g. according to the criteria listed in Figure 4.1). The selected PWS cover the west of the Netherlands within the range of less than 60 km to the coast, which experienced more increased precipitation than the other parts of the country in the past decades (Buishand et al., 2013; Rahimpour et al., 2016a). This part of the country includes the majority of urban areas with dense populations with more than 300,000 inhabitants (i.e. The Hague, Delft, and Rotterdam).

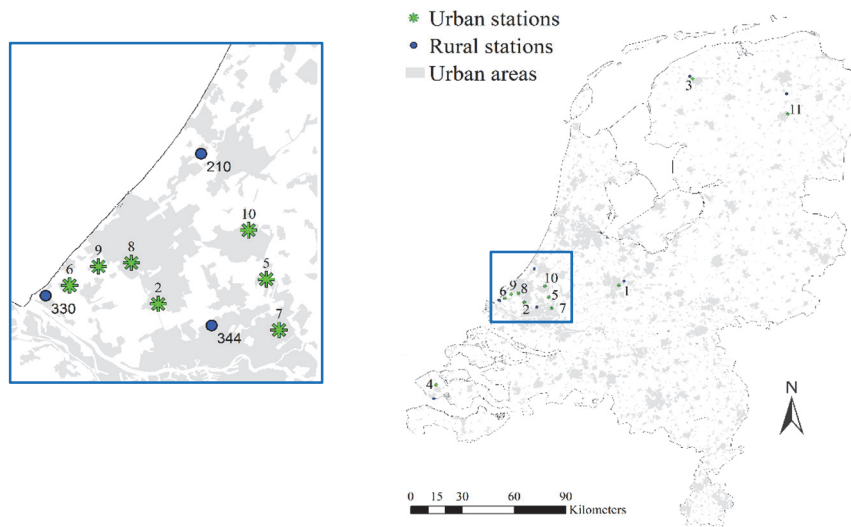


Figure 4.2. Urban (PWS) and rural (AWS) stations that were used in this study. The urban stations with more than 1000 addresses per square kilometre marked with asterisk and their labels correspond to the rows in Table 4.3. Gray-shading display urban areas in the Netherlands (EEA, 2014).

Table 4.3 describes more of the details of the selected stations for further analysis. These stations have similar designs and are classified as urban stations by the Dutch amateur website (<http://www.hetweeractueel.nl>). The local climate zone (LCZ) around each PWS (buffer with 0.3 km radius) is

Type: see details in Table 4.1; LCZ: local climate zone for 0.3 km radius around the personal amateur weather stations (PWS) (OMR: open mid-rise, OLR: open low-rise); OAD: address density per km²; STED: urbanity degree (1: very strong urban ≥ 2500 addresses per km²; 2: strong urban 1500–2500 addresses per km²; 3: moderate urban 1000–1500 addresses per km²); POP: population; PD: population density per km²; D: distance between urban (PWS) and paired rural (AWS) (km); AWS: corresponding KNMI stations

classified as open mid-rise (OMR) or open low-rise (OLR) following the classification by Stewart and Oke (2012). These classes define the slight reduction of the visible sky, abundant plant cover and scattered trees over urban areas. OMR consists of buildings of 3-9 stories made of heavy materials and thick walls. Likewise, OLR consists of small buildings of 1-3 stories that are built of wood, tile, brick or stone (Id, 2011). Further, the land-use information regarding the degree of urbanity, address density and population density were extracted for approximately 5 km around each station (Suomi et al., 2012) from the available database of the Dutch national statistics of 2015 (CBS, 2015). The population around the stations were further considered to select suitable urban stations for further investigation. For very small population density, the averaged observed UHI was close to zero. The results of temperature- population density relationship indicate that the applied criteria for station selection based on considered metadata was effective. The selected PWSs are located in urban areas with more than 1000 addresses per square kilometre (see Table 4.3).

Table 4-3. Information of selected urban stations extracted for a 5 km radius around the station. Row: the numbers correspond to labels in Figure 4.2.

Row	PWS	Lat	Lon	Elevation (m)	City	Province	Type	LCZ	OAD	STED	POP	PD	D	AWS
1	IUTRECHT23	52.08	5.14	9	Utrecht	Utrecht	(I)	OMR	3184	1	321915	3415	3.5	260
2	IDELFT1	51.98	4.34	-1	Delft	Zuid-Holland	(II)	OMR	3384	1	99095	4340	7.5	344
3	IFRIESLA8	53.21	5.77	0	Leeuwarden	Friesland	(II)	OLR	2285	2	95950	1219	2	270
4	IZEELAND16	51.51	3.61	2	Middelburg	Zeeland	(II)	OLR	1717	2	47520	980	6.5	310
5	IZHBLEIS1	52.01	4.54	-7	Lansingerland (Bleiswijk)	Zuid-Holland	(II)	OLR	1187	3	56505	1041	9.4	344
6	IZUIDHOL94	52.01	4.17	0	Westland ('s-Gravenzande)	Zuid-Holland	(II)	OLR	1329	3	102695	1291	3.5	330
7	IZUIDHOL36	51.95	4.57	4	Capelle aan den IJssel	Zuid-Holland	(II)	OLR	2240	2	66025	4644	8.7	344
8	IZUIDHOL92	52.03	4.29	0	The Hague (Wateringse Veld)	Zuid-Holland	(II)	OLR	4720	1	105855	6179	12	344
9	IZUIDHOL80	52.02	4.23	0	Westland (Poeldijk)	Zuid-Holland	(VII)	OMR	1329	3	102695	1291	8	330
10	IZUID-HO15	52.07	4.51	-3	Zoetermeer	Zuid-Holland	(II)	OLR	2503	1	123090	3565	12	210
11	IDRENTHE29	53.01	6.59	9	Assen	Drenthe	(II)	OLR	1436	3	67205	154	12.5	280

4.2.3. Data analysis

This study analysed the temperature and precipitation variables for rural and urban areas. The hourly observation meteorological parameters were investigated with night time (the time interval between sunset and sunrise [LT]) and day time (the time interval between sunrise and sunset [LT]). More

details for sunrise and sunset time is available at www.timeanddate.com/sun/netherlands. UHIs within urban areas vary spatially based on the properties of the surroundings (Rovers et al., 2014). UHI were calculated using a PWS air temperature (T_{Urban}) minus the air temperature of the closest AWS (T_{Rural}) (Oke, 1973; Steeneveld et al., 2011), which is written as follows:

$$UHI = T_{Urban} - T_{Rural} \quad (4.1)$$

The average of the observations during the investigated period may be more appropriate than other indices for use in detecting the physical and temporal behaviours of the measurements (Brandsma and Wolters, 2012). However, sometimes the maximum value is needed to characterize the urban measurements independent of their spatiotemporal variations. These maximum values, regardless of their frequencies of occurrence, may have the strongest impacts on human life. Therefore, the UHI_{ave} and UHI_{max} (the mean and maximum observed UHI values of each month, respectively) were derived from the hourly values.

However, the extreme precipitation intensities could be influenced by many factors, such as atmospheric dynamic advection processes, atmospheric moisture availability and other process (Attema et al., 2014; Berg et al., 2013; Panthou et al., 2014). The relationship between extreme precipitation and temperature (analogous to the Clausius-Clapeyron relation) plays an important role in precipitation formation (Barbero et al., 2017). The Clausius-Clapeyron relation indicates the maximum capacity of an air mass for holding water vapour, which increases 6-7% per degree of temperature increase (Allen and Ingram, 2002). This percentage of water vapour enhancement could decrease or increase due to various factors, such as the region, duration, season or temperature range (Berg et al., 2013; Lenderink and van Meijgaard, 2008).

To understand the relation between temperature and precipitation, we followed the method described by Lenderink and van Meijgaard (2008). In this respect, the hourly precipitations were paired with their corresponding temperatures for all wet hours (precipitation > 0 mm) at each station for the nights from 2011 to 2015. To examine the temperature-precipitation relationships of the investigated stations, scaling can be used with either the dew-point temperature or air temperature as the reference (Lenderink et al., 2011). Although the preference is to use the dew-point (e.g. including temperature and humidity), in this study, only the air temperature observations were used due to the lack of sufficient dew-point observations at the urban stations.

For each station, the sorted P90th-temperature was split into 20 bins between 0 and 20 °C with intervals of 1 °C. Furthermore, a sensitivity analysis of the bin width shows that a 0.5°C bin width does not influence the results. The 90th percentile of the hourly precipitations (P90th) was defined as extreme precipitation (ranked from highest to lowest). The wet time fraction (WTF) was estimated using the ratio of the total number of P90th events to the total number of wet hours for each bin. Then, the precipitation fractional (PF) was used to assess the variations of the intensities of the P90th events. The PF was calculated by the fractional contribution of the P90th to total precipitation in each bin (Mishra et al., 2012). The WTF and PF are defined as follows:

$$WTF = \frac{N_{P90th^i}}{N_{P_i}} \quad (4.2)$$

$$PF = \frac{\sum_{i=0}^{20} P90th_i}{\sum_{i=0}^{20} P_i} \quad (4.3)$$

where P is the amount of precipitation, N_{P90th^i} represents the number of hourly extreme precipitation events above the 90th percentile (P90th) in each bin (i) and N_{P_i} is the number of wet hours in each bin.

Investigating the hourly maximum UHI and precipitations for a long time series could be useful for urban climate studies (Steenefeld et al., 2011). The statistical method to evaluate the intensities and frequencies of the maximum observations could be applied to detect the probability distributions of temperature and precipitation (Data, 2009). The extreme distribution of the maximum UHI and precipitation can be explained by the GEV method (Coles, 2001; Overeem et al., 2008b; Steenefeld et al., 2011). Analysing the data via the GEV method leads to the quantification of the degree of observed extremes and their distributions. The maximum hourly values were fitted to GEV as follows:

$$F(x; \mu, \sigma, \epsilon) = \begin{cases} \exp\left(-\left[1 + \epsilon \frac{x-\mu}{\sigma}\right]^{-\frac{1}{\epsilon}}\right), & \& \quad \epsilon \neq 0 \\ \exp\left(-\exp\left(-\frac{x-\mu}{\sigma}\right)\right), & \& \quad \epsilon = 0 \end{cases} \quad (4.4)$$

$$\text{where: } \left[x: 1 + \epsilon \frac{x-\mu}{\sigma} > 0 \right], \quad \begin{cases} \mu \in \mathbb{R} \\ \sigma > 0 \\ \epsilon \in \mathbb{R} \end{cases}$$

where x is the maximum hourly UHI (or precipitation) and $F(x)$ is the cumulative distribution. The distribution maximum is defined by the parameter location (μ), and the spread of the distribution is defined by the scale parameter ($\sigma > 0$). The shape parameter (ϵ) defines the extreme value distribution types. The maximum likelihood (Jenkinson, 1955) was used to estimate the distribution parameters. The fitting distribution approximations are generally accurate due to the primary statistical theory of the maximum likelihood approach (Data, 2009). The goodness of fit for the GEV estimations and their uncertainties were tested by calculating their confidence intervals and standard errors. The parametric bootstrap method was applied to obtain

the confidence intervals. A large enough replicate sample size of 10^4 was chosen to run the parametric bootstrap method (Pattengale et al., 2009).

4.3. Results

4.3.1. The UHI intensities

The variations of UHI, as derived from the nearest AWS, were investigated between 2011 and 2015 (Figure 4.3) by considering the diurnal course of the average UHI. Figure 4.3 shows the variations of the average hourly UHI for 24 hours during the investigated 5-year period. The UHI depicts a sinusoidal shape between 0 and 24 h (LT), with its greatest values exceeding 2°C at 18 h (LT).

A distinct diurnal course of UHI at each station shows stronger and weaker values for UHI in night-time and in the morning, respectively. The average UHI approaches zero degree close to sunrise (between 05:00 and 06:00 h LT) and reaches the largest negative values at about 08:00 h LT. In the morning and afternoon the averaged UHI gradually increases and reaches a maximum at about 18:00 h LT. The stronger UHI in night-time hours was also found in previous studies (Hamdi and Schayes, 2008; Wolters and Brandsma, 2012). They described the UHI disappearing after sunrise in the morning is due to the effective heat storage, shadowing and low solar radiation which make urban areas to warm up slower than the rural areas. The UHI was detected in all seasons for all stations with a seasonal influence on the magnitude of observed UHI. Figure 4.4 shows the average of hourly UHI in night-cycle for the investigated PWS within the cities for the spring

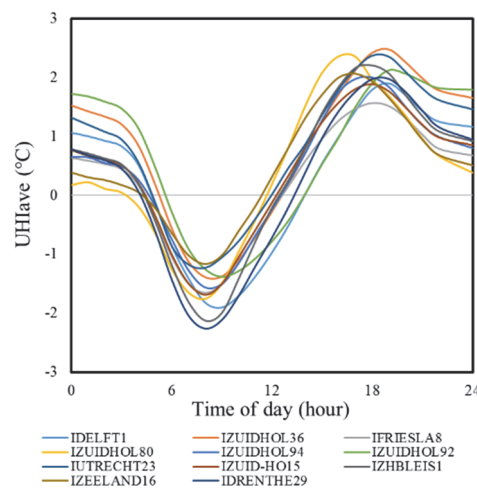


Figure 4.3. Hourly variation of mean observed urban heat island values from 2011 to 2015. The UHI at night-time decreases near sunrise

(MAM), summer (JJA), autumn (SON) and winter (DJF). The magnitudes of the UHI averaged over all cities were $-0.08 - 0.63^{\circ}\text{C}$ for the winter and $0.26 - 1.30^{\circ}\text{C}$ for the summer. Likewise, those of the spring were $0.36 - 1^{\circ}\text{C}$, and those in the autumn were $-0.01 - 0.81^{\circ}\text{C}$. The UHI could be observed on some days in the winter, although on average, the UHI were minimal during the winter months. The UHI intensity and its statistical distribution most likely depend on other investigated weather parameters as well as the characteristics of the city and countryside. In The Netherlands, cold night or warm nights generally occur with clear sky or fair weather, respectively. The UHI development in both aforementioned situations occurs more during calm conditions with little wind speed, and is also dependent on sea level pressure and humidity (Steenefeld et al., 2010; Wolters and Brandsma, 2012).

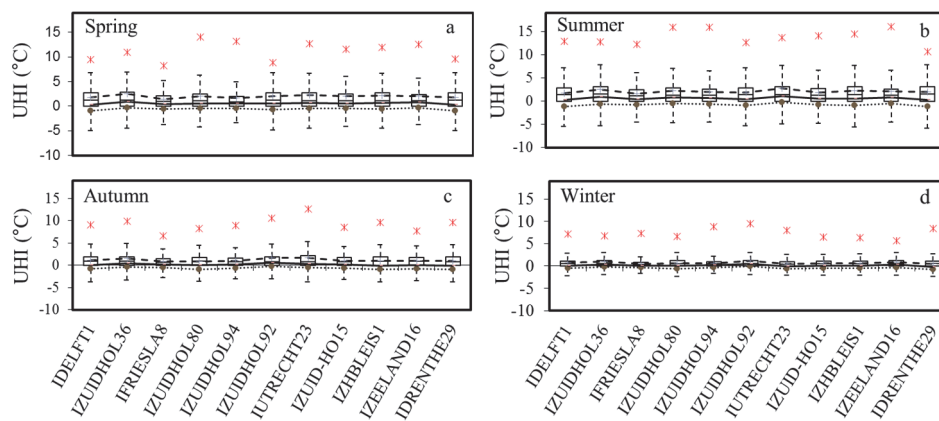


Figure 4.4. Box-Whisker plot for the PWS hourly UHI from 2011 to 2015. UHI is plotted conditional on their occurrence during spring (a), summer (b), autumn (c) winter (d). The whiskers are set to 1.5 times the inter-quartile range (IQR). The lines show the 0.25 (dotted), 0.5 (solid), and 0.75 (dashed) quantiles. The red crossed dots indicate the maximum data points for outliers.

4.3.2. UHI versus population density

A quantitative relationship between UHI and cities has often been investigated by correlating the population and its UHI (Oke, 1973). Further, the UHI intensities and magnitudes are strongly dependent on the degree of urban development (e.g. urban sky visibility factors) at the investigated location (Van Hove et al., 2011). Population density has a stronger link to building topology and the characteristics of cities than does population number, and PD is further strongly linked to sky visibility factors (Giridharan et al., 2005). In this respect, The UHI intensity and its dependency on the PD were investigated for the individual months of 2011-2015. The linear regression was obtained using least squares estimations comparing UHI (i.e. UHIave and UHI_{max}) and population densities for the individual months. The

relationships between UHI and PD for the daytime and diurnal cycles tend to have weak correlation coefficients (results not shown). Alternatively, a significant positive relation between the UHI and PD was obtained for the night-time cycle. The coefficients of determination (R^2) for nightly UHIave and PD were estimated to be between 0.56 and 0.71 for the individual months (see Table 4.4).

Table 4-4. The linear relationship properties between UHI ($^{\circ}\text{C}$) and population density (10^3 per km^2) during the night-time cycle for the individual months between 2011 and 2015. R^2 : coefficient of determination, a: slope and b: intercept values of the regression line.

Index	UHIave				UHImax			
	R2	P-value	a	b	R2	P-value	a	b
Jan	0.60	0.005	0.12	0.03	0.67	0.002	0.34	3.49
Feb	0.57	0.007	0.10	0.23	0.45	0.025	0.75	3.17
Mar	0.71	0.001	0.19	0.42	0.32	0.07	0.27	4.95
Apr	0.69	0.002	0.22	0.66	0.32	0.068	0.31	5.5
May	0.66	0.002	0.17	0.60	0.29	0.085	0.25	4.93
Jun	0.71	0.001	0.20	0.67	0.55	0.009	0.80	3.79
Jul	0.66	0.002	0.19	0.50	0.33	0.065	0.30	4.75
Aug	0.56	0.008	0.18	0.39	0.30	0.08	0.23	4.9
Sep	0.61	0.004	0.24	0.15	0.29	0.085	0.33	4.63
Oct	0.70	0.001	0.18	0.02	0.47	0.02	0.39	4.6
Nov	0.67	0.002	0.17	-0.13	0.56	0.008	0.91	2.47
Dec	0.57	0.008	0.10	-0.09	0.49	0.016	0.26	3.12

The positive relationship between UHImax and PD can be observed for all months, despite the smaller R^2 (between 0.29 and 0.67). The averaged slopes for UHIave and UHImax are 0.17°C and 0.43°C , respectively, over all months. The regression line for UHIave has intercept values close to 0°C , as expected for rural areas with population densities near 0. For UHImax, the intercept values of the regression lines were larger (between 2.7°C and 5.5°C) than those for UHIave. The greater intercept values for UHImax show that strong positive deviations of temperature could exist when the UHIave is close to 0°C .

4.3.3. Precipitation

Figure 4.5(a) shows that the total cumulative precipitation in urban areas increased more than that in rural areas between 2011 and 2015. The difference between the urban and rural cumulative precipitations from 2011 to 2015 was estimated to be nearly 65 mm (48–81 mm 95% CI, $p < 0.05$).

Figure 4.5(b) shows the hourly precipitation in the cities was generally greater than in their neighbouring rural areas.

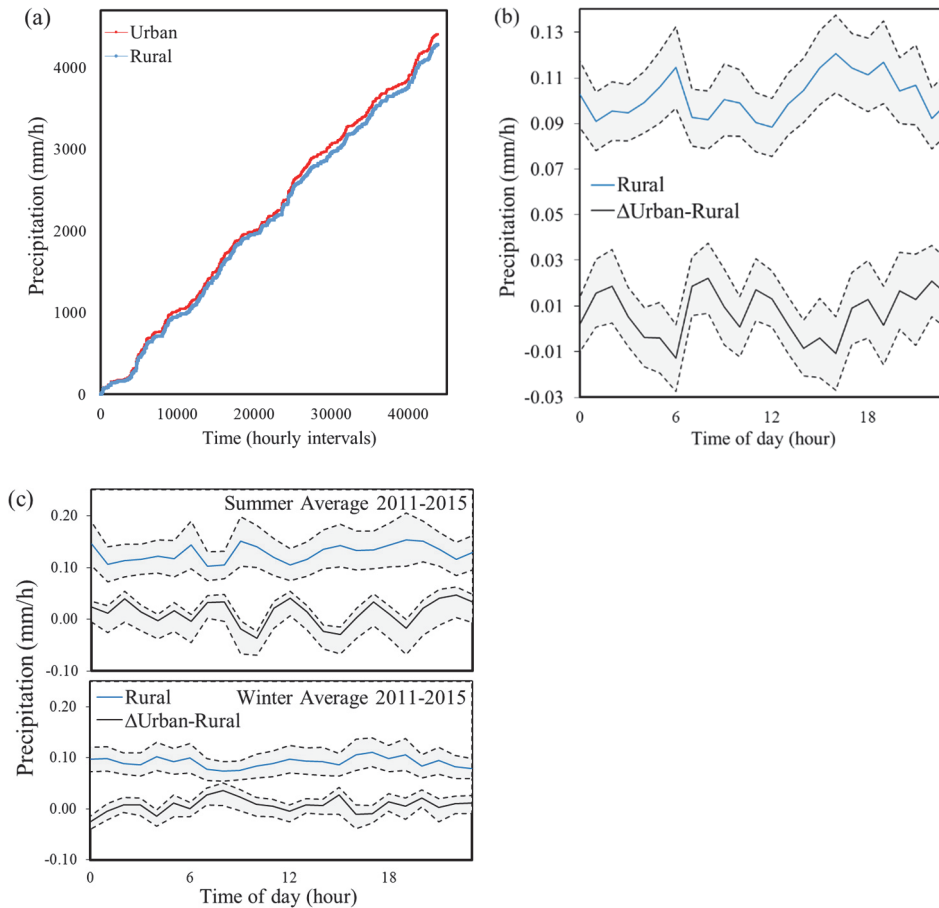


Figure 4.5. (a): A time series plot of the hourly-accumulated precipitation that averaged for urban stations (red line) and rural stations (blue line). (b): Mean (solid line) and 95% confidence interval of hourly precipitation between January 2011 and December 2015. The rural stations (blue) and the differences of hourly precipitation between cities (PWS) and rural station (AWS) (black). (c): The rural hourly precipitation (blue line) and the differences of hourly precipitation between cities (PWS) and rural station (AWS) (black line) between January 2011 and December 2015 for summer (upper panel) and winter (lower panel). The shaded areas show 95% confidence intervals.

In the evening, the strengthened difference between urban and rural temperatures led to an increase in magnitude of UHI circulation with dynamically up ward flow in urban areas, which could increase the possibility of precipitation occurrences in the evening and night-time. The decreased precipitation in the afternoon may indicate that the air convection in the afternoon is less marked with the smaller UHI. The average hourly

precipitation amounts for the 5 yr were approximately 0.11 mm (0.09 – 0.12 mm at the 95% confidence interval) in cities and 0.10 mm (0.09 – 0.11 mm at the 95% confidence interval) in rural areas. The difference shows that the hourly precipitation that occurred was 7% greater in cities than in rural areas. The average of the hourly precipitation amount in the summer was 0.14 mm (0.10 – 0.18 mm at the 95% confidence interval) in cities and 0.13 mm (0.09 – 0.16 mm at the 95% confidence interval) in rural areas (Figure 4.5(c)). Additionally, the average of the hourly precipitation amount in the winter was 0.1 mm (0.07 – 0.12 mm at the 95% confidence interval) in cities and 0.09 mm (0.06 – 0.11 mm at the 95% confidence interval) in rural areas. Higher values of the hourly precipitation and bigger differences between the city and rural precipitations occurred in the summer. These differences are more prominent during the night in the summer (0.15 mm in cities and 0.12 mm in rural areas).

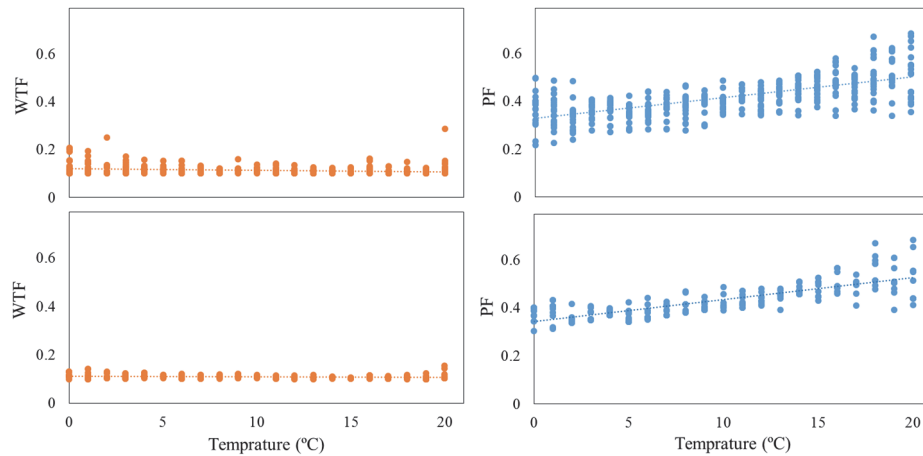


Figure 4.6. Relationship between mean hourly temperature ($^{\circ}\text{C}$) in each bin and wet time fraction (WTF) as well as precipitation fractional (PF) of extreme precipitation (greater than 90th percentile) for urban stations (upper panels) and rural stations (bottom panels) for night-time during 2011-2015.

Although the precipitation enhancement may be caused by many external influences, an overall enhancement of the precipitation could be expected based on the temperature increases. The urban extreme precipitation occurrences may have been expected to be more intense due to the warmer convective precipitation (Lenderink et al., 2011; Mishra et al., 2012).

The relation between temperature and extreme precipitation (P90th) was further investigated by the wet time fraction (WTF) and precipitation fractional (PF). The estimated relationships between temperature and WTF or PF for each bin do not show a robust linear relationship (Figure 4.6). However, the estimated relationships show that the regression slopes

between the hourly temperatures and P90th values are more strongly influenced by PF variations than by WTF, suggesting that the temperature has a greater impact on the intensity of the extreme precipitation than on its frequency.

4.3.4. Extreme value statistics

The UHI, temperature and precipitation distributions were assessed by considering their diurnal maximum hourly occurrences for the individual months. The position of the probability distribution functions was characterized by the GEV distribution function for the hourly UHImax and the maximum hourly precipitation. The estimated location parameters simply show the means of the distributions of the maximum hourly UHI and precipitation. Figure 4.7(a) shows the UHI based on the investigated stations against the corresponding temperatures (e.g. both urban and rural) stratified by months. The UHI distribution was greater between March and September than during other months. The estimated location parameter of the maximum hourly precipitation over urban and rural stations was plotted against the estimated location parameter for the maximum hourly UHI for each month, as shown in Figure 4.7(b). The lowest values of the location parameter occurred in December and the highest values occurred in April and August. These results suggest that the highest values of the maximum hourly precipitation and UHImax were evident in the summer months, and the difference between urban and rural precipitation tends to be greater in

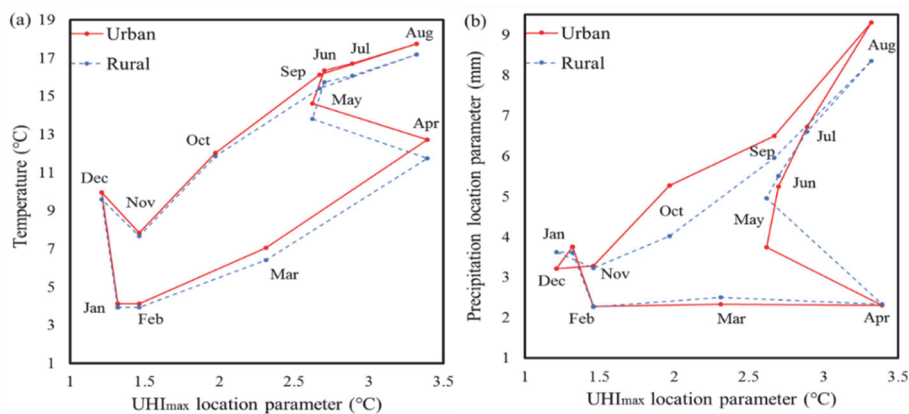


Figure 4.7. Estimated location parameter for the hourly maximum UHI against hourly temperature (a) and estimated location parameter for the maximum hourly precipitation (b) averaged for cities (red solid line) and rural (blue dashed line) for the individual months.

months with larger values for UHImax (Figure 4.7(b)). In particular, the average maximum hourly precipitations in urban and rural areas were 9.30 mm and 8.36 mm, respectively, in August. This difference reveals the

maximum hourly precipitation in urban areas is approximately 11% larger than that in rural areas in August.

Zhou et al. (2013) demonstrated the seasonal dependency of UHI intensity in the form of hysteresis loop for European cities. They found the inter-annual variations of UHI intensity depends on the boundary temperature. For Dutch cities, Figure 4.7 shows a distinct seasonal cycle of the temperature and precipitation, which follows a closed loop and is based on urban-related warming. This cycle reveals the weakest and strongest urban-related warmings for the winter and summer, respectively. The maximum hourly UHI was depicted as having different amplitudes in the spring and autumn. The clockwise rotation of the UHI loop leads to the conclusion that urban areas warm up more quickly in the spring and cool off faster in the autumn. Stronger maximum hourly precipitations occurred in the summer and early autumn than in the other two seasons. Furthermore, the results show that more intense hourly extreme precipitation occurred in the autumn than that in the spring. The seasonality of precipitation in the Netherlands, as indicated by previous studies (such as Rahimpour et al., (2016)'s study), shows that precipitation is enhanced in the summer and early autumn. Figure 4.7 reveals that the urban precipitation in the late spring is more suppressed than the rural precipitation. Likewise, urban precipitation enhancement is larger than rural precipitation enhancement in the late summer and early autumn. Although there are different physical mechanisms behind the variation in precipitation, the results of the present study reveals a distinct seasonal cycle for temperature and precipitation in Dutch cities, following a loop wherein the urbanization effect is strongest between August and October and weakest in the winter and spring.

4.4. Discussion

Differences between the urban and countryside climates were investigated using amateur and automatic weather station networks. The PWS data of sufficiently high quality could provide long-term observations for the analysis of urban climates (Steenefeld et al., 2011). Unreliable data were excluded via QC of the PWS data (section 2.1). The measured variables of the selected PWS (Table 4.3) make it possible to detect the urban climate in more detail, not only in terms of air temperature but also in terms of other parameters. Differences between temperature and precipitation in urban and rural areas were investigated. The UHI intensities reveal diurnal and seasonal inconsistencies, and could be influenced by mesoscale (Gedzelman et al., 2003) or synoptic weather conditions (Morris and Simmonds, 2000). The average monthly UHI indicate that urban areas were warmer than rural areas, except for some winter days. The UHI were found to be strongest in the late spring and summer and weakest in the winter. This could be attributed to

seasonal influences on meteorological conditions. This distinct annual cycle is most likely caused by wind speed and insolation variations during the year (Wolters and Brandsma, 2012) because the winter in the Netherlands is known to have higher wind speeds, and the effects of surface properties (materials) on albedo and the surface energy budget differ in the winter and summer. The similar result was found by Arnds et al., (2017) with a radial gradient about 2 K for Hamburg. They showed it has seasonal cycle with greater values between April and September and lower in winter. The observed UHI annual cycle suggests that irradiation and vegetation period might be a relevant factor besides the weather condition frequency. UHI intensity enhancement in spring and summer also indicates that the vegetation period could induce greater differences in latent heat flux between urban and rural areas, even though Dutch cities are relatively green (Arnds et al., 2017).

The averaged UHI variations in Figure 4.3 demonstrate that the UHI intensity reaches a maximum in the evening (2°C at 18 (LT)). The results show that UHI and urban impacts may be similar for other European cities such as Poznan in central Europe, which was recently reported by Pórolniczak et al. (2017). The causes of UHI increases in the evening could be related to the much lower cooling rates of urban areas than those of rural areas after sunset. This difference is related to the high thermal capacity in urban areas and the low emissions of longwave radiation back the sky due to building densities (Unger, 2004). Conversely, the UHI was minimized near sunrise, and this reduction continued into the morning. The negative values of UHI during the morning hours show that urban areas are cooler than their surrounding countryside. In other words, the mornings experienced the urban cool island (UCI) instead of UHI. The maximum value of UCI averaged for all investigated cities was approximately 1.6°C at 8 a.m. (LT). The UCI at all stations indicate that the investigated cities experienced shadow effects, which means that sunlight was prevented from reaching the cities in the morning (Oke, 1982). The UCI of some winter days could be caused by the higher average wind speeds in winter, which make stronger advection of rural air into cities (Wolters and Brandsma, 2012).

The UHI was found during the nights of all investigated urban areas. In addition to temperature and dew-point, high sea level pressures with clear weather conditions in the Netherlands (Wolters and Brandsma, 2012) and greater humidity in rural areas than cities (which may be caused by the minimal evaporation (less vegetation) in cities during the day and higher temperatures at night) may lead to intensive UHI. Therefore, it can be deduced that the impacts of UHI extreme values can be diluted by combining the night and day datasets. This agrees with previous studies in the

Netherlands (Brandsma and Wolters, 2012; Steeneveld et al., 2011; Klok et al., 2012; Van Hove et al., 2015).

The PD around each PWS station was linked to the monthly UHI between 2011 and 2015. The possible relationships between UHI and population densities were significant only at night. The slopes of the regression lines for UHI_{max} (extreme cases) are statistically significant and greater than those of UHI_{ave} for all months. The medians of the linear slopes were obtained as 0.18 and 0.32 (°C/10³ km²) for UHI_{ave} and UHI_{max}, respectively. Wolters and Brandsma (2012) also linearized the relationship between UHI and population densities for the nights between June 23rd and July 24th in 2010. Their findings confirm our estimations; they found the medians of the relationship slopes to be 0.18 and 0.31 (°C/10³ km²) for UHI_{ave} and UHI_{max}, respectively.

In addition to studying UHI, our study attempted to quantify the hourly precipitation discrepancies between cities and their surrounding areas. The overall features of the hourly precipitation analysis reveal greater values in cities than in the countryside, and the highest precipitation difference in the summer. The observed enhanced cumulative precipitation in urban areas is in agreement with the previous study for urbanisation impacts on urban climates by Daniels et al. (2015), which showed a 7% enhancement of precipitation in Dutch cities. Thus, we confer further confidence to the recorded observations of the amateur stations.

The extreme precipitation sensitivity to temperature seems physically implausible due to other physical processes and factors (Attema and Lenderink, 2014; Lenderink and Van Meijgaard, 2010). However, the change from stratiform precipitations to more convective precipitations can be expected at higher temperatures (Lin and Chen, 2011). Precipitation enhancement (amount and intensity of short duration e.g. hourly) could be partially attributed to thermal effects from UHI in combination with stagnant weather systems resulting from other factors such as increases in the surface roughness and the strengthening air convection due to urbanization (Ren, 2015). The UHI (a low level heat source) impacts on local flows (upward/downward motion) and circulations may lead to suppressing or increasing convection or updrafts (Han and Baik, 2008). Further, the velocity perturbations in a stably stratified atmosphere could be decreased by the UHI generated gravity waves (Han et al., 2014). Thus, water vapor transport and upward movement of convergence can be triggered by the UHI circulation, and the existence of enough moisture can lead to more precipitation in urban areas (Yang et al., 2017).

An enhanced precipitation difference was detected at night is in agreement with results from other urban areas (Dou et al., 2015; Ikebuchi et al., 2007; Yang et al., 2013), for example, Dixon and Mote (2003) found the UHI enhancement increased night-time precipitation frequency in late spring and summer in Atlanta. The likely similar results reported by Chen et al. (2015) and Yang et al. (2017) showed that the higher UHI intensity might induce the stronger convection and cause the larger hourly precipitation in urban areas than in the rural areas in the late evening and night-time. Furthermore, pronounced precipitation difference during the night-time hours could be related to the interaction between the weakening sea breeze and the UHI (Mitra et al., 2012; Shepherd et al., 2010). Although the above discussion provide valuable information on urban climate, they are mostly proved for big cities in the United States with different climate conditions (e.g. air quality, urban morphology, building style and materials). Therefore, for Dutch urban case, further investigations are needed to better understand physical mechanisms regarding the urban situation in the Netherlands. The reader is referred to (van Hove et al., 2010) for more detailed discussions about the effects of such conditions in the Netherlands. It is to note that the catch efficiency of precipitation could be influenced by location of stations. The rural stations in open area are exposed to wind more than urban stations that surrounded by obstacles. The possibility of larger catch efficiency of precipitation in urban stations than that in rural stations may cause uncertainty in the observed precipitation differences between urban and rural. Although this study explores the potential of PWS data for the analysis of temperature and precipitation variations in cities, the rigorous assessment for data quality remains a challenge in urban climate research. It is worth of defining a new possible research direction to double check the effects of current set-up characteristics of the stations on the quality of collected data, for instance, the factors like PWS placement, maintenance and sensor quality, which were assumed fulfilling the manufacturer's specified accuracy. For future studies, it would be desirable to address the effects of such factors. Furthermore, for obtaining more reliable results on precipitation discrepancy between urban and non-urban areas, efforts are needed to examine the impact of bias corrections on observed precipitation variations. The ignored undetected errors in this study (i.e. wind speed-induced errors and installation and siting of PWS and other undetected forcing factors) could impact the obtained precipitation discrepancy between urban and nonurban areas. Therefore, the more reliable results could be obtained by comprehensive quality assessment and separating sources of uncertainty and erroneous metadata.

4.5. Conclusions

The influences of urbanization on the local climate were investigated by analysing data from amateur meteorological stations in residential areas and automatic stations in their nearby countryside. The agreement between the results obtained in the present study and those of previous studies reflects the utility of amateur weather observations. The effects of urban areas on temperature (e.g. represented by UHI) and precipitation were analyzed over 5 yr. Despite the relatively small sizes of Dutch cities (with <10 km radii), these cities do influence their climates. Dutch UHIs determined here are substantial and comparable to those of other European cities. The average UHI exceeded 2°C after sunset, indicating that UHI is a nocturnal phenomenon, while UCIs occur after sunrise in the morning. The cooling effect was found to be almost imperceptible at night.

The UHI intensities and their statistical distributions most likely depend on other weather parameters as well as the city and countryside properties. The links between the UHI and population densities (the significant linear relationships at night found in all months) show that higher UHI can occur in more densely populated urban areas. Additionally, the hourly extreme precipitation was strongest in the summer and more intensive in the autumn than in the spring. This study quantified the precipitation enhancement over urban areas as being greater than that in nearby rural areas. The hourly precipitation in Dutch cities was estimated to be, on average, 7% greater than that in the countryside. The hourly temperature dependence of extreme precipitation shows that precipitation increases at a greater rate in cities than that in rural.

Chapter 5

Response of extreme precipitation over the Netherlands to urbanisation *

* This chapter is based on:
Rahimpour, V., Zeng, Y., Mannaerts, C.M., Su, Z., 2018. Response of extreme precipitation over the Netherlands to urbanisation. In review: Journal of Applied Meteorology and Climatology.

ABSTRACT

Knowledge of the response of extreme precipitation to urbanisation is essential to ensure societal preparedness for the extreme events caused by climate change. To quantify this response, this study proposes scaling extreme precipitation according to temperature using the statistical quantile regression and binning methods. The method performs a linear regression between the 95th percentile of daily precipitation and the corresponding daily dew point temperature, surface air temperature and atmospheric air temperature at 850 hPa during the period of 1985-2014. The positive scaling rates (3-7% at most stations) that describe the relationship of precipitation with the dew point and atmospheric air temperatures show non-stationary behaviour. The return levels of extreme precipitation are investigated using monthly blocks of the maximum daily precipitation, considering the dependency of precipitation on the dew point and atmospheric air temperatures and the North Atlantic Oscillation (NAO) index. Consideration of the land cover types upwind of the stations in different directions reveals that greater amounts of precipitation occur in urban areas than non-urban areas, especially after the spring months. The return levels for the maximum daily precipitation are 5-7% greater over urban stations than those over non-urban stations in August for all of the classified station types under light flow conditions. Analysis of the intensity-duration-frequency curves for urban and non-urban precipitation in August reveals that the assumption of stationarity leads to the underestimation of precipitation extremes due to the sensitivity of extreme precipitation to the dew point and atmospheric air temperatures. The study concludes that non-stationary models should be used to estimate the return levels of extreme precipitation by considering the probable covariates. In addition to the external forces that drive extreme precipitation, such as large-scale weather modes, circulation types and temperature changes, urbanisation has significant impacts on extreme precipitation in the Netherlands, particularly short-duration events.

5.1. Introduction

Extreme precipitation events have been shown to have significant impacts on the environment and society (Alfieri et al., 2015; Kundzewicz et al., 2013; Feyen et al., 2012). Ample studies have demonstrated that increases in extreme precipitation events are expected as the climate warms (Aalbers et al., 2017; Attema et al., 2014; Lenderink and Attema, 2015). Higher air temperatures increase the water vapour holding capacity of the atmosphere (6-7%/°C). This increase is known as the Clausius-Clapeyron (C-C) relationship and is used in many studies as a physical basis for assessments of the variations in extreme precipitation with the dew point and air temperatures (Allen and Ingram, 2002; Lenderink et al., 2011; Min et al., 2011; Westra et al., 2014). Lenderink and van Meijgaard (2008) used data describing the hourly extreme precipitation in the Netherlands (i.e., the De Bilt station is taken as a representative station) and found that the rate of increase in extreme precipitation exceeds the C-C rate. Enhancements in the dependency of extreme precipitation on the C-C rate appear due to increases in latent heat driven by moisture convergence or convective precipitation (Berg et al., 2013; Haerter and Berg, 2009; Lenderink and Van Meijgaard, 2010). In the above studies, the statistical quantile regression (QR; Koenker, Roger, 1999; Koenker and Bassett, 1978) and binning methods (Lenderink and van Meijgaard, 2008) are used to determine the scaling factor between extreme precipitation and the dew point or air temperatures.

The incidence of extreme precipitation is increasing in the Netherlands, and several studies have identified increases in mean annual precipitation and trends in extreme indices for gauge-based observations due to climate change and internal variability across the Netherlands (Aalbers et al., 2017; Buishand et al., 2013; Rahimpour et al., 2017). Fairly rapid urbanisation has also occurred during the last several decades in the Netherlands, based on the expansion of urban areas (Daniels et al., 2015b; Hazeu et al., 2011) and the increase in population growth rates (e.g., 1.05% in 2015) (*World Urbanization Prospects The 2014 Revision*, n.d.). Due to the lack of long-term observations (i.e., precipitation, dew point and air temperatures) for Dutch cities, efforts to investigate extreme precipitation in urban areas in the Netherlands have been limited. Daniels et al. (2015) simulated the effects of the urban land-use type on precipitation for a 4-day period in May 1999 over the Netherlands and reported that no clear local response could be identified. In another study, Daniels et al. (2016) investigated the impacts of land-use changes during 19 summer days from 2000 to 2010. They found that the influence of the urban land-use type on precipitation is not negligible, and it caused an increase in precipitation by 7-8% in this decade for the Netherlands. Moreover, a similar result was found by Rahimpour et al. (2018) for hourly extreme precipitation at local urban stations when compared to

nearby rural stations. These studies emphasize that variations in extreme precipitation may also occur due to urbanisation and human activities that impact regional and local climates.

Given the above discussion, this study presents a physically based statistical analysis that assesses changes in extreme precipitation over the urban and non-urban areas in the Netherlands. The study is structured as follows. Section 2 describes the datasets and statistical methods used to assess the observed parameters and evaluate the non-stationary models. Section 3 highlights the results of scaling and analysing extreme precipitation and the performance of the differences in precipitation extremes between urban and non-urban areas. Section 4 presents more details underlying the results obtained in this study and suggests possible mechanisms, and Section 5 gives the conclusions of this study.

5.2. Data and Methods

For defining urban and non-urban stations, the stations are classified by considering the types of areas located upwind of the stations in different directions. To understand the variability in extreme precipitation over urban and non-urban areas, a non-stationary analysis with suitable covariates is needed. The air and dew point temperatures and a large-scale mode of climate variability are selected as non-stationary covariates at each rain gauge station.

5.2.1. Data

Precipitation data in the Netherlands are available from the national weather institute (KNMI). These data are collected by 1) a network of automatic gauges that consists of 35 stations (<http://www.knmi.nl/nederland-nu/klimatologie/daggegevens>); and 2) a network of manual rain gauges that includes 325 stations (<http://www.knmi.nl/nederland-nu/klimatologie/monv/reeksen>). This study considers the daily validated datasets (which contain less than 1% missing data) corresponding to 231 rain gauges for the 30-year period extending from 1985 to 2014. The humidity and daily surface air temperature at a height of 1.5 m are obtained from the hourly automatic gauges without any missing data between 1985 and 2014. The 5-minute radar-recorded precipitation on a 2.4-km grid is used when the short-term observational records at the rain gauges are unavailable. The validated (bias-corrected) radar records covering 17 years (1998-2014) from the two radar stations in the Netherlands (De Bilt and Den Helder) are used. The ERA and ECMWF datasets (i.e., the ERA-Interim reanalysis data for 1985-2014), which have a resolution of 0.125*0.125, are used to provide estimates of the mean sea-level pressure and the daily atmospheric air temperatures at 850 hPa (T_a) (Dee et al., 2011). The North

Atlantic Oscillation (NAO) index is used to represent a large-scale mode of climate variability, and it describes the variability in the North Atlantic Ocean from 80° W to 30° E and between 35° N and 65° N as the normalised monthly sea-level pressure (SLP) difference between stations in the Azores and Iceland (Hurrell, 1995).

5.2.2. Circulation conditions

To obtain atmospheric circulation conditions, the method developed by Jenkinson and Collison (1977) is used to classify weather types. The Jenkinson-Collison type (JCT) classification scheme reproduces the subjective Lamb weather types. In this method, the circulation type is classified based on the variability in pressure around a region that contains 16 grid points. A domain that is larger than the study area (3-13°E47-58°N) is used to implement the classification scheme for mean sea-level pressure. The cost733class software package (Philipp et al., 2016) is used to create weather types corresponding to the eight prevailing wind directions, plus one unclassified type. Types 1 to 8 represent the wind directions (W, NW, N, NE, E, SE, S, and SW, where W = 1, etc.), and 9 represents the unclassified weather type (light flow) (for more information on this method, see Philipp et al., 2014).

5.2.3. Urban land cover

The Coordination of Information on the Environment (CORINE) land cover dataset, which corresponds to the year 2012 and has a resolution of 100*100-m (EEA, 2017), is used to define urban and non-urban stations, consistent with previous studies in the Netherlands (e.g., Chrysanthou et al., 2014; Daniels et al., 2014; Rahimpour et al., 2017). The urban extent in this study consists of six categories: i) discontinuous urban fabric; ii) industrial or commercial units and public facilities; iii) road and rail networks and the associated land; iv) port areas and airports; v) mineral extraction sites, dump sites, and construction sites; and vi) green urban areas and sport and leisure facilities.

5.2.4. Analysis

The dew point temperature (T_d) is derived using a formula adopted from KNMI (2000):

$$T(^{\circ}\text{C}) = t(\text{K}) - 273.15 \quad (5.1)$$

$$e_s(T) = A * e^{\left\{\frac{B * T}{T + C}\right\}} \quad \text{where } A = 6.11, B = 17.504, \text{ and } C = 241.2 \quad (5.2)$$

$$e = \frac{\{e_s(T) * RH\}}{100\%} \quad (5.3)$$

$$T_d = C / [\{B / (\ln e - \ln A)\} - 1] \quad (5.4)$$

where the temperature $t(\text{K})$ and relative humidity (RH) are measured

directly, and the vapour pressure (e) is a consequence of the relative humidity and the saturation vapour pressure ($e_s(T)$) under the given conditions. The daily data values are extracted for 231 rain gauge locations from the gridded dataset for the daily mean and maximum of the surface air temperature and the dew point temperature (for a more detailed discussion, see Sluiter (2009, 2012, 2014)).

To avoid the effects of other factors, such as spatial differences in ground cover, on the differences in air temperature, data describing the daily atmospheric air temperature at 850 hPa (approximately 1.5 km) produced by ECMWF are used as a covariate for understanding the impacts of this quantity on precipitation. These atmospheric air temperature data (i.e., T_a) from ERA-Interim are provided at T255 resolution with 60 levels up to 0.1 hPa, which is adequately above the boundary layer of the atmosphere in comparison with the surface air temperature.

Regression slopes are estimated using the 95th percentile of daily precipitation (P95th) associated with the changes in daily temperature on the Celsius scale (T), which is extracted at the rain gauge locations by bringing the datasets (T_{mean} , T_{max} , T_d , and T_a) to the point scale corresponding to the rain gauge stations. In previous studies, the precipitation scaling has been estimated using binned pairs of events (e.g., temperature and precipitation quantiles for each bin). Here, the scaling is estimated directly using QR (Koenker and Bassett, 1978) and the binning method. For a set of data pairs (x_i, y_i) for $i = 1, 2, \dots, n$, the QR for a given percentile (p) is expressed as:

$$y_i = \beta_0^{(p)} + \beta_1^{(p)} x_i + \varepsilon_i^{(p)} \quad (5.5)$$

where ε_i is an error term with zero mean, and the percentile (p) lies between 0 and 1. Here, y_i represents the logarithmically transformed daily precipitation, and x_i is the corresponding temperature (T_{mean} , T_{max} , T_d , or T_a). The exponential transformation for the regression coefficient $\beta_1^{(p)}$ is used to estimate the change in the regression slope ($\frac{\delta P_{95\text{th}}}{\delta T} (\%)$) as follows (Hardwick Jones et al., 2010; Wasko and Sharma, 2014):

$$\frac{\delta P_{95\text{th}}}{\delta T} (\%) = 100 * (e^{\beta_1^{(p)}} - 1) \quad (5.6)$$

The regression slope is also estimated using the binning method by Lenderink and van Meijgaard (2008). In this method, the observed daily events (precipitation ≥ 1 mm) for each station from 1985 to 2014 are paired with their corresponding predictor variable (i.e., T_{mean} , T_{max} , T_d , or T_a);

1. the pairs are sorted in ascending order according to their corresponding temperatures;

2. the ranked pairs are split into 20 bins at 1°C intervals such that approximately the same number of events are placed in each bin;
3. the linear regressions are performed by forming a dataset for each bin based on the median of their temperatures and the logarithm of the 95th percentile of precipitation; and
4. the change in the regression slope ($\frac{\delta P_{95th}}{\delta T}$ (%)) is estimated by applying the regression equation between each highest to lowest temperature where the 95th percentile of precipitation occurs.

Statistical methods can be applied to evaluate the intensities, quantitative properties and distributions of extreme precipitation (Data, 2009). The generalised extreme value (GEV) method is used to estimate the return levels of extreme precipitation (Coles, 2001). Consecutive non-overlapping blocks are identified by applying the block maxima approach to precipitation at the investigated time durations (i.e., from 5 minutes to 24 hours). The GEV distribution (equation 5.7) is determined by the location parameter (μ), the scale parameter ($\sigma > 0$), and the shape parameter (ϵ), which are measures of the mean, spread and skewness of the distributions of extreme events in a time series (Coles, 2001). Since the climate is non-stationary, the maximum likelihood (ML) method (Jenkinson, 1955) is selected for use in this study (Data, 2009).

$$F(x; \mu, \sigma, \epsilon) = \begin{cases} \exp\left(-\left[1 + \epsilon \frac{x - \mu}{\sigma}\right]^{\frac{1}{\epsilon}}\right), & \epsilon \neq 0 \\ \exp\left(-\exp\left(-\frac{x - \mu}{\sigma}\right)\right), & \epsilon = 0 \end{cases} \quad (5.7)$$

$$\text{where: } \left[x: 1 + \epsilon \frac{x - \mu}{\sigma} > 0 \right], \quad \begin{cases} \mu \in \mathbb{R} \\ \sigma > 0 \\ \epsilon \in \mathbb{R} \end{cases}$$

The stationary GEV distribution assumes constant parameters without any covariates, whereas the non-stationary GEV considers the dependency of the GEV distribution on a covariate or time (Coles, 2001). In this study, the appropriate extreme value analysis, which includes non-stationary distributions, is obtained by the incorporation of covariates into the extreme distribution. The dependence of the location and scale parameters is derived by considering the covariates for each station as follows:

$$\mu = \mu_0 + \sum_{i=1}^k \mu_i (y_i) \quad (5.8)$$

$$\sigma = \sigma_0 + \sum_{i=1}^k \sigma_i (y_i) \quad (5.9)$$

where y_i represents the i th covariate, μ_0 and σ_0 represent a constant offset, and μ_i and σ_i represent a linear dependence on the covariates. The non-stationary properties of the extremes in the present study are obtained using T_d , T_a and the NAO index as the covariates for the location and scale parameters, and the shape parameter is held constant.

The GEV distribution parameters for the observed extreme precipitation at each station are estimated by means of ML estimation (Jenkinson, 1955). The goodness of fit for the influence of covariates is assessed using the log-likelihood ratio test (LRT) (Zhang et al., 2010) with the aid of the following equation:

$$D=2[l^S - l^{NS}] \quad (5.10)$$

Here, l^S and l^{NS} represent the log likelihood of the stationary model and the non-stationary model, respectively. Therefore, the effect of the inclusion of the covariates on the model fit is assessed using the LRT (Zhang et al., 2010). The probability of occurrence of a severe event P is defined as the likelihood of the event happening at least one time on average in N years, so $P = \frac{1}{N}$. For a period N , the long-term return level (r_N) of the occurrence of extreme precipitation can be determined using equation (5.11) (Coles, 2001). Moreover, the confidence intervals of the estimates are derived by 10^4 bootstrap samples of the observations.

$$P(x > r_N) = 1 - F(r_N; \mu, \sigma, \varepsilon) = \frac{1}{N} \quad (5.11)$$

5.3. Results

The rain gauge-based precipitation for a recent 30-year period extending from 1985 to 2014 is investigated using the corresponding mean and maximum surface air temperature, dew point temperature and atmospheric temperature at 850 hPa, which are brought to the point scale of the rain

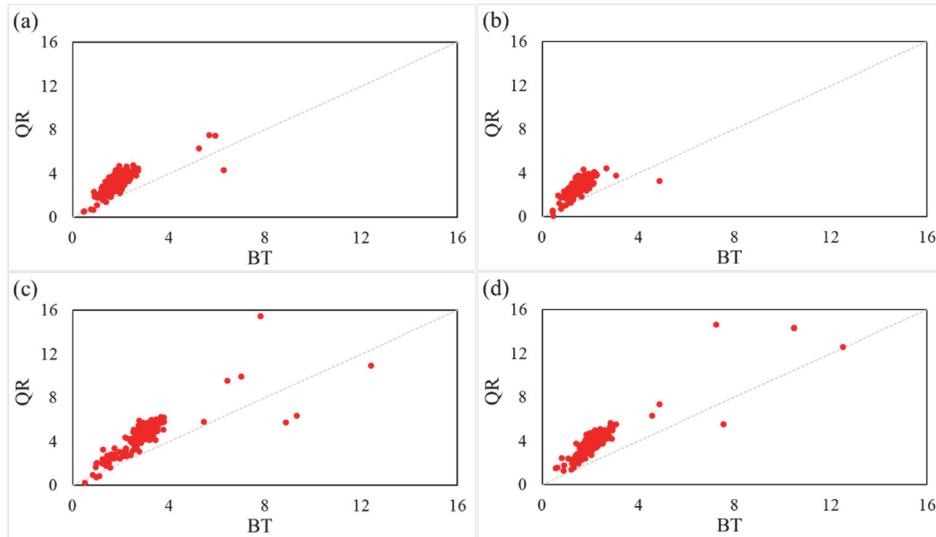


Figure 0.1. Regression slopes ($\frac{\delta P_{95th}}{\delta T}$ (%)) for 231 rain gauge stations (red circles) obtained from quantile regression (QR) and binning method (BT). Panel (a) to panel (d) show precipitation relationship with mean, maximum, dew point and atmospheric temperatures, respectively. The one-one line is shown by grey solid line.

gauges. The regression slopes are estimated using QR between the 95th percentile of precipitation (≥ 1 mm) and the predictors (Tmean, Tmax, Td and Ta). The robustness of the obtained change in the regression slope ($\frac{\delta P_{95th}}{\delta T}$ (%)) determined using the QR method is checked using the binning method (Figure 5.1). Both methods imply a positive scaling relationship for all of the investigated predictor variables for all of the stations. When the entire data set is used, QR gives more robust results, and the variability in the estimates is less than that obtained using the binning method with an equal number of bins (Wasko and Sharma, 2014). The change in the regression slopes obtained using QR.estimated using the binning method are relatively small compared to those

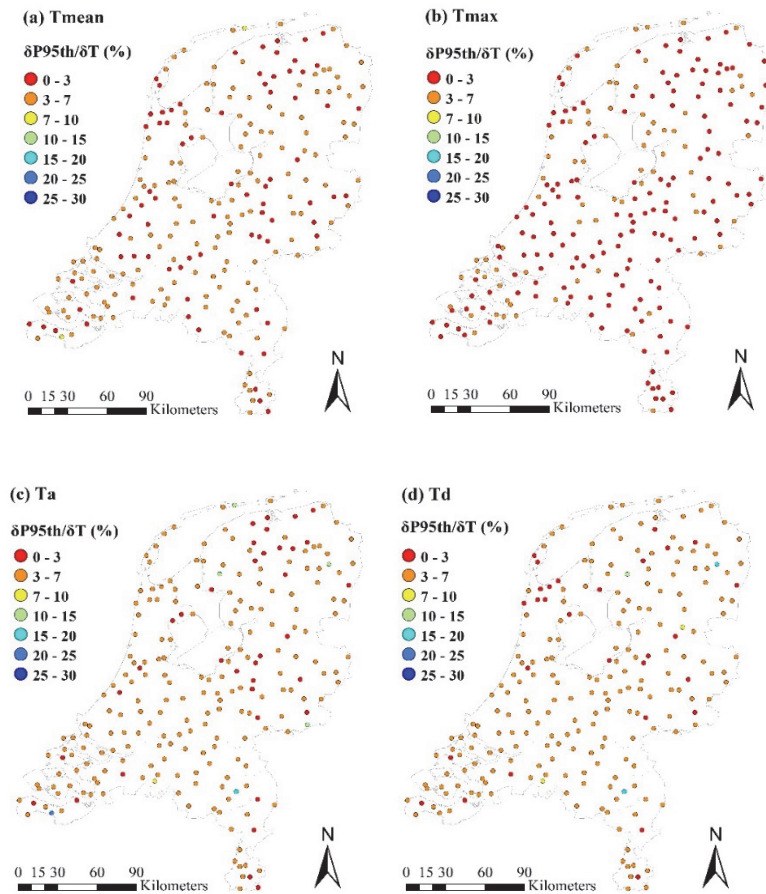


Figure 0.2. Estimated regression slopes ($\frac{\delta P_{95th}}{\delta T}$ (%)) for the 231 rain gauge stations in the Netherlands obtained from the mean surface temperature (Tmean), maximum surface temperature (Tmax), atmospheric temperature at 850 hPa pressure level (Ta) and dew point temperature (Td).

Figures 5.2(a) and 5.2(b) show the regression slopes between P95th and the mean and maximum daily temperature for each station. The regression slopes for the mean temperature are relatively similar to those for the maximum temperature at most of the stations. Increases in atmospheric temperature can induce more intense precipitation (Bengtsson, 2010; Wentz et al., 2007). Similar to the surface air temperature, the regression slope indicates a positive change for all of the stations (Figure 5.2(c)). The relationship between the P95th of precipitation and the dew point temperature, which represents a measure of absolute humidity, is considered instead of the surface air temperature (Figure 5.2(d)). The regression slopes

for P95th-Td indicate greater changes than P95th-Tmean at most of the stations. This result reveals that changes in relative humidity become important, as does the dew point temperature. In fact, the increase in the dew point temperature is somewhat more robust than that in temperature (Attema et al., 2014). Lenderink et al. (2011) found more reliable spatial variations in the changes in the dew point temperature compared to those in the surface air temperature over Europe. Therefore, and because precipitation forms in clouds, Td and Ta may be the predictor variables that are most appropriately used to estimate the temperature sensitivity of the P95th when compared with Tmean and Tmax.

Considering the circulation conditions, the study makes use of the JCT scheme with nine types to classify the weather and circulation type on each day. The frequencies of daily precipitation (08-08 UTC) occurrences are investigated according to the weather types for 231 rain gauges throughout the Netherlands from 1985 to 2014. Figure 5.3(a) shows that the median of the precipitation events is slightly larger for the southerly and westerly weather types than those events for the easterly and northerly weather types. Although the average precipitation is fairly similar among the different weather types, the amount and number of extreme precipitation events (i.e., the upper outliers on the box-and-whisker plots) show the impacts of circulation conditions on the occurrence of extreme precipitation. Therefore, a reliable assessment of the impacts of urban areas on extreme precipitation might be obtained by considering the land-cover type upwind of each station for each wind direction.

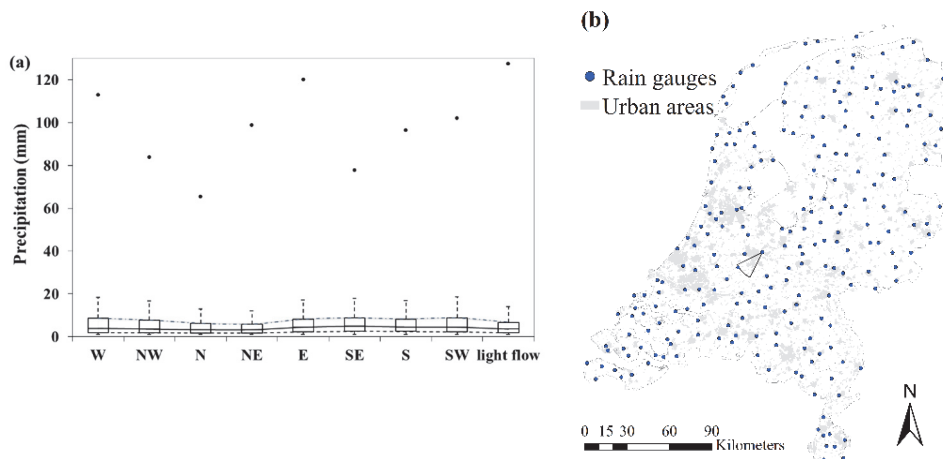


Figure 0.3. (a) Variations in precipitation among the nine weather types during 1985-2014. (b) Locations of rain gauge stations (blue closed circles) and areas of urban land cover (grey shading) in the Netherlands (EEA, 2014). The eighth of a circle with a radius of 20 km radius for the southwesterly geostrophic wind direction (W8) is for the De Bilt station.

To reach this goal, we consider the possible effects of the weather types on precipitation events by defining the urban and non-urban stations separately for each wind direction. The land cover types within 8 octants (eighths of a circle, given the 8 prevailing wind directions) surrounding each station are extracted from the CORINE dataset (Figure 5.3(b)). These octants extend to a distance of 20 km from each station. Depending on the wind direction, the manual rain gauges are classified as urban stations for the corresponding octant when the six aforementioned land-cover categories cover more than 25% of the entire area of the octant; otherwise, they are classified as rural stations. Therefore, the stations are classified in terms of the percentage of urban land use in the eight upwind directions and one in the whole buffer around the stations for the unclassified weather type (i.e., light flow). Throughout the study, the discrepancy between the urban and non-urban areas is evaluated by taking the difference between the average of all of the urban stations and the average of all of the non-urban stations for each wind direction.

To depict the distribution of extreme precipitation in the Netherlands, the monthly maximum of the maximum daily precipitation at the De Bilt station over a 30-year period is shown by a box-and-whisker plot (Figure 5.4(a)). Strikingly, some data points fall above the whiskers, which extend to 1.5 times the inter-quartile range. Moreover, these data points reflect positively skewed distributions, whereas the lower whiskers are limited to the boxes.

The maximum average occurs between July and October, which have larger boxes than the other months. Therefore, it is unreasonable to say that extreme precipitation is stationary in the Netherlands due to the distribution of extreme precipitation and the seasonal variations in their occurrence during this 30-year period. The seasonal variability and non-stationary nature of extreme precipitation are consistent with previous studies that have examined the Netherlands (Buishand et al., 2013; Rahimpour et al., 2017, 2016b). The seasonal precipitation changes are made obvious by the occurrence of larger boxes in the box-and-whisker plots for the summer and autumn, whereas smaller boxes are seen for winter and spring. Figure 5.4(b) demonstrates the fluctuations in the return levels associated with the assessment of impacts using the covariates for the non-stationary estimates (based on the annual block maxima approach) for the De Bilt station. This figure shows that the return levels vary for different return periods with the observed temperature (i.e., T_d and T_a) and the variations in the NAO index. Furthermore, the small correlation coefficient between T_d/T_a and the maximum precipitation show that both covariates can be used together.

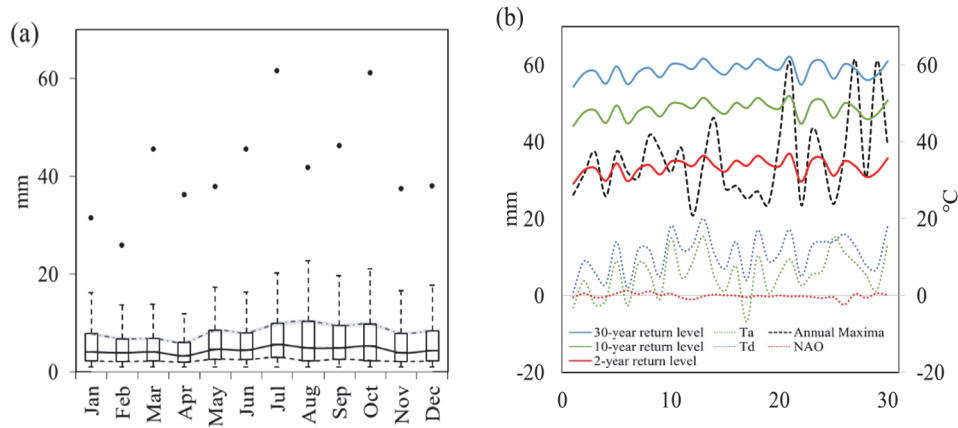


Figure 0.4. (a): Box-and-whisker plot of the maximum daily precipitation and the extended inter-quartile range (i.e., the whiskers extend to 1.5 times the inter-quartile range) for the De Bilt station during 1985-2014. The outlying data points are indicated by black dots. The median of the daily maximum precipitation is displayed by the black solid line shaded in the 95% confidence interval. The dashed and dot-dashed lines show the 0.25 and 0.75 quantiles. (b): The GEV model is fitted to determine the influences of T_a , T_d and the NAO index on annual maximum daily precipitation in De Bilt from 1985 to 2014. The dotted green, dotted blue, dashed black, dotted red, solid red, solid green, and solid blue lines depict T_a , T_d , the annual maxima, the NAO index, and the 2-, 10- and 30-year return level. This diagnostic plot shows that the 2-year return level approximates the median of the GEV distribution.

The seasonal evolution is resolved by considering sub-annual (monthly) blocks, which are sufficiently long to obtain an appropriate convergence of the probability distribution functions (PDFs) of the maximum daily precipitation using the GEV model (Rahimpour et al., 2016a). The suitability of one-month blocks (i.e., no significant improvement is achieved through the use of two-month blocks) has been verified in our previous study (Rahimpour et al., 2016a) for rain gauge stations within the Netherlands during a similar period, and one-month blocks are used in that study to estimate GEV distributions. In this respect, the parameters of the GEV distribution are fitted for all of the precipitation maxima from each month separately (i.e., from January, February and so on) to avoid overlapping precipitation extremes from different seasons. The monthly non-stationary GEV models for the precipitation maxima are estimated using three covariates (i.e., T_d , T_a and the NAO index) in combination with the location and scale parameters at each station. They are combined as linear covariates for the location and scale parameters in Equations (5.8) and (5.9), respectively. The significance of the non-stationary models is tested using the LRT to assess the goodness of fit at each station. Table 5.1 demonstrates the improvement in the non-stationary models in determining their best-fit for parameters' distribution and shows the influence of the covariates at most of the stations for the individual months.

Table 0-1. Percent goodness of fit for the stationary (S) and non-stationary (NS) models

	Jan	Feb	Mar	Apr	May	Jun	Jul	Aug	Sep	Oct	Nov	Dec
S	12	8	12	19	13	7	12	14	8	16	10	12
NS	88	92	88	81	87	93	88	86	92	84	90	88

Assessing the influence of the covariates using the non-stationary GEV models results in less uncertain estimates (i.e., with smaller confidence intervals) at most of the stations, in that they fall within the confidence intervals of those obtained using the stationary GEV models. The best-fitting GEV model at each station (as determined by taking the effects of the covariates on the location and scale parameters into account) is used to estimate the return levels for each month at each station. Figure 5.5 shows the median of the estimated return levels given different return periods and months over all of the stations in the Netherlands. This figure shows clearly that most of the occurrences of precipitation with higher values happen between July and September, and high return levels of extreme precipitation prevail in August. The average precipitation return levels during the given return periods obtained using the non-stationary models are larger than those obtained using the stationary models. These differences show that the stationary models underestimate the return levels, especially in the summer months.

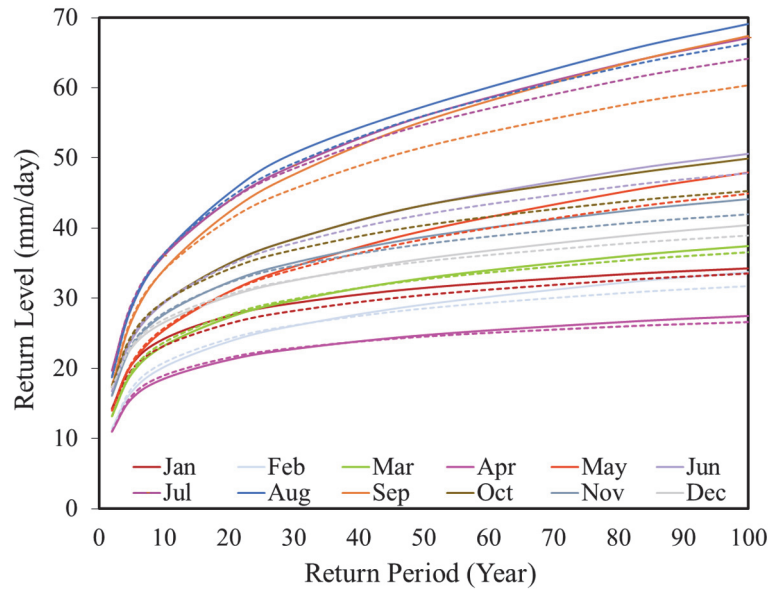


Figure 0.5. Monthly return level for the maximum daily precipitation (median of all rain gauge stations) vs. the return period from the stationary models (dotted lines) and the non-stationary models (solid lines) in the Netherlands from 1985 to 2014.

The urban impacts on extreme precipitation are investigated using the rain gauges and the gridded datasets and by evaluating the return levels of extreme precipitation using the non-stationary models. The variations in the different return levels (i.e., 2, 5, 10 and 30-year) from January to December for the urban and non-urban stations are investigated using the non-stationary models and 30 years of historical data. Figure 5.6 shows that the return levels of extreme precipitation for the urban stations vary similarly to those of the non-urban stations; small values occur in winter, and large values occur in summer. The 2-year return level of daily extreme precipitation varies between 10.7 mm and 20.6 mm for the urban stations and between 10.9 mm and 19.9 mm for the non-urban stations. Likewise, similar differences between the ranges of the urban and non-urban return levels are estimated for the 5-, 10- and 30-year return levels (i.e., 15.5-30.4 mm, 18.2-31.1 mm and 21.5-54.1 mm for the urban stations and 15.5-29 mm, 18.4-36.3 mm and 22.6-51.1 mm for the non-urban stations). The differences in return levels between the urban and non-urban stations increase for larger return periods. The return levels for the urban stations are 5-7% (i.e., the percentage of the ratio between the difference in the return levels of the urban and non-urban stations at each return period and the return levels for the non-urban areas) greater than those of the non-urban

Response of extreme precipitation over the Netherlands to urbanisation

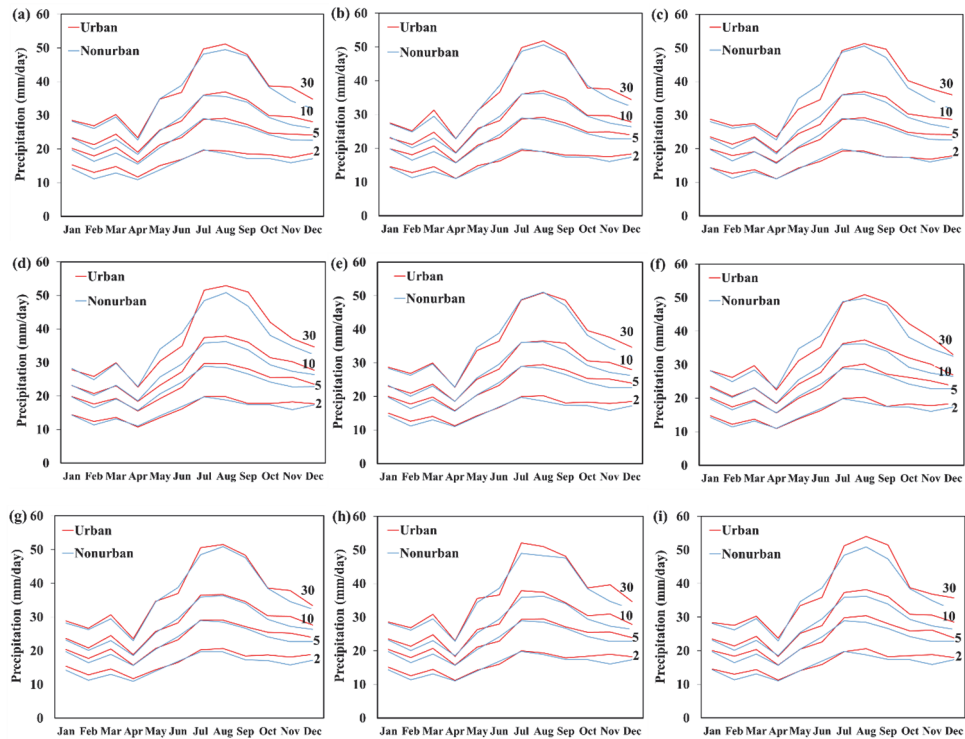


Figure 0.6. Two-, 5-, 10- and 30-year return levels derived using non-stationary models averaged over urban (red lines) and non-urban (blue lines) rain gauge stations in the Netherlands from January to December. Panels (a) to (i) reflect the stations classified as W1 to W9 due to the land use types upwind of the stations.

stations in August throughout the urban type classified as W9. The return levels of extreme precipitation are larger for the urban stations than those for the non-urban stations over all of the months except those between April and June. The discrepancies seen between the urban and non-urban areas during the second half of the year may be partly caused by the increases in temperature and convection caused by the urban heat island (UHI) effect on winter precipitation (Trusilova et al., 2009, 2008).

To extract additional detail on the discrepancies in extreme precipitation between the urban and non-urban areas, precipitation intensities, rather than quantities, are investigated at short time intervals. The precipitation extremes in the Netherlands in August over short time intervals ranging from 5 minutes to 24 hours are investigated using 17 years (1998 to 2014) of

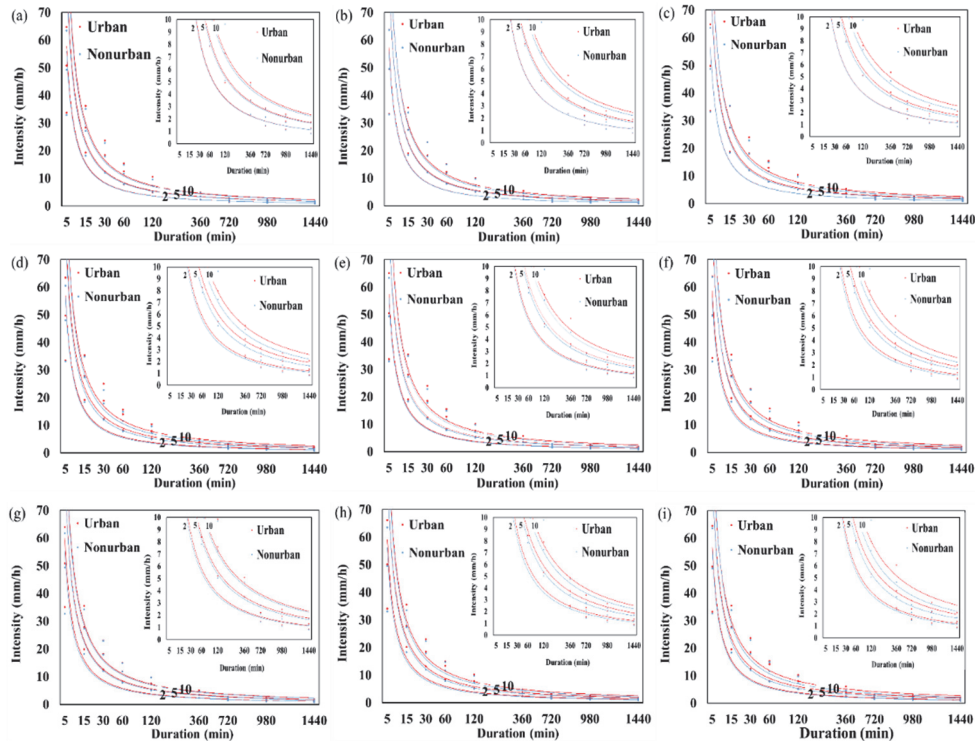


Figure 0.7. Precipitation intensity return levels for 2-, 5- and 10-year return periods for nine stations classified as urban and non-urban within the Netherlands. The estimates are obtained using the non-stationary assumption at each station and averaged over the urban and non-urban stations. The regression lines for the urban (red) and non-urban (blue) stations are indicated by power-law trend lines.

precipitation radar data. The 5-minute radar data are extracted for 231 locations (i.e., the locations of the rain gauges) in the Netherlands. Furthermore, the 5-minute precipitation values are aggregated for 15, 30, 60, 120, 360, 720, 980, and 1440 minutes at the location of each station. The intensity is obtained by dividing the precipitation amount by the duration of the period. The return levels for the intensity of precipitation for August are estimated using a non-stationary GEV model at each station. Similar to the non-stationary models applied to the daily rain gauge data, T_d and T_a are used as covariates of the precipitation intensities and applied to the extremes of the precipitation intensities. The NAO index is excluded from the covariates of extreme precipitation intensity in August because of its negligible impact in the summer months (Haylock and Goodess, 2004). Figure 5.7 shows the intensities at different durations and repetition times (i.e., 2, 5 and 10-year return levels) averaged over the urban and non-urban stations separately. This figure shows that, on average the return levels for

precipitation intensities over the urban areas are larger than those over the non-urban areas over all of the classified stations (particularly for the urban type classified as W9). Although there is some variation in the maximum daily precipitation in the urban and non-urban areas, the urban areas show the highest values; in particular, the differences are clearly larger for longer return periods over all of the classified urban stations. The power (polynomial) regression lines exhibit similar behaviour in the urban and non-urban precipitation intensity return levels, whereas they are larger in the urban areas than in the non-urban areas. The effects of urban areas on extreme precipitation are clearer for shorter durations, where the urban and non-urban areas display larger differences between the precipitation return levels. Therefore, urbanisation leads to increases in precipitation intensity and flood peaks.

In fact, the results demonstrate the overall features of the discrepancies between the urban and non-urban stations; accurate intensity-duration-frequency (IDF) curves at each station are necessary for designing infrastructure and projecting future precipitation return levels. Accurate estimates are difficult to produce due to local differences in precipitation extremes for short durations and limited numbers of long observational time series during the last few years. The differences between the urban and non-urban IDF curves require more consideration of non-stationary models combined with the effects of urbanisation in projecting future extreme precipitation, whereas incorporating non-stationary models requires additional study of the choice of covariates. Understanding the physical causes that underlie extreme precipitation (i.e., circulation and temperatures changes) and the impacts of urbanisation on climate may assist in the development of non-stationary models that can be used to produce improved assessments of the risks related to climate change.

5.4. Discussion

The scaling relationship between precipitation and temperatures is used to simplify the nature of precipitation changes and understand the changes in intensity that may occur in a warming climate (Lenderink et al., 2011; Lenderink and Attema, 2015). The relationship between precipitation and air temperatures is investigated directly using data collected at rain gauges in the Netherlands. This work is carried out using QR and the binning method for each individual station. The binning method is performed by dividing the precipitation values into 20 temperature bins that range from 0 to 20°C and have widths of 1°C. The percentage change in the P95th precipitation quantile in each temperature bin is then estimated for each station. The trend line of the fitted linear regression reveals the relationship between precipitation and temperature as a scaling rate (i.e., $\frac{\delta P_{95th}}{\delta T}$ (%)). Moreover, QR

is also performed for the above process to obtain the trend in precipitation with temperature. Unlike the binning method, QR estimates trends directly (i.e., it is unbiased with the sample size), and no discretisation of the data is required (Wasko and Sharma, 2014). Results obtained using the daily precipitation and temperatures (T_{mean} , T_{max} , T_d , and T_a) show similar trends in precipitation with the temperatures by both binning and QR methods. However, the regression slopes ($\frac{\delta P_{95th}}{\delta T}$ (%)) estimated using QR are slightly larger than those obtained using the binning method. The scaling of precipitation with temperature indicates the efficacy of the dew point and atmospheric air temperatures as covariates that may influence the occurrence of extreme precipitation. From our understanding of the physical basis of precipitation, we expect the effects of the covariates listed above to have importance for the occurrence of extreme precipitation under favourable atmospheric conditions. Moreover, our results are consistent with previous studies that indicate that large stratiform precipitation can change to convective precipitation as temperature increases (Berg et al., 2013).

The influence of atmospheric circulation conditions is studied using the JCT classification scheme for all days between 1985 and 2014. The basic statistics of precipitation are investigated separately for each weather type on each day, and the results demonstrate the dependency of variations in the frequency and intensity of precipitation on the weather types. Whereas the mean of daily precipitation is higher for the W and SW weather types, the maximum daily precipitation is associated with the light flow weather type. Although westerly winds are dominant in the Netherlands, it is unclear which weather type and circulation pattern favour extreme precipitation. Regardless of the lack of available long-term meteorological observations in urban areas in the Netherlands that can be used to assess urban micro-climates and their effects on climatic variables (i.e., precipitation), this study considers rain gauge stations as either urban and non-urban stations for the different wind directions, depending on the types of areas located upwind of the stations (see section 2). This practice helps to produce a comparable discrepancy between the urban and non-urban areas in each classified urban type and tends to produce results that are generally applicable within the country.

The seasonal variations in precipitation are relatively uniform in summer and winter (Attema and Lenderink, 2014; Buishand et al., 2013; Rahimpour et al., 2016a), while there is a coastal gradient in spring and autumn due to the proximity of the North Sea and the influence of the NAO index (Attema et al., 2014). Moreover, extreme convective precipitation is more likely to occur in the summer months, and extreme stratiform precipitation is expected to occur in other seasons (Daniels et al., 2016; Overeem et al., 2009). Therefore, monthly data are valuable for characterising the dominant extreme precipitation. Trends in the monthly maximum precipitation that are

significant at the 5% level have been found by previous studies; hence, precipitation displays non-stationary variations (Buishand et al., 2013; Rahimpour et al., 2017, 2016a). The GEV parameters for extreme precipitation are estimated for each station in every month. The non-stationary GEV model is developed based on the dew point and atmospheric air temperatures (i.e., T_d and T_a) and a large-scale mode of climate variability (i.e., the NAO index) to demonstrate the distribution of monthly extreme precipitation and the return levels. The estimates obtained using non-stationary models fall within the confidence intervals of those obtained using stationary models at most of the stations in the Netherlands. The non-stationary increase in extreme precipitation identified in this study is in accordance with previous studies that have identified a statistically significant increasing trend in extreme precipitation in the Netherlands (Buishand et al., 2013; Overeem et al., 2008a; Rahimpour et al., 2017). The non-stationary models tend to produce more conservative estimates of the return levels of extreme precipitation. The results show that the downwind impacts of urban areas on the return levels of extreme precipitation over the country are relatively small in late spring (i.e., between April and June) and larger at other times. The exception in late spring may be caused by the suppression of shower activity (over the almost 50 km distance to the coast where most of the urban areas in the Netherlands are located) due to low sea-surface temperatures. Daniels et al. (2015a) reported that the precipitation over the coastal areas in the Netherlands in spring is almost 25% less than that over inland areas because of triggering mechanisms (air travelling over the land and planetary boundary layer growth affect cloud formation).

However, urbanisation alters the surface roughness and enhances the turbulence over urban areas (Hamdi et al., 2014). The deeper boundary layers and temperature increases that occur in urban areas change the atmospheric water balance and enhance the water-holding capacity of air (Chen and Hossain, 2016). The largest discrepancy between the urban and non-urban return levels is found under light flow conditions (i.e., the urban type classified as W9). Extreme precipitation events are further found to be most strongly affected by urban land use in the summer months, especially August, and under the urban type classified as W9, among others. The UHI has been found to be higher in August than in other months in the Netherlands (Rahimpour et al., 2018; Wolters and Brandsma, 2012). The higher extreme precipitation in August is in accordance with the findings of previous Dutch studies on precipitation frequency during days where convection plays a relatively important role and maxima occur during the evening and near sunset (Overeem, 2009). Intense precipitation may be caused by increases in the strength of convection due to intensive UHI (Chen et al., 2015; Rahimpour et al., 2018; Yang et al., 2017). The temperature discrepancy between urban and non-urban areas enhances instability and

convective activity over areas downwind from urbanised areas (Lin and Chen, 2011). Increased moisture and upward convergent movement are triggered by UHI circulation patterns (Yang et al., 2017). Thus, the higher temperatures in urban areas that are caused by the UHI circulation and sufficient water vapour could cause more precipitation in urban areas. In other words, moist convection increases precipitation downwind based on the strong UHI and the absence of wind under conducive thermodynamic conditions (Han et al., 2014). In this respect, August is examined using high spatial resolution radar data to highlight the maximum precipitation return levels for different time durations for the urban and non-urban areas. The precipitation intensity return levels indicate similar occurrences for the urban and non-urban stations, with more intensive events for the urban stations. The difference in precipitation intensities between the urban and non-urban stations is clearer for shorter time durations (i.e., 5 minutes) and decreases for longer durations (i.e., 1 day).

The better fits obtained using non-stationary models at most of the stations reveal that the IDF curves derived using the stationarity assumption underestimate extreme precipitation, and this statement is even more true given the increase in the frequency of extreme events that will occur in the future. If an IDF curve based on stationary estimates is used for designing urban infrastructure, neglecting other factors and the impacts of urbanisation, the probability of infrastructure failure is high due to the more extreme precipitation events that are identified by the non-stationary models. In this respect, to obtain accurate IDF curves, the estimation methods should be updated by considering the influence of additional climate variability on extreme precipitation events. However, the selection of covariates is important in finding the precipitation return levels. The results show that ignoring the effects of urbanisation can lead to uncertain estimates of the intensity, duration and frequency of events extreme precipitation, especially for short-duration precipitation. Although this study does not evaluate the uncertainties of the covariates, it shows that extreme precipitation associated with temperature differences between the urban and non-urban areas tend to give less uncertain estimates of return levels in the future. Therefore, the current IDF curves in the Netherlands should be revised by considering appropriate covariates for infrastructure design in the future.

For obtaining more reliable results on precipitation discrepancy between urban and non-urban areas, efforts are needed to examine the impact of bias corrections on observed precipitation variations. The ignored undetected errors in this study (i.e. wind speed-induced errors and seasonal variations) could impact the obtained precipitation discrepancy between urban and nonurban areas. The catch efficiency of precipitation, for example, might be

larger in urban areas than that of non-urban areas where urban stations surrounded by obstacles are exposed to less wind than non-urban stations in open areas. Therefore, the results could be influenced by bias corrected precipitation data regarding temperature, wind speed, drop size and snow percentage (Ding et al., 2007; Sun et al., 2013). Further, it is acknowledged that the investigated rain gauge and gridded radar datasets may not truly reveal the full micro-climate over urban areas (i.e., other factors influence urban meteorology). A larger number of meteorological stations located in Dutch cities would be needed to fully characterize these micro-climates, and these additional stations are currently unavailable. Note that the estimated precipitation return levels and IDF curves require longer-term observations in each region, and the trends in the covariates such as the NAO index may not persist in the coming years and use of climate model simulations might enable extrapolation into the future. Therefore, care should be taken in extrapolating features seen in historical data into the future, especially for longer return periods, during which different physical causes (i.e., natural or anthropogenic forces) may influence the precipitation.

When scaling precipitation on temperatures for local scales, the influences of different mechanisms such as the regional and seasonal precipitation variations should be considered (Schroeer and Kirchengast, 2017). Precipitation dependency on local temperature can be found in regions such as the Netherlands with enough moisture availability (Lenderink and van Meijgaard, 2008; Westra et al., 2014). It is to note that local temperature and global mean temperature usually scales linearly. However, connecting scaling relationship for local temperature and precipitation could be a controversial issue (IPCC, 2014) where different factors involved (e.g. thermodynamic effects (Barbero et al., 2017) and dynamic factors (Drobinski et al., 2018)). Furthermore, changes in the temporal resolution of extreme precipitation and the covariates may cause changes in the scaling rate and the estimated return levels. Sub-daily and hourly long-term data could provide more valuable information for obtaining robust assessments of the sensitivity of the scaling relationship between extreme precipitation and desirable predictor variables, such as the dew point temperature. For instance, Barbero et al. (2017) reported that the response of precipitation to temperature at an hourly resolution is better than that at a daily resolution. Furthermore, other factors, such as the types and sizes of cloud condensation nuclei and the geographical characteristics of stations, can also affect extreme precipitation.

5.5. Conclusions

Knowledge of the impacts of climate warming and urbanisation on the observed trends in extreme precipitation can lead to improved estimates for

the return levels of extreme precipitation. This study considers the factors that likely influence extreme precipitation and extends existing statistical approaches by scaling extreme precipitation and examining non-stationary models that consider covariates (i.e., the dew point and air temperatures). The investigation of the appropriate covariates is done through applying QR and the binning method to precipitation and temperature datasets covering the Netherlands. Since the scaling of precipitation with increasing temperature is positive, the results suggest that the dew point and atmospheric temperatures are appropriate covariates for extreme precipitation. A linear combination of the dew point and the atmospheric temperature at the 850-hPa level, as well as the NAO index, which represents a large-scale influence mode, are applied to estimate the monthly precipitation return levels for different return periods. The study shows that presuming a non-stationary climate could lead to improved estimates of precipitation return levels where the stationary models underestimate the precipitation return levels.

The study makes use of the JCT with nine types to classify weather and circulation types. The dependence of precipitation on circulation conditions leads to the classification of stations as urban and non-urban areas based on their upwind land-use types for each wind direction to investigate the response of extreme precipitation to alternative land-cover types. The maximum daily precipitation for each month is compared between the stations in the regions downwind of urban areas (i.e., urban stations) and the other stations (i.e., non-urban stations). August has the highest return level and frequency for maximum daily precipitation throughout the year. The urban type classified as W9 (light flow conditions) demonstrates the magnitude of the differences between the urban and non-urban precipitation return levels.

This study concludes that, apart from large-scale climate changes, increases in extreme precipitation can be induced by urbanisation. Due to land use and urban climate change, the use of non-stationary models is advised to produce improved estimates of precipitation return levels and to project the frequency and intensity of precipitation in the future.

Chapter 6
Synthesis

The land and atmosphere and land interactions induced by human activities impact the Earth's climate. Climate has changed throughout historical times via the variations of different forcing factors. Climate change at, for example, global, regional and even local scales has been detected by relevant climatic indicators. According to climatological studies, temperature and the frequency and intensity of precipitation have increased. It is predicted that extreme events will increase considerably. Because of land surface forcing, the response of extreme precipitation to the conversion of land into urban areas is important for knowledge about the hydrological cycle. Extreme precipitation variability and water system stability estimates tend to be important issues for human life, particularly in urban areas, which often experience convective precipitation with large amounts of precipitation. The scientific analysis of extreme precipitation can generate essential information for understanding the climate system and adaptation to extremes by increasing confidence in the related risk calculation.

6.1. Precipitation facts

Climate change can cause changes in the frequency of precipitation and extreme events over a majority of land areas (Aguilar et al., 2009; Chen et al., 2012; Doherty et al., 1999; Gutowski et al., 2010; Zhang et al., 2010). The observed climate change in the last century is associated with natural and anthropogenic causes (Van Minnen et al., 2013). Natural variability (e.g., internal modes of climate variability and large-scale circulation) explains much of the global warming at the beginning of the century and the observed climate change in recent decades, although the majority of the increasing climate change seems to be the result of human activities (e.g., anthropogenic heats) over the most recent years (Min et al., 2011, 2009; Stone et al., 2012; Trusilova et al., 2008; Zhang et al., 2013). Global warming can increase the frequency and intensity of precipitation events (IPCC, 2014), as warmer air tends to hold a lot more water vapour than colder air (Barnett et al., 2008; Willett et al., 2008). Increases in extreme precipitation events have consistently been reported to correspond with increases in temperatures (Trenberth et al. 2007, Easterling et al. 2000) and water vapour in the atmosphere (Christensen et al. 2007). The temperature in the Netherlands, for example, increased by 1.8°C from 1901 to 2013, with the increase of 1.4°C from 1951 to 2013, which is clearly higher than the global average increase in temperature (KNMI, 2014). This temperature change increased the atmospheric moisture and subsequently increased precipitation. Climate scenarios for the Netherlands have been developed to describe what people will experience in upcoming years. Climate change will result in a 3-6% increase in precipitation (depending on KNMI climate scenario assumptions), which will lead to more extreme precipitation in the coming years over the Netherlands (KNMI, 2014).

Extensive work has already been dedicated to studying precipitation patterns in the Netherlands (Attema et al., 2014; Buishand et al., 2013; Daniels et al., 2014). The above findings agree with previous reports that regions at high latitudes and in the wet tropics are expected to experience increased precipitation. This scenario, if true, has crucial consequences for the Netherlands. For example, higher precipitation peaks and changes in the pattern and frequency of rainfall will directly impact water management in the Netherlands. The precipitation extremes in autumn 1998 revealed the vulnerability of Dutch regional water systems and caused approximately 0.5 billion euros of damage (Smits et al., 2004).

Extreme precipitation index trends indicate that conditions have become wetter from 1961 to 2014 in the Netherlands. From the analysis in Chapter 3, the spatial patterns of the extreme precipitation indices showed coherent changes between the recent and earlier multi-decadal periods after 1961. A prevailing pattern of significant positive changes was found in the total annual precipitation and extreme precipitation indices in the Netherlands. The maximum of the daily precipitation index, for example, was found from a downward slope in the earlier multi-decadal period to an upward slope in the recent multi-decadal period (Rahimpour et al., 2016b). Furthermore, the percentile indices showed that the increasing change in high quantile precipitation (i.e., P95th and P99th) is more rapid and disproportionate than that of the annual total precipitation across the Netherlands. The long-term change of extreme indices against the WMO 30-year period indicated significant positive trends in the wet indices, resulting in larger annual values (Rahimpour et al., 2017).

6.2. Precipitation effects of land surface

Understanding the particular land surface effect on local climate is useful for improving the urban level of comfort and designing better disaster reaction strategies for hazards, including extreme events. Although natural variability could induce precipitation instability (variation around the mean of observations), land surface changes have similar impacts on precipitation, which makes attribution of precipitation difficult. Land surface changes and surface roughness exert an influence on surface energy (i.e., vertical extent and transport processes in the ABL) against the natural environment. For example, energy can transfer between the land and the lowest layer of the atmosphere as latent and sensible heats (via evapotranspiration and convection, respectively). In vegetated and grassland areas, part of sun's heat is consumed by the evaporation of water, which makes these areas cooler than other areas that have a higher sensible heat. Consequently, the weather may change due to differences in the temperature and water availability (i.e., atmospheric moisture) between two places (e.g., a vegetated area and its

surrounding areas). Urbanisation has a very pronounced effect on land surface change, which could potentially cause changes in atmospheric parameters and therefore affect changes in the spatiotemporal distribution of precipitation attributes. Urbanisation forms urban canopy layers of buildings, changes the local land cover, modifies the radiation, thermal and dynamic characteristics of the underlying surface, and makes the land cover in the urban area very different from that of surrounding rural areas. Since there is less vegetation and uncovered soil in cities than in non-urban areas, the vast majority of the sun's energy is absorbed by urban constructions and asphalt. Therefore, during the warm hours of a day, the relatively low amount of evaporative cooling in urban areas leads to higher temperatures in urban areas than in rural areas. Cars and industrial facilities generate additional urban heat from industrial and domestic heating and cooling devices (Brand, 2010). These differences cause a horizontal gradient of energy and moisture from the surrounding environment to the urban area, which impacts boundary layer characteristics. Urban influences on precipitation have been extensively studied in recent decades, and urban surface roughness, urban aerosols and UHIs have been identified as the main mechanisms of urban-induced precipitation. A comprehensive literature review of urban modifications to precipitation is given by Shepherd (2005) and Han et al. (2014). Surface roughness is greater in urban areas than in surrounding areas, which leads to changes in airflow, and diverted air can result in updrafts downwind of urban areas (Cotton and Pielke Sr, 2007). The urban modification of precipitation further depends on the sources of water vapour and the degree of surface roughness. Changes in aerosol concentrations could increase precipitation when the available water vapour is high and convection is strong (Han et al., 2014). Evidence of human-induced aerosol enhancement can be detected by monitoring weekly cycles of observed meteorological variables such as precipitation (Beck, 2012; Stallins et al., 2013; Stjern, 2011). However, the existence of a consistent weekly cycle has neither been found over Europe (Beck, 2012; Stjern, 2011) nor been found for precipitation from 1951 to 2010 over the Netherlands (Daniels et al., 2015b). The UHI as a heat source in the lower level of atmosphere produces dynamic upward motion/flow. This UHI-induced flow initiates moist convection under the proper thermodynamic conditions, which could be responsible for urban-modified precipitation. The UHI has been identified during the last decade across the Netherlands (Theeuwes et al., 2016; Van Hove et al., 2011; Wolters and Brandsma, 2012). In Chapter 4, the UHI, temperature and precipitation distributions were investigated for individual months. The seasonal change in the magnitude of the observed UHI revealed greater values after late spring. The temperature impacts on the frequency and intensity of extreme precipitation were displayed by the plotted relation between the hourly temperature and extreme precipitation (Figure 4.6), where the difference between the urban and rural precipitation tended to be greater in summer months.

6.3. Seasonality of extreme precipitation

Although total annual precipitation is usually used in water studies, the temporal distribution and seasonal timing of precipitation are important for agriculture, floods, soil erosion and many water and environmental processes. There are valid reasons for the investigation of the seasonal variability of extreme precipitation; daily precipitation in the Netherlands follows a pronounced annual cycle. Daniels et al. (2014) demonstrated that seasonal precipitation means were higher in summer and autumn and lower in winter and spring during the 1951-2009 period. Moreover, changes in precipitation have been found to be inhomogeneous throughout the year. For 1910-2009, Buishand et al. (2013) found an average change in the mean annual precipitation of 25%, with values of 16% and 35% in summer and winter, respectively. Winter precipitation on average is slightly (8%) higher than summer precipitation in the Netherlands (Sluijter et al., 2011). However, this difference in precipitation greatly varies from year to year (e.g., the amount of winter precipitation was higher in 1998 and lower in 2003) (Van Minnen et al., 2013). Based on the occurrence and distribution of heavy precipitation (more than 10 mm), the summer half-year (between June and November) had a higher percentage of heavy rainfall, especially in July and August, during the 1961-2014 period than during earlier periods (Rahimpour et al., 2016a). Furthermore, the two most widely used extreme precipitation indices (i.e., monthly maximum 1-day and consecutive 5-day precipitation (mm), P_{x1} and P_{x5} , respectively) indicate that after 1961, the occurrence of maximum precipitation in summer and autumn has increased (Rahimpour et al., 2016b).

EVT has been used for analysing 1-day extreme precipitation, which has been widely applied in hydrology and climatology (Beirlant et al., 2006; Coles, 2001). Extreme precipitation is mostly investigated by annual or seasonal/monthly maxima. The block maxima approach aims to acquire the probability distribution of the maximum value of blocks, dividing observed time series into equal-length blocks. In Chapter 2, three statistical approaches (the use of block maxima, a stationary model and a nonstationary model) were examined to model the annual cycle of daily extreme precipitation. The GEV model is considered a canonical model for the block maxima approach. The models were developed for the annual cycle of daily extreme precipitation for each station across the Netherlands. Choosing monthly maxima instead of annual maxima reduces seasonal variation in blocks, and as a result, the assumption of independent and iid events is easier to fulfil (Maraun et al., 2009). The sensitivity of block length was examined for one-month and two-month blocks, and the one-month block length was identified as the most suitable option. The developed GEV models include the annual cycle in the form of harmonic functions for the location and scale parameters and an invariant shape

parameter. The parametric form of the developed model reduces the uncertainty of GEV parameter estimations.

The time dependence of extreme precipitation characteristics was revealed by GEV harmonic functions and by analysing a set of daily observations from 231 rain gauges across the Netherlands. Furthermore, the nonstationary GEV models were determined by fitting the GEV models with the monthly North Atlantic Oscillation (NAO) as the dominant teleconnection pattern for seasonal climatic variations in the Netherlands. The selected nonstationary models indicated that the observed variation in extreme precipitation was linked to the NAO. The larger-scale parameter led to a greater spread of the extreme precipitation distribution. The NAO index was on average associated with the extreme precipitation intensification in the Netherlands. This link between the NAO and extreme precipitation not only undermines the basic assumption of stationary data for precipitation but also reveals the fluctuations of precipitation intensity in the Netherlands are connected with the NAO pattern.

The nonstationary model estimated narrower confidence intervals (CI) than the stationary models for the location and scale parameters of all stations between March and November. A narrower CI was found for the shape parameter of all stations for all months. The seasonal variation of the location parameter was stronger than that of the scale parameter in the western part of the country. The maximum values and relative amplitude of the location parameter were found in the summer half-year (between June and November) in the west and in the winter half-year (between December and May) in the east. The maximum values for the relative amplitude of the scale parameter occurred in spring (March-May) in the west of the country and in early summer in the east of the country. The monthly maximum daily precipitation amounts and trends increased more dramatically over the recent multi-decadal period than over the previous period (Chapter 3), and the differences between these two multi-decadal periods were greatest in July and August and smallest in June. This discrepancy between trends had the smallest value in March and the largest values in July and August.

The monthly return level pattern was estimated with the nonstationary models at each station. The information from all months was applied with the sinusoidal model of the location and scale parameters, which led to a reduction in the degrees of freedom in the model (Maraun et al., 2009), implying a reduction in the uncertainty of the return levels or other derived quantities. The 10-year return level was estimated by the highest value in the summer half-year and varied from approximately 20 mm in winter to nearly 33 mm in summer (Figure 2.5). Similarly, the 50-year return level of extreme precipitation varied between 28 mm and 50 mm. Although large quantities of moisture are transferred from the North Sea to the Netherlands by the

prevailing south or southwest wind (Sistermans and Nieuwenhuis, 2004; Stolk, 1989), precipitation is probably reduced by the lower water temperature of the North Sea off the western Netherlands. The changes in circulation (van Haren et al., 2013) and the increases in SST near the Netherlands (Lenderink et al., 2009) could lead to higher extreme precipitation along the west coast during the summer half-year. The west coast has lower extreme precipitation than the inland areas in late winter and spring and higher extreme precipitation in summer and autumn. Changes in extreme precipitation in the winter half-year could be induced by the NAO index, which notably increased before the early 1990s and has decreased strongly in recent decades.

The distinct seasonal cycle of the maximum hourly precipitation during the 5-year period from 2011 to 2015 follows the seasonal pattern of urban-related warming (Chapter 4). The demonstrated closed loop (Figure 4.7) showed that hourly precipitation occurred more in summer and early autumn than in other seasons. Likewise, similar results were found for the maximum hourly UHI, which depicted the strongest values in summer and quicker warm-up and cool-off rates in spring and autumn, respectively. Furthermore, the return levels were estimated with nonstationary models by taking the NAO index, dew point and atmospheric temperature values as the covariates of the location and scale parameters (Chapter 5). Compared with the return levels derived using the nonstationary models, the return levels were underestimated using the stationary models, especially for summer months. The estimations showed that of the highest extreme precipitation values will occur between July and September, with high return levels of extreme precipitation prevailing in August.

6.4. Spatial precipitation pattern and trends

The spatial patterns and regional differences of extreme precipitation could provide details for a better understanding of the risks of hydrological events to human life. The KNMI statistics revealed that the daily precipitation anywhere in the Netherlands is between 50-62 mm and 73-90 mm for every 10-year and 100-year period, respectively. In addition the chance of extreme precipitation (due to a higher annual precipitation amount) is greater in the west, southeast and middle of the country (i.e., the Hague, Vaals and Veluwe areas); the towns within the east and south of the country (Twente and Brabant) have already been confronted with flooding for a considerable time, making these hydrological issues more severe (Hooimeijer and van der Toorn Vrijthoff, 2014). In Chapter 2, the spatial pattern of daily extreme precipitation characteristics from the GEV parameter was illustrated by the relatively high location values in the west of the Netherlands (especially along the central west coast), as well as in the middle of the country (the Veluwe area). The southwest and southeast corners of the country (the province of Limburg) also had higher location

parameter values than other parts of the country. The relative amplitude of the location parameter decreased from the west towards the east (i.e., from 30% to 1%). The annual mean of the scale parameter was the highest in the west, southwest and middle of the country and the lowest in the north and south of the country. The relative amplitude of the scale parameter showed a gradient from west to the east (i.e., from 1% to 40%) that was weaker along the west coast areas than in other parts of the country.

The monthly maximum daily precipitation exhibited greater changes in the west of the country than in the east of the country, especially in August (Chapter 3). The estimated return levels for the 10-year and 50-year return periods revealed constant high values for all months in the southeastern corner of the country, possibly due to the orography of this part of the Netherlands. Return levels with higher values were estimated over the forestlands in the middle of the country in spring. Moreover, the return levels across the north part of the country increased from the winter half-year to the summer half-year. The return levels in the east of the country were still lower than those in the west of the country. The prevailing westerly winds and distance to the coast may also be reasons for this difference (Lenderink et al., 2007).

6.5. Urbanisation effects

Regarding the urbanised areas of the Netherlands, 90% of the Dutch population is concentrated in urban regions with at least 90,000 inhabitants. The urbanisation and average population growth rates indicate urbanisation has been fairly rapid in the Netherlands. Urban area development has occurred in the Netherlands over the recent multi-decadal period (Feranec et al., 2007), and Hazeu and De Wit (2004) detected a 4.76% change in the land surface of the Netherlands between 1986 and 2000. Additionally, Daniels et al. (2015b) found that the urban land use along the west coast of the Netherlands increased from 14% in 1960 to 33% in 2010. This increase in urban land use might have contributed to influences on the local climate. Therefore, in addition to other external factors, land use type should be treated as an external factor that affects extreme precipitation patterns.

Projected precipitation maps based on KNMI scenarios were produced with historical precipitation data (from 1980 to 2010) scaled using the delta change method to represent future precipitation data (van den Hurk et al., 2014). The possible impacts of other factors, such as urbanisation, on precipitation variation were disregarded in this approach. The effects of local land use on climate and extreme events are debatable in the Netherlands (Daniels et al., 2015b; Dekkers et al., 2012; Hazeu et al., 2011). The possible influence of land surface change on extreme precipitation events remains an interesting topic to study, particularly for land use changes due to urbanisation. In this

respect, the precipitation discrepancy between urban and non-urban areas is considered throughout the present thesis to detect possible urbanisation effects on extreme precipitation changes in the Netherlands.

The evidence of precipitation discrepancies between urban and non-urban areas presented in this study is in accordance with previous studies of urban impacts on precipitation. Statistical analyses of rain gauge stations (Chapter 3), amateur stations (Chapter 4) and radar data (Chapter 5) throughout the thesis consistently indicated that urban impacts enhance extreme precipitation. Higher precipitation was found in urban areas than in non-urban areas, depending on factors such as the studied index, month, coastal distance, time duration and geostrophic wind direction. Analysis of urban and non-urban precipitation indicated that the extreme precipitation occurrences in urban areas were larger than those in non-urban areas. The possible impacts of urbanisation on extreme precipitation (e.g., variability in probability and distribution) are persistent, and scenarios of future extreme events may need to be updated to reflect these impacts.

In Chapter 3, the patterns of extreme precipitation indices for urban stations were similar to those for the non-urban stations from 1961 to 2014. Discrepancies between the urban and non-urban stations were investigated by the categorized stations in different regions, which were influenced by similar external forces such as distance to the coast and SST impacts. The urban stations revealed a higher positive change in extreme indices than the non-urban stations over the last 54 years. The slopes of the index changes with respect to the WMO reference period were steeper at the urban stations than at the non-urban stations for the recent few decades. Regions were created based on the distance to the coast to disentangle the coast-inland precipitation gradient; via this method, the differences between urban and non-urban precipitation in the same region can be attributed to urban land use influences. The estimated standardized monthly maximum daily precipitation (PI) for the WMO reference period was greater overall in urban areas than in non-urban areas in the same defined regions (Rahimpour et al., 2017). Although there were some exceptions, depending on the selected region and month, the difference in extreme precipitation index change between the urban and non-urban stations were the greatest in the populated western part of the country than in other parts of the country.

In Chapter 4, the study investigated the temperature and precipitation variations due to urbanisation impacts. Urban stations were paired with their nearest rural stations to reduce other external forces in the investigation of urban impacts on temperature and precipitation. The average hourly precipitation amount was estimated to be approximately 7% greater in urban areas than in the surroundings for a 5-year period (2011-2015). The hourly

precipitation in the urban areas increased more than that in the surrounding areas in late summer and early autumn. In addition to other physical causes underlying this discrepancy, the UHI affected urban precipitation. The urban impacts were evident when the maximum hourly precipitation was plotted against the maximum hourly UHI. The urban-related discrepancy showed a distinct seasonal cycle that was the largest from August to October and smaller in other months. Higher differences in the hourly precipitation between urban areas and surrounding areas were found during the night in summer. The location parameter of the monthly maximum one-hour precipitation for the same period was estimated, with the highest and lowest values in August and December, respectively. These differences between urban and rural precipitation are in accordance with the highest location parameter values for the maximum hourly precipitation and UHI effect in summer. The maximum estimated hourly precipitation in urban areas was approximately 11% higher than that in surrounding areas in August. This intensive precipitation may be caused by the greater UHI effect associated with increased water vapour and convergence due to upward air movement (Chen et al., 2015; Yang et al., 2017).

A better understanding of extreme precipitation variations was provided in Chapter 5 using quantile regression and a binning method for scaling the high quantile precipitation. The positive regression slopes were estimated between the 95th percentile of precipitation (P95th) and the dew point and air temperatures. The dew point and atmospheric air temperatures were found to be appropriate predictor variables to represent the temperature sensitivity of P95th under surface air temperature changes induced by climate warming (Lenderink et al., 2011; Lenderink and Attema, 2015). In this respect, these variables were applied as covariates for extreme precipitation events. In particular, these variables might have affected extreme precipitation under favourable atmospheric conditions, i.e., large stratiform to convective precipitation for lower to higher temperatures (Berg et al., 2013).

The geostrophic wind direction (JCT scheme) was used to classify the weather type of each day. Because of the impacts of circulation conditions on precipitation, urban and non-urban areas were defined by considering the upwind land cover of a station within a 20 km radius for different wind directions. This method for analysing precipitation has already been applied by previous studies in the Netherlands (Daniels et al., 2015b; Witter, 1984), in which a precipitation enhancement of 20% was detected in the downwind regions of urban areas across the Netherlands. The return levels of the urban and non-urban stations in this study were estimated by nonstationary models for individual months from 1985 to 2014. A similar variation in the return levels of maximum daily precipitation was found for urban and non-urban areas throughout the year. The estimate range showed that return levels vary, with

larger values over urban areas than over non-urban areas. The return levels of maximum daily precipitation were found, on average, to be 5-7% larger in urban areas than in non-urban areas. The downwind effects of precipitation return levels were revealed over the year, with the exception of April to June. The low SST and the air travelling from the coast over the land could suppress shower activity in the spring season over the Dutch coast, which contains the most urbanised areas in the country (Daniels et al., 2015a). The largest estimations in August might be due to the higher temperature discrepancy between the urban and non-urban areas (i.e., UHI increases lead to enhanced convection) (Overeem, 2009; Rahimpour et al., 2018; Wolters and Brandsma, 2012). The relatively high precipitation downwind of urban areas might be triggered by the higher temperature in urban areas than in non-urban areas (due to the UHI circulation) and moist convection under favourable atmospheric conditions (Han et al., 2014).

Increases in the intensity and amplitude of heavy precipitation in the coming years have been projected over Europe (Fischer and Knutti, 2016; Gao et al., 2016; Scoccimarro et al., 2016). Regarding future precipitation, van Luijtelaar et al. (2008) demonstrated that the daily rainfall intensity could be expected to increase by 10% to 50% in 2100 for a 10-year return period in the Netherlands. At Uccle, Belgium (which has a similar climate as the Netherlands), Willems (2013) demonstrated that the storm intensity for a 10-year return period could increase by more than fifty percent by the end of the 21st century. In Chapter 5, the differences between the extreme precipitation of urban and non-urban areas were further demonstrated using high spatial and temporal resolution radar data for short time durations. All stations had similar precipitation intensity return levels, and urban areas had more intensive precipitation than non-urban areas. The higher precipitation in the shorter durations for urban areas may be due to urbanisation effects that increase the precipitation intensity and flood peak. The speed at which this consequence occurs will depend on the details of the estimated extreme variation a given site. By being familiar with the effects of possible changes within the expected precipitation trend, the capability to assess future water management needs will increase substantially.

6.6. Future research

Extreme precipitation events can cause severe impacts on infrastructural, agricultural, biological and socio-economic systems (Berg et al., 2013; Gutowski et al., 2010; Nicholls and Alexander, 2007). Moreover, severe damage and street inundations could be induced by precipitation extremes that exceed the capacity of urban sewer systems. Improved knowledge of the impacts of climate change and urbanisation on extreme precipitation events could clarify the conditions that people will face in coming years. The stability

of land-atmosphere interactions is the main driver of weather and/or climate modifications. However, the strength of land-atmosphere coupling as a single metric is questionable due to the influences of different atmospheric parameters on the strength of this coupling (Guo et al., 2006; Koster et al., 2006). The observed large-scale precipitation change, for example, is hardly attributed to human activities (e.g., land surface change) because of the high spatiotemporal variability and regional sensitivity of precipitation (Allen and Ingram, 2002; Zhang et al., 2007). Therefore, the roles of external forcing on extreme precipitation at a local scale for urban and non-urban areas should be studied in more detail to disentangle changes in extreme precipitation caused by changes in climate and urbanisation.

The major limitation of this study was related to the use of observed data, which provides spatially and temporally limited information for long-term periods at a given location. Due to the lack of a sufficient number of meteorological observations, especially in cities and urban areas, the robustness of findings about the impacts of urbanisation on local climates is questionable. The extreme precipitation attributions were limited by the incompleteness of the analysis assumptions and the available spatiotemporal data. Further studies should pay more attention to data (quality of observations and types of sources) and analysis approaches. Extreme precipitation analysis could be improved by the use of additional data sources, such as radar and satellite records, which are detailed and spatially adjusted. Personal weather stations are another source of observations that, after quality control, can provide valuable time series of meteorological parameters at the local scale. Considering data quality (especially for observations in cities) and investigating homogenized hourly and sub-hourly data would help to elucidate the mechanism underlying precipitation occurrences. High-resolution synoptic observations can enable the detection of precipitation changes for convective and stratiform systems separately. This method would disentangle the extreme precipitation trends caused by changes in climate and urbanisation. For example, scaling convective precipitation associated with other meteorological variables in urban areas may improve our understanding of the effects of urbanisation on precipitation extremes.

Knowledge of the meteorological causes of extreme precipitation events is important for future studies. This study showed that dew point and air temperature changes could be explanatory factors for extreme precipitation. In addition to these factors, further studies on the influences of urbanisation on vertical instability and wind shear are important to understand the formation and intensity of precipitation.

In addition to the data sources, the best fit of predictors could be assessed by adopting a new approach using the multivariate statistical method, which helps

to understand the physical causes behind the seasonal and spatial variations in extreme precipitation. Future investigations of nonstationary extreme events could be extended to include the evaluation of further meteorological aspects and regional characteristics, which might permit a more reliable prediction of the variation and distribution of extreme precipitation in the Netherlands. It should be noted that for drawing firm conclusion, new observations in the case study with similar local conditions (e.g., some measurements in rural areas and a few in the urban-influenced neighbours and others far away) are needed to better quantify the instrumental errors and uncertainties.

Bibliography

- Aalbers, E.E., Lenderink, G., van Meijgaard, E., van Den Hurk, B.J.J.M., 2017. Local-scale changes in mean and heavy precipitation in Western Europe, climate change or internal variability? *Clim. Dyn.* 0, 0. doi:10.1007/s00382-017-3901-9
- Ackerman, B., Changnon, S., Dzurisin, G., 1978. Summary of METROMEX, volume 2: Causes of precipitation anomalies. Urbana.
- Aguilar, E., Aziz Barry, A., Brunet, M., Ekan, L., Fernandes, A., Massoukina, M., Mbah, J., Mhanda, A., do Nascimento, D.J., Peterson, T.C., Thamba Umba, O., Tomou, M., Zhang, X., 2009. Changes in temperature and precipitation extremes in western central Africa, Guinea Conakry, and Zimbabwe, 1955–2006. *J. Geophys. Res.* 114, D02115. doi:10.1029/2008JD011010
- Akaike, H., 1974. A New Look at the Statistical Model Identification. *IEEE Trans. Automat. Contr.* 19, 716–723. doi:10.1109/TAC.1974.1100705
- Alfieri, L., Feyen, L., Dottori, F., Bianchi, A., 2015. Ensemble flood risk assessment in Europe under high end climate scenarios. *Glob. Environ. Chang.* 35, 199–212. doi:10.1016/j.gloenvcha.2015.09.004
- Allen, M.R., Ingram, W.J., 2002. Constraints on future changes in climate and the hydrologic cycle. *Nature* 419, 224–232. doi:10.1038/nature01092
- Altaratz, O., Koren, I., Remer, L.A., Hirsch, E., 2014. Cloud invigoration by aerosols—Coupling between microphysics and dynamics. *Atmos. Res.* 140, 38–60.
- Anagnostopoulou, C., Tolika, K., 2012. Extreme precipitation in Europe: statistical threshold selection based on climatological criteria. *Theor. Appl. Clim.* 107, 479–489. doi:10.1007/s00704-011-0487-8
- Arnbjerg-Nielsen, K., Willems, P., Olsson, J., Beecham, S., Pathirana, A., Bülow Gregersen, I., Madsen, H., Nguyen, V.T. V., 2013. Impacts of climate change on rainfall extremes and urban drainage systems: A review. *Water Sci. Technol.* 68, 16–28. doi:10.2166/wst.2013.251
- Arnds, D., Böhner, J., Bechtel, B., 2017. Spatio-temporal variance and meteorological drivers of the urban heat island in a European city. *Theor. Appl. Climatol.* 128, 43–61. doi:10.1007/s00704-015-1687-4
- Attema, J.J., Lenderink, G., 2014. The influence of the North Sea on coastal precipitation in the Netherlands in the present-day and future climate. *Clim. Dyn.* 42, 505–519. doi:10.1007/s00382-013-1665-4
- Attema, J.J., Loriaux, J.M., Lenderink, G., 2014. Extreme precipitation response to climate perturbations in an atmospheric mesoscale model. *Environ. Res. Lett.* 9, 014003. doi:10.1088/1748-9326/9/1/014003
- Barbero, R., Fowler, H.J., Lenderink, G., Blenkinsop, S., 2017. Is the intensification of precipitation extremes with global warming better detected at hourly than daily resolutions? *Geophys. Res. Lett.* 44, 974–983. doi:10.1002/2016GL071917

- Barnett, T.P., Pierce, D.W., Hidalgo, H.G., Bonfils, C., Santer, B.D., Das, T., Bala, G., Wood, A.W., Nozawa, T., Mirin, A.A., Cayan, D.R., Dettinger, M.D., 2008. Human-Induced Changes in the Hydrology of the Western United States. *Science* (80-.). 319, 1080–1083. doi:10.1126/science.1152538
- Beck, C., 2012. Are there weekly cycles in occurrence frequencies of large-scale circulation types? *Atmos. Sci. Lett.* 13, 238–243. doi:10.1002/asl.389
- Beirlant, J., Goegebeur, Y., Segers, J., Teugels, J.L., 2006. *Statistics of extremes: theory and applications*. John Wiley & Sons.
- Bengtsson, L., 2010. The global atmospheric water cycle. *Environ. Res. Lett.* 5. doi:10.1088/1748-9326/5/2/025202
- Berg, P., Moseley, C., Haerter, J.O., 2013. Strong increase in convective precipitation in response to higher temperatures. *Nat. Geosci.* 6, 181–185. doi:10.1038/ngeo1731
- Brand, S., 2010. *Whole earth discipline*. Atlantic Books Ltd.
- Brandsma, T., GP., K., HRA., W., 2003. Empirical estimation of the effect of urban heat advection on the temperature series of De Bilt (The Netherlands). *Int. J. Climatol.* 23, 829–845. doi:10.1002/joc.902
- Brandsma, T., Wolters, D., 2012. Measurement and statistical modeling of the urban heat island of the city of Utrecht (Netherlands). *J. Appl. Meteorol. Climatol.* 51, 1046–1060. doi:10.1175/JAMC-D-11-0206.1
- Buishand, A., Jilderda, R., Wijngaard, J., 2010. Regional differences in the extreme rainfall climatology in the Netherlands. *Trienn. Sci. Rep.* 2007-2009 34.
- Buishand, T.A., 1991. Extreme rainfall estimation by combining data from several sites. *Hydrol. Sci. J.* 36, 345–365. doi:10.1080/02626669109492519
- Buishand, T.A., De Martino, G., Spreeuw, J.N., Brandsma, T., 2013. Homogeneity of precipitation series in the Netherlands and their trends in the past century. *Int. J. Climatol.* 33, 815–833. doi:10.1002/joc.3471
- Buishand, T.A., Velds, C.A., 1980. *Neerslag en verdamping*. Koninklijk Nederlands Meteorologisch Instituut.
- Buishand, T.A., Wijngaard, R., J.B., J. en, 2009. *Regionale verschillen in extreme neerslag*.
- Burauskaite-Harju, A., Grimvall, A., Brömssen, C. Von, 2012. A test for network-wide trends in rainfall extremes. *Int. J. Climatol.* 32, 86–94. doi:10.1002/joc.2263
- Burnham, K.P., Anderson, D.R., 2002. Model selection and multimodel inference: a practical information-theoretic approach, *Ecological Modelling*. doi:10.1016/j.ecolmodel.2003.11.004
- Burnham, K.P., Anderson, R.P., 2004. Multimodel Inference: Understanding AIC and BIC in Model Selection. *Sociol. Methods Res.* 33, 261–304. doi:10.1177/0049124104268644

- Casanueva, A., Rodríguez-Puebla, C., Frías, M.D., González-Reviriego, N., 2014. Variability of extreme precipitation over Europe and its relationships with teleconnection patterns. *Hydrol. Earth Syst. Sci.* 18, 709–725. doi:10.5194/hess-18-709-2014
- CBS, 2015. Toelichting Wijk- en Buurtkaart 2013, 2014 en 2015, www.cbs.nl.
- Chen, H., Sun, J., Chen, X., Zhou, W., 2012. CGCM projections of heavy rainfall events in China. *Int. J. Climatol.* 32, 441–450. doi:10.1002/joc.2278
- Chen, S., Li, W.-B., Du, Y.-D., Mao, C.-Y., Zhang, L., 2015. Urbanization effect on precipitation over the Pearl River Delta based on CMORPH data. *Adv. Clim. Chang. Res.* 6, 16–22. doi:10.1016/j.accre.2015.08.002
- Chen, X., Hossain, F., 2016. Revisiting Extreme Storms of the Past 100 Years for Future Safety of Large Water Management Infrastructures. *Earth's Futur.* 4, 306–322. doi:10.1002/2016EF000368
- Christensen, J.H., Hewitson, B., Busuioc, A., Chen, A., Gao, X., Held, R., Jones, R., Kolli, R.K., Kwon, W.K., Laprise, R., 2007. Regional climate projections, in: *Climate Change, 2007: The Physical Science Basis. Contribution of Working Group I to the Fourth Assessment Report of the Intergovernmental Panel on Climate Change*, University Press, Cambridge, Chapter 11. pp. 847–940.
- Chrysanthou, A., Van Der Schrier, G., Van Den Besselaar, E.J.M., Klein Tank, A.M.G., Brandsma, T., 2014. The effects of urbanization on the rise of the European temperature since 1960. *Geophys. Res. Lett.* 41, 7716–7722. doi:10.1002/2014GL061154
- Claeskens, G., and Hjort, N.L., 2008. *Model selection and model averaging.*, Cambridge University Press. doi:10.1080/02664760902899774
- Coles, S., 2001. *An introduction to statistical modeling of extreme values*, Springer Series in Statistics. doi:10.1007/978-1-4471-3675-0
- Cotton, W.R., Pielke Sr, R.A., 2007. *Human impacts on weather and climate.* Cambridge University Press.
- Daniels, E.E., 2016. Land surface impacts on precipitation in the Netherlands.
- Daniels, E.E., Hutjes, W. A., Lenderink, G., Ronda, R.J., Holtslag, A.A.M., 2015a. Land Surface Feedbacks on Spring Precipitation in the Netherlands. *J. Hydrometeorol.* 16, 232–243. doi:10.1175/JHM-D-14-0072.1
- Daniels, E.E., Lenderink, G., Hutjes, R., Holtslag, A., 2016. Relative impacts of land use and climate change on summer precipitation in the Netherlands. *Hydrol. Earth Syst. Sci.* 20, 4129–4142. doi:10.5194/hess-20-4129-2016
- Daniels, E.E., Lenderink, G., Hutjes, R.W.A., Holtslag, A.A.M., 2015b. Short Communication Observed urban effects on precipitation along the Dutch West coast. *Int. J. Climatol.* 35, 2119, 2111–2119. doi:10.1002/joc.4458
- Daniels, E.E., Lenderink, G., Hutjes, R.W.A., Holtslag, A.A.M., 2014. Spatial precipitation patterns and trends in The Netherlands during 1951-2009. *Int. J. Climatol.* 34, 1773–1784. doi:10.1002/joc.3800

- Data, C., 2009. Guidelines on analysis of extremes in a changing climate in support of informed decisions for adaptation. World Meteorological Organization.
- De Jongh, I.L.M., Verhoest, N.E.C., De Troch, F.P., 2006. Analysis of a 105-year time series of precipitation observed at Uccle, Belgium. *Int. J. Climatol.* 26, 2023–2039.
- De Lima, M.I.P., Carvalho, S.C.P., P. De Lima, J.L.M., S. Coelho, M.F.E., 2010. Trends in precipitation: Analysis of long annual and monthly time series from mainland Portugal. *Adv. Geosci.* 25, 155–160. doi:10.5194/adgeo-25-155-2010
- Dee, D.P., Uppala, S.M., Simmons, A.J., Berrisford, P., Poli, P., Kobayashi, S., Andrae, U., Balmaseda, M.A., Balsamo, G., Bauer, P., Bechtold, P., Beljaars, A.C.M., van de Berg, L., Bidlot, J., Bormann, N., Delsol, C., Dragani, R., Fuentes, M., Geer, A.J., Haimberger, L., Healy, S.B., Hersbach, H., H??lm, E. V., Isaksen, L., K??llberg, P., K??hler, M., Matricardi, M., McNally, A.P., Monge-Sanz, B.M., Morcrette, J.J., Park, B.K., Peubey, C., de Rosnay, P., Tavolato, C., Th??paut, J.N., Vitart, F., 2011. The ERA-Interim reanalysis: Configuration and performance of the data assimilation system. *Q. J. R. Meteorol. Soc.* 137, 553–597. doi:10.1002/qj.828
- Dekkers, J.E.C., Koomen, E., Jacobs-Crisioni, C.G.W., Rijken, B., 2012. Scenario-based projections of future land use in the Netherlands. *Spat. Inf. Lab. Res. Memo.* SL-11 1–51.
- Diermans, F., Ogink, H., van Dansik, J., Gloudemans, E., 2005. Neerslagstatistiek, extreem gevoel? H2O 38, 25.
- Ding, Y., Yang, D., Ye, B., Wang, N., 2007. Effects of bias correction on precipitation trend over China. *J. Geophys. Res. Atmos.* 112, 1–11. doi:10.1029/2006JD007938
- Dixon, P.G., Mote, T.L., 2003. Patterns and Causes of Atlanta’s Urban Heat Island–Initiated Precipitation. *J. Appl. Meteorol.* 42, 1273–1284. doi:10.1175/1520-0450(2003)042<1273:PACOAU>2.0.CO;2
- Dobson, A.J., Barnett, A., 2008. An introduction to generalized linear models. CRC press.
- Dodd, E.L., 1923. The greatest and the least variate under general laws of error. *Trans. Am. Math. Soc.* 25, 525–539.
- Doherty, R.M., Hulme, M., Jones, C.G., 1999. A gridded reconstruction of land and ocean precipitation for the extended tropics from 1974 to 1994. *Int. J. Climatol.* 19, 119–142. doi:10.1002/(SICI)1097-0088(199902)19:2<119::AID-JOC358>3.0.CO;2-X
- Dou, J., Wang, Y., Bornstein, R., Miao, S., 2015. Observed spatial characteristics of Beijing urban climate impacts on summer thunderstorms. *J. Appl. Meteorol. Climatol.* 54, 94–105. doi:10.1175/JAMC-D-13-0355.1
- Drobinski, P., Silva, N. Da, Panthou, G., Bastin, S., Muller, C., Ahrens, B.,

- Borga, M., Conte, D., Fosser, G., Giorgi, F., Güttler, I., Kotroni, V., Li, L., Morin, E., Öno, B., Quintana-Segui, P., Romera, R., Torma, C.Z., 2018. Scaling precipitation extremes with temperature in the Mediterranean: past climate assessment and projection in anthropogenic scenarios. *Clim. Dyn.* 51, 1237–1257. doi:10.1007/s00382-016-3083-x
- Easterling, D.R., Evans, J.L., Groisman, P.Y., Karl, T.R., Kunkel, K.E., Ambenje, P., 2000. Observed Variability and Trends in Extreme Climate Events: A Brief Review *. *Bull. Am. Meteorol. Soc.* 81, 417–425. doi:10.1175/1520-0477(2000)081<0417:OVATIE>2.3.CO;2
- EEA, 2017. Landscapes in Transition. An account of 25 years of land cover change in Europe. EEA Rep. 226. doi:10.2800/81075
- EEA, 2014. CORINE land cover nomenclature illustrated guide 1–96.
- Einfalt, T., Quirnbach, M., Langst?dtler, G., Mehlig, B., 2011. Climate change tendencies observable in the rainfall measurements since 1950 in the Federal Land of North Rhine-Westphalia and their consequences for urban hydrology. *Water Sci. Technol.* 63, 2633–2640. doi:10.2166/wst.2011.165
- Embrechts, P., Klüppelberg, C., Mikosch, T., 1997. Modelling extremal events, volume 33 of Applications of Mathematics.
- Erell, E., Pearlmutter, D., Williamson, T., 2011. *Urban Microclimate: Designing the Spaces Between Buildings*: Earthscan. London/washington. DC.
- Feranec, J., Hazeu, G., Christensen, S., Jaffrain, G., 2007. Corine land cover change detection in Europe (case studies of the Netherlands and Slovakia). *Land use policy* 24, 234–247. doi:10.1016/j.landusepol.2006.02.002
- Feyen, L., Dankers, R., Bódis, K., Salamon, P., Barredo, J.I., 2012. Fluvial flood risk in Europe in present and future climates. *Clim. Change* 112, 47–62. doi:10.1007/s10584-011-0339-7
- Fischer, E.M., Knutti, R., 2016. Observed heavy precipitation increase confirms theory and early models. *Nat. Clim. Chang.* 6, 986–991. doi:10.1038/nclimate3110
- Fisher, R.A., Tippett, L.H.C., 1928. Limiting forms of the frequency distribution of the largest or smallest member of a sample. *Math. Proc. Cambridge Philos. Soc.* 24, 180–190. doi:10.1017/S0305004100015681
- Flato, G.M., Boer, G.J., Lee, W.G., McFarlane, N. a., Ramsden, D., Reader, M.C., Weaver, a. J., 2000. The Canadian Centre for Climate Modelling and Analysis global coupled model and its climate. *Clim. Dyn.* 16, 451–467. doi:10.1007/s003820050339
- Fréchet, M., 1928. Sur la loi de probabilité de l'écart maximum, in: *Annales de La Societe Polonaise de Mathematique*. [sn].
- Frei, C., Schär, C., 2001. Detection Probability of Trends in Rare Events: Theory and Application to Heavy Precipitation in the Alpine Region. *J. Clim.* 14, 1568–1584. doi:10.1175/1520-0442(2001)014<1568:DPOTIR>2.0.CO;2

- Gao, Y., Lu, J., Leung, L.R., 2016. Uncertainties in projecting future changes in atmospheric rivers and their impacts on heavy precipitation over Europe. *J. Clim.* 29, 6711–6726. doi:10.1175/JCLI-D-16-0088.1
- Gedzelman, S.D., Austin, S., Cermak, R., Stefano, N., Partridge, S., 2003. Mesoscale aspects of the Urban Heat Island around New York City. *Sci. York* 75, 29–42. doi:10.1007/s00704-002-0724-2
- Gellens, D., 2003. Etude des précipitations extrêmes. Etablissement des fractiles et des périodes de retour événements pluviométriques. These Dr. Univ. Libr. Bruxelles. Université libre de Bruxelles.
- Giridharan, R., Lau, S.S.Y., Ganesan, S., 2005. Nocturnal heat island effect in urban residential developments of Hong Kong. *Energy Build.* 37, 964–971.
- Griffiths, G.M., Chambers, L.E., Haylock, M.R., Manton, M.J., Nicholls, N., Baek, H.J., Choi, Y., Della-Marta, P.M., Gosai, a., Iga, N., Lata, R., Laurent, V., Maitrepierre, L., Nakamigawa, H., Ouprasitwong, N., Solofa, D., Tahani, L., Thuy, D.T., Tibig, L., Trewin, B., Vediapan, K., Zhai, P., 2005. Change in mean temperature as a predictor of extreme temperature change in the Asia-Pacific region. *Int. J. Climatol.* 25, 1301–1330. doi:10.1002/joc.1194
- Groisman, P.Y., Karl, T.R., Easterling, D.R., Knight, R.W., Jamason, P.F., Hennessy, K.J., Suppiah, R., Page, C.M., Wibig, J., Fortuniak, K., Razuvaev, V.N., Douglas, A., Førland, E., Zhai, P.M., 1999. Changes in the probability of heavy precipitation: Important indicators of climatic change. *Clim. Change.* doi:10.1023/A:1005432803188
- Gumbel, E.J., 1958. *Statistics of extremes.* 1958. Columbia Univ. Press. New York 247.
- Guo, Z., Dirmeyer, P.A., Koster, R.D., Sud, Y.C., Bonan, G., Oleson, K.W., Chan, E., Versegny, D., Cox, P., Gordon, C.T., McGregor, J.L., Kanae, S., Kowalczyk, E., Lawrence, D., Liu, P., Mocko, D., Lu, C.-H., Mitchell, K., Malyshev, S., McAvaney, B., Oki, T., Yamada, T., Pitman, A., Taylor, C.M., Vasic, R., Xue, Y., 2006. GLACE: The Global Land–Atmosphere Coupling Experiment. Part II: Analysis. *J. Hydrometeorol.* 7, 611–625. doi:10.1175/JHM511.1
- Gutowski, W.J., Arritt, R.W., Kawazoe, S., Flory, D.M., Takle, E.S., Biner, S.S., Caya, D., Jones, R.G., Laprise, R.R., Leung, L.R., Mearns, L.O., Moufouma-Okia, W., Nunes, A.M.B., Qian, Y., Roads, J.O., Sloan, L.C., Snyder, M. a., Raymond, A., L Ruby, L., Gutowski Jr., W.J., 2010. Regional Extreme Monthly Precipitation Simulated by NARCCAP RCMs. *J. Hydrometeorol.* 11, 1373–1379. doi:10.1175/2010JHM1297.1
- Haerter, J.O., Berg, P., 2009. Unexpected rise in extreme precipitation caused by a shift in rain type? *Nat. Publ. Gr.* 2, 372–373. doi:10.1038/ngeo523
- Haines, A., Kovats, R.S., Campbell-Lendrum, D., Corvalan, C., 2006. Climate change and human health: Impacts, vulnerability and public health. *Public Health* 120, 585–596. doi:10.1016/j.puhe.2006.01.002

- Hamdi, R., Schayes, G., 2008. Sensitivity study of the urban heat island intensity to urban characteristics. *Int. J. Climatol.* 28, 973–982.
- Han, J.-Y., Baik, J.-J., 2008. A Theoretical and Numerical Study of Urban Heat Island-Induced Circulation and Convection. *J. Atmos. Sci.* 65, 1859–1877. doi:10.1175/2007JAS2326.1
- Han, J.-Y., Baik, J.-J., Khain, A.P., 2012. A Numerical Study of Urban Aerosol Impacts on Clouds and Precipitation. *J. Atmos. Sci.* 69, 504–520. doi:10.1175/JAS-D-11-071.1
- Han, J.-Y., Baik, J.-J., Lee, H., 2014. Urban impacts on precipitation. *Asia-Pacific J. Atmos. Sci.* 50, 17–30. doi:10.1007/s13143-014-0016-7
- Hanel, M., Buishand, T.A., 2010. On the value of hourly precipitation extremes in regional climate model simulations. *J. Hydrol.* 393, 265–273. doi:10.1016/j.jhydrol.2010.08.024
- Hardwick Jones, R., Westra, S., Sharma, A., 2010. Observed relationships between extreme sub-daily precipitation, surface temperature, and relative humidity. *Geophys. Res. Lett.* 37, 1–5. doi:10.1029/2010GL045081
- Hartmann, D.L., Tank, A.M.G.K., Rusticucci, M., Alexander, L. V, Brönnimann, S., Charabi, Y.A.R., Dentener, F.J., Dlugokencky, E.J., Easterling, D.R., Kaplan, A., 2013. Observations: atmosphere and surface, in: *Climate Change 2013 the Physical Science Basis: Working Group I Contribution to the Fifth Assessment Report of the Intergovernmental Panel on Climate Change*. Cambridge University Press.
- Hausfather, Z., Menne, M.J., Williams, C.N., Masters, T., Broberg, R., Jones, D., 2013. Quantifying the effect of urbanization on U.S. Historical Climatology Network temperature records. *J. Geophys. Res. Atmos.* 118, 481–494. doi:10.1029/2012JD018509
- Haylock, M.R., Goodess, C.M., 2004. Interannual variability of European extreme winter rainfall and links with mean large-scale circulation. *Int. J. Climatol.* 24, 759–776. doi:10.1002/joc.1033
- Hazeu, G.W., 2003. CLC2000 Land Cover database of the Netherlands - Monitoring land cover changes between 1986 and 2000 107.
- Hazeu, G.W., Bregt, A.K., de Wit, A.J.W., Clevers, J.G.P.W., 2011. A Dutch multi-date land use database: Identification of real and methodological changes. *Int. J. Appl. Earth Obs. Geoinf.* 13, 682–689. doi:10.1016/j.jag.2011.04.004
- Hazeu, G.W., De Wit, A.J.W., 2004. CORINE land cover database of the Netherlands: monitoring land cover changes between 1986 and 2000. *EARSel eProceedings* 3, 382–387.
- Hirsch, R.M., Archfield, S.A., 2015. Flood trends: Not higher but more often. *Nat. Clim. Chang.* 5, 198.
- Hooimeijer, F., van der Toorn Vrijthoff, W., 2014. *More urban water: Design and management of Dutch water cities*. CRC Press.
- Horton, R.E., 1921. Thunderstorm-Breeding Spots. *Mon. Weather Rev.* 49,

- 193–193. doi:10.1175/1520-0493(1921)49<193a:TS>2.0.CO;2
- Hosking, J.R.M., 1990. L-Moments: Analysis and Estimation of Distributions Using Linear Combinations of Order Statistics. *J. R. Stat. Soc. Ser. B* 52, 105–124. doi:10.2307/2345653
- Hu, Z., Yu, B., Chen, Z., Li, T., Liu, M., 2012. Numerical investigation on the urban heat island in an entire city with an urban porous media model. *Atmos. Environ.* 47, 509–518. doi:10.1016/j.atmosenv.2011.09.064
- Hundecha, Y., Bárdossy, A., 2005. Trends in daily precipitation and temperature extremes across western Germany in the second half of the 20th century. *Int. J. Climatol.* 25, 1189–1202. doi:10.1002/joc.1182
- Hurrell, J.W., 1995. Decadal Trends in the North Atlantic Oscillation: Regional Temperatures and Precipitation. *Science* 269, 676–9. doi:10.1126/science.269.5224.676
- Id, S., 2011. K Ey To D Atasheets. *Buildings* 1–11.
- Ikebuchi, S., Tanaka, K., Ito, Y., Moteki, Q., 2007. Investigation of the Effects of Urban Heating on the Heavy Rainfall Event by a Cloud Resolving Model CReSiBUC. *Annu. Disaster Prev. Res. Institute, Kyoto Univ.* 50, 105–111.
- IPCC: [Field, C.B., V. Barros, T.F. Stocker, D. Qin, D.J. Dokken, K.L. Ebi, M.D. Mastrandrea, K.J. Mach, G.-K. Plattner, S.K. Allen, M. Tignor, and P.M. Midgley, (eds.)], 2012. *Managing the Risks of Extreme Events and Disasters to Advance Climate Change Adaptation*. Cambridge University Press, Cambridge, UK, and New York, NY, USA, 582 pp. doi:10.1017/CBO9781139177245
- IPCC, 2014. *Climate Change 2013 – The Physical Science Basis: Working Group I Contribution to the Fifth Assessment Report of the Intergovernmental Panel on Climate Change*. Cambridge University Press, Cambridge. doi:DOI: 10.1017/CBO9781107415324
- Jarraud, M., 2008. *Guide to meteorological instruments and methods of observation (WMO-No. 8)*. World Meteorol. Organ. Geneva, Switz.
- Jenkinson, A.F., 1955. The frequency distribution of the annual maximum (or minimum) values of meteorological elements. *R. Meteorol. Soc.* 81, 158–171. doi:10.1002/qj.49708134804
- Jenkinson, A.F., Collison, F.P., 1977. An initial climatology of gales over the North Sea. *Synop. Climatol. branch Memo.* 62, 18.
- Jiang, Q., Kresin, F., Bregt, A.K., Kooistra, L., Pareschi, E., Putten, E. Van, Volten, H., Wesseling, J., 2016. *Citizen Sensing for Improved Urban Environmental Monitoring 2016*.
- Jones, P.D., Jonsson, T., Wheeler, D., 1997. Extension to the North Atlantic oscillation using early instrumental pressure observations from Gibraltar and south-west Iceland. *Int. J. Climatol.* 17, 1433–1450. doi:10.1002/(SICI)1097-0088(19971115)17:13<1433::AID-JOC203>3.0.CO;2-P
- Junkermann, W., Vogel, B., Sutton, M.A., 2011. The climate penalty for clean fossil fuel combustion. *Atmos. Chem. Phys.* 11, 12917–12924.

- doi:10.5194/acp-11-12917-2011
- Karagiannidis, A.F., Karacostas, T., Maheras, P., Makrogiannis, T., 2012. Climatological aspects of extreme precipitation in Europe, related to mid-latitude cyclonic systems. *Theor. Appl. Climatol.* 107, 165–174. doi:10.1007/s00704-011-0474-0
- Katz, R.W., Parlange, M.B., Naveau, P., 2002. Statistics of extremes in hydrology. *Adv. Water Resour.* 25, 1287–1304. doi:10.1016/S0309-1708(02)00056-8
- Kaufmann, R.K., KAREN C. SETO, ANNEMARIE SCHNEIDER, ZOUTING LIU, L.Z., WANG, A.W., 2007. Climate Response to Rapid Urban Growth: Evidence of a Human-Induced. doi:10.1175/JCLI4109.1
- Kendall, M.G., 1948. Rank correlation methods. Griffin, Oxford, England.
- Khain, A.P., 2009. Notes on state-of-the-art investigations of aerosol effects on precipitation: a critical review. *Environ. Res. Lett.* 4, 1–20. doi:10.1088/1748-9326/4/1/015004
- Klein Tank, A.M.G., 2007. EUMETNET/ECSN optional programme: European Climate Assessment & Dataset (ECA&D) Algorithm Theoretical Basis Document (ATBD), version 4. R. Netherlands Meteorol. Inst. KNMI.
- Klein Tank, A.M.G., Können, G.P., 2003. Trends in Indices of Daily Temperature and Precipitation Extremes in Europe, 1946–99. *J. Clim.* 16, 3665–3680. doi:10.1175/1520-0442(2003)016<3665:TIIODT>2.0.CO;2
- Klein Tank, A.M.G., Lenderink, G., 2009. Climate change in the Netherlands; Supplements to the KNMI'06 scenarios. Bilt, K. Ned. Meteorol. Inst.
- Klein Tank, A.M.G., Wijngaard, J.B., Können, G.P., Böhm, R., Demaree, G., Gocheva, A., Mileta, M., Pashiardis, S., Hejkrlik, L., Kern-Hansen, C., Heino, R., Bessemoulin, P., Müller-Westermeier, G., Tzanakou, M., Szalai, S., Palsdóttir, T., Fitzgerald, D., Rubin, S., Capaldo, M., Maugeri, M., Leitass, A., Bukantis, A., Aberfeld, R., van Engelen, A.F. V., Forland, E., Mielus, M., Coelho, F., Mares, C., Razuvaev, V., Nieplova, E., Cegnar, T., Antonio Lopez, J., Dahlstrom, B., Moberg, A., Kirchhofer, W., Ceylan, A., Pachaliuk, O., Alexander, L. V., Petrovic, P., 2002. Daily dataset of 20th-century surface air temperature and precipitation series for the European Climate Assessment. *Int. J. Climatol.* 22, 1441–1453. doi:10.1002/joc.773
- Klein Tank, A.M.G., Zwiers, F.W., Zhang, X., 2009. Guidelines on Analysis of extremes in a changing climate in support of informed decisions for adaptation, Climate Data and Monitoring. World Meteorological Organization.
- Klok, L., Zwart, S., Verhagen, H., Mauri, E., 2012. The surface heat island of Rotterdam and its relationship with urban surface characteristics. *Resour. Conserv. Recycl.* 64, 23–29.
- KNMI, 2014. KNMI'14 climate scenarios for the Netherlands; A guide for professionals in climate adaptation 34.
- KNMI, 2000. Handbook for the meteorological observation. 91–110.

- Koenker, Roger, and J.A.M., 1999. Goodness of fit and related inference processes for quantile regression. *J. Am. Stat. Assoc.* 94, 1296–1310.
- Koenker, R., Bassett, G., 1978. Regression Quantiles. *Econometrica* 46, 33. doi:10.2307/1913643
- Koster, R.D., Guo, Z., Dirmeyer, P. a., Bonan, G.B., Chan, E., Cox, P.M., Gordon, C.T., Kanae, S., Kowalczyk, E., Lawrence, D.M., Liu, P., Lu, C.H., Malyshev, S., MacAvaney, B., McGregor, J.L., Mitchell, K., Mocko, D., Oki, T., Oleson, K.W., Pitman, A., Sud, Y.C., Taylor, C.M., Versegny, D., Vasic, R., Xue, Y., Yamada, T., 2006. GLACE: The Global Land – Atmosphere Coupling Experiment. Part I: Overview. *J. Hydrometeorol.* 7, 611–625. doi:http://dx.doi.org/10.1175/JHM511.1
- Kundzewicz, Z.W., Pińskwar, I., Brakenridge, G.R., 2013. Large floods in Europe, 1985–2009. *Hydrol. Sci. J.* 58, 1–7. doi:10.1080/02626667.2012.745082
- Kunkel, K.E., Karl, T.R., Brooks, H., Kossin, J., Lawrimore, J.H., Arndt, D., Bosart, L., Changnon, D., Cutter, S.L., Doesken, N., Emanuel, K., Groisman, P.Y., Katz, R.W., Knutson, T., O'Brien, J., Paciorek, C.J., Peterson, T.C., Redmond, K., Robinson, D., Trapp, J., Vose, R., Weaver, S., Wehner, M., Wolter, K., Wuebbles, D., 2013. Monitoring and understanding trends in extreme storms: State of knowledge. *Bull. Am. Meteorol. Soc.* 94, 499–514. doi:10.1175/BAMS-D-11-00262.1
- Leadbetter, M.R., Lindgren, G., 1983. Rootz en, H.(1983) Extremes and related properties of random sequences and processes.
- Lenderink, G., Attema, J., 2015. A simple scaling approach to produce climate scenarios of local precipitation extremes for the Netherlands. *Environ. Res. Lett.* 10, 085001. doi:10.1088/1748-9326/10/8/085001
- Lenderink, G., Mok, H.Y., Lee, T.C., Van Oldenborgh, G.J., 2011. Scaling and trends of hourly precipitation extremes in two different climate zones - Hong Kong and the Netherlands. *Hydrol. Earth Syst. Sci.* 15, 3033–3041. doi:10.5194/hess-15-3033-2011
- Lenderink, G., van Meijgaard, E., 2010. Linking increases in hourly precipitation extremes to atmospheric temperature and moisture changes. *Environ. Res. Lett.* 5, 9. doi:10.1088/1748-9326/5/2/025208
- Lenderink, G., van Meijgaard, E., 2008. Increase in hourly precipitation extremes beyond expectations from temperature changes. *Nat. Geosci* 1, 511–514.
- Lenderink, G., Van Meijgaard, E., 2010. Linking increases in hourly precipitation extremes to atmospheric temperature and moisture changes. *Environ. Res. Lett.* 5, 9. doi:10.1088/1748-9326/5/2/025208
- Lenderink, G., van Meijgaard, E., Selten, F., 2009. Intense coastal rainfall in the Netherlands in response to high sea surface temperatures: analysis of the event of August 2006 from the perspective of a changing climate. *Clim. Dyn.* 32, 19–33. doi:10.1007/s00382-008-0366-x
- Lenderink, G., van Ulden, a., van den Hurk, B., Keller, F., 2007. A study on

- combining global and regional climate model results for generating climate scenarios of temperature and precipitation for the Netherlands. *Clim. Dyn.* 29, 157–176. doi:10.1007/s00382-007-0227-z
- Leopold, L.B., 1968. Hydrology for- Urban Land Planning - Effects of Urban Land Use. *Geol. Surv. Circ.* 554, 1–18.
- Levizzani, V., Amorati, R., Meneguzzo, F., 2002. A review of satellite-based rainfall estimation methods. ... *Comm. Proj. Music* ... 70.
- Lin, C.-Y., Chen, W.-C., 2011. Impact of the Urban Heat Island Effect on Precipitation over a Complex Geographic Environment in Northern Taiwan 339–353. doi:10.1175/2010JAMC2504.1
- Madsen, H., Lawrence, D., Lang, M., Martinkova, M., Kjeldsen, T.R., 2014. Review of trend analysis and climate change projections of extreme precipitation and floods in Europe. *J. Hydrol.* 519, 3634–3650.
- Mann, H.B., 1945. Nonparametric Tests Against Trend. *Econometrica* 13, 245–259. doi:10.2307/1907187
- Maragatham, R.S., 2012. Trend Analysis of Rainfall Data -a Comparative Study of Existing Methods. *Int. J. Phys. Math. Sci.* 2, 13–18.
- Maraun, D., Osborn, H., J., W.R. and T., 2009. The annual cycle of heavy precipitation across the United Kingdom: a model based on extreme value statistics. *Encycl. Atmos. Sci.* 4, 1549–1555. doi:10.1002/joc
- McLaren, C., Null, J., Quinn, J., 2005. Heat Stress From Enclosed Vehicles: Moderate Ambient Temperatures Cause Significant Temperature Rise in Enclosed Vehicles 116. doi:10.1542/peds.2004-2368
- Miao, S., Chen, F., Li, Q., Fan, S., 2011. Impacts of urban processes and urbanization on summer precipitation: A case study of heavy rainfall in Beijing on 1 August 2006. *J. Appl. Meteorol. Climatol.* 50, 806–825. doi:10.1175/2010JAMC2513.1
- Mills, G., 2014. Urban climatology: History, status and prospects. *Urban Clim.* 10, 479–489. doi:10.1016/j.uclim.2014.06.004
- Min, S.-K., Zhang, X., Zwiers, F.W., Friederichs, P., Hense, A., 2009. Signal detectability in extreme precipitation changes assessed from twentieth century climate simulations. *Clim. Dyn.* 32, 95–111. doi:10.1007/s00382-008-0376-8
- Min, S.-K., Zhang, X., Zwiers, F.W., Hegerl, G.C., 2011. Human contribution to more-intense precipitation extremes. *Nature* 470, 378–381. doi:10.1038/nature09763
- Mishra, V., Wallace, J.M., Lettenmaier, D.P., 2012. Relationship between hourly extreme precipitation and local air temperature in the United States. *Geophys. Res. Lett.* 39, 1–7. doi:10.1029/2012GL052790
- Mitra, C., Shepherd, J.M., Jordan, T., 2012. On the relationship between the premonsoonal rainfall climatology and urban land cover dynamics in Kolkata city, India. *Int. J. Climatol.* 32, 1443–1454. doi:10.1002/joc.2366

- Moore, R.J., 1987. Combined regional flood frequency analysis and regression on catchment characteristics by maximum likelihood estimation.
- Morris, C.J.G., Simmonds, I., 2000. Associations between varying magnitudes of the urban heat island and the synoptic climatology in Melbourne, Australia. *Int. J. Climatol. A J. R. Meteorol. Soc.* 20, 1931–1954.
- Mudersbach, C., Jensen, J., 2011. an Advanced Statistical Extreme Value Model for Evaluating Storm Surge Heights Considering Systematic Records and Sea Level Rise Scenario. *Coast. Eng. Proc.* 1, 23. doi:10.9753/icce.v32.currents.23
- Neter, J., Kutner, M.H., Nachtsheim, C.J., Wasserman, W., 1996. Applied linear statistical models. Irwin Chicago.
- Nicholls, N., Alexander, L., 2007. Has the climate become more variable or extreme? *Progress 1992-2006. Prog. Phys. Geogr.* 31, 77–87. doi:10.1177/0309133307073885
- Niyogi, D., Pyle, P., Lei, M., Arya, S.P., Kishtawal, C.M., Shepherd, M., Chen, F., Wolfe, B., 2011. Urban modification of thunderstorms: An observational storm climatology and model case study for the Indianapolis urban region. *J. Appl. Meteorol. Climatol.* 50, 1129–1144. doi:10.1175/2010JAMC1836.1
- Oke, 1973. City size and the urban heat island. *Atmos. Environ.* 7, 769–779. doi:10.1016/0004-6981(73)90140-6
- Oke, T.R., 2004. Initial guidance to obtain representative meteorological observations at urban sites. *World Meteorol. Organ.* 51. doi:Reporte
- Oke, T.R., 1982. The energetic basis of the urban heat island. *Q. J. R. Meteorol. Soc.* 108, 1–24. doi:10.1002/qj.49710845502
- Overeem, A., 2009. Climatology of extreme rainfall from rain gauges and weather radar.
- Overeem, A., Buishand, A., 2012. Statistiek van extreme gebiedsneerslag in Nederland. KNMI.
- Overeem, A., Buishand, A., Holleman, I., 2008a. Rainfall depth-duration-frequency curves and their uncertainties. *J. Hydrol.* 348, 124–134. doi:10.1016/j.jhydrol.2007.09.044
- Overeem, A., Buishand, T.A., Holleman, I., 2009. Extreme rainfall analysis and estimation of depth-duration-frequency curves using weather radar. *Water Resour. Res.* 45, n/a-n/a. doi:10.1029/2009WR007869
- Overeem, A., Holleman, I., Buishand, A., 2008b. Extreme rainfall climatology from weather radar.
- Pall, P., Allen, M.R., Stone, D. a., 2007. Testing the Clausius-Clapeyron constraint on changes in extreme precipitation under CO2 warming. *Clim. Dyn.* 28, 351–363. doi:10.1007/s00382-006-0180-2
- Panthou, G., Mailhot, A., Laurence, E., Talbot, G., 2014. Relationship between surface temperature and extreme rainfalls: a multi-timescale and event-based analysis. *J. Hydrometeorol.* 1, 140613122546006. doi:10.1175/JHM-D-14-0020.1

- Pattengale, N., Alipour, M., Bininda-Emonds, O., Moret, B., Stamatakis, A., 2009. How Many Bootstrap Replicates Are Necessary? *Research in Computational Molecular Biology* 5541, 184–200. doi:10.1007/978-3-642-02008-7_13
- Peterson, T.C., 2003. Assessment of urban versus rural in situ surface temperatures in the contiguous United States: No difference found. *J. Clim.* 16, 2941–2959. doi:10.1175/1520-0442(2003)016<2941:AOUVRI>2.0.CO;2
- Philipp, A., Beck, C., Esteban, P., Krennert, T., Lochbihler, K., Spyros, P., Pianko-kluczynska, K., Post, P., Alvarez, R., Spekat, A., Streicher, F., 2014. User guide.
- Philipp, A., Beck, C., Huth, R., Jacobeit, J., 2016. Development and comparison of circulation type classifications using the COST 733 dataset and software. *Int. J. Climatol.* 36, 2673–2691. doi:10.1002/joc.3920
- Półrolniczak, M., Kolendowicz, L., Majkowska, A., Czernecki, B., 2017. The influence of atmospheric circulation on the intensity of urban heat island and urban cold island in Poznań, Poland. *Theor. Appl. Climatol.* 127, 611–625. doi:10.1007/s00704-015-1654-0
- R Foundation for Statistical Computing, Vienna, A.I. 3-900051-07-0, 2011. R Development Core Team. *R A Lang. Environ. Stat. Comput.* 55, 275–286.
- Rahimpour, V., Zeng, Y., Mannaerts, C.M., Su, Z., 2018. Urban impact on air temperature and precipitation over the Netherlands 75, 95–109. doi:https://doi.org/10.3354/cr01512
- Rahimpour, V., Zeng, Y., Mannaerts, C.M., Su, Z., 2017. Detecting the effect of urban land use on extreme precipitation in the Netherlands. *Weather Clim. Extrem.* 17, 36–46. doi:10.1016/j.wace.2017.07.003
- Rahimpour, V., Zeng, Y., Mannaerts, C.M., Su, Z., 2016a. Attributing seasonal variation of daily extreme precipitation events across The Netherlands. *Weather Clim. Extrem.* 14, 56–66. doi:10.1016/j.wace.2016.11.003
- Rahimpour, V., Zeng, Y., Mannaerts, C.M., Su, Z., 2016b. Land Cover Effects on Extreme Precipitation in the Netherlands, in: *Living Planet Symposium*. p. 175.
- Ren, G.Y., 2015. Urbanization as a major driver of urban climate change. *Adv. Clim. Chang. Res.* 6, 1–6. doi:10.1016/j.accre.2015.08.003
- Rioned, S., 2006. *Stedelijke Wateropgave*.
- Rootzén, H., Katz, R.W., 2013. Design life level: quantifying risk in a changing climate. *Water Resour. Res.* 49, 5964–5972.
- Rosenfeld, D., Dai, J., Yu, X., Yao, Z., Xu, X., Yang, X., Du, C., 2007. Inverse relations between amounts of air pollution and orographic precipitation. *Science* 315, 1396–1398. doi:10.1126/science.1137949
- Roth, M., Buishand, T.A., Jongbloed, G., Klein Tank, A.M.G., Van Zanten, J.H., 2012. A regional peaks-over-threshold model in a nonstationary climate. *Water Resour. Res.* 48, 1–12. doi:10.1029/2012WR012214
- Rovers, V., Bosch, P., Albers, R., Spit, T., 2014. *Climate proof cities*. TNO.

- Rozoff, C.M., Cotton, W.R., Adegoke, J.O., 2003. Simulation of St.Louis, Missouri, Land use impacts on thunderstorms. *J.Appl.Meteorol.* 42, 716–738.
- Rust, H.W., Maraun, D., Osborn, T.J., 2009. Modelling seasonality in extreme precipitation. *Eur. Phys. J. Spec. Top.* 174, 99–111. doi:10.1140/epjst/e2009-01093-7
- Ryu, Y.-H., Baik, J.-J., 2012. Quantitative Analysis of Factors Contributing to Urban Heat Island Intensity. *J. Appl. Meteorol. Climatol.* 51, 842–854. doi:10.1175/JAMC-D-11-098.1
- Sailor, D.J., 2011. A review of methods for estimating anthropogenic heat and moisture emissions in the urban environment. *Int. J. Climatol.* 31, 189–199. doi:10.1002/joc.2106
- Santos, M., Fragoso, M., 2013. Precipitation variability in Northern Portugal: Data homogeneity assessment and trends in extreme precipitation indices. *Atmos. Res.* 131, 34–45. doi:10.1016/j.atmosres.2013.04.008
- Schlünzen, K.H., Hoffmann, P., Rosenhagen, G., Riecke, W., 2010. Long-term changes and regional differences in temperature and precipitation in the metropolitan area of Hamburg. *Int. J. Climatol.* 30, 1121–1136. doi:10.1002/joc.1968
- Schmith, T., 2001. Global warming signature in observed winter precipitation in Northwestern Europe? *Clim. Res.* 17, 263–274. doi:10.3354/cr017263
- Schneider, A., Friedl, M.A., Potere, D., 2009. A new map of global urban extent from MODIS satellite data. *Environ. Res. Lett.* 4, 044003. doi:10.1088/1748-9326/4/4/044003
- Schroerer, K., Kirchengast, G., 2017. Sensitivity of extreme precipitation to temperature: the variability of scaling factors from a regional to local perspective. *Clim. Dyn.* 0, 0. doi:10.1007/s00382-017-3857-9
- Scoccimarro, E., Gualdi, S., Bellucci, A., Zampieri, M., Navarra, A., 2016. Heavy precipitation events over the Euro-Mediterranean region in a warmer climate: results from CMIP5 models. *Reg. Environ. Chang.* 16, 595–602.
- Seber, G.A.F., Lee, A.J., 2012. Linear regression analysis. John Wiley & Sons.
- Sen, P.K., 1968. Estimates of the Regression Coefficient Based on Kendall's Tau. *J. Am. Stat. Assoc.* 63, 1379–1389. doi:10.2307/2285891
- Shem, W., Shepherd, M., 2009. On the impact of urbanization on summertime thunderstorms in Atlanta: Two numerical model case studies. *Atmos. Res.* 92, 172–189. doi:10.1016/j.atmosres.2008.09.013
- Shepherd, J.M., 2006. Evidence of urban-induced precipitation variability in arid climate regimes. *J. Arid Environ.* 67, 607–628. doi:10.1016/j.jaridenv.2006.03.022
- Shepherd, J.M., 2005. A review of current investigations of urban-induced rainfall and recommendations for the future. *Earth Interact.* 9, 1–27. doi:10.1175/EI156.1
- Shepherd, J.M., Carter, M., Manyin, M., Messen, D. and Burian, S., 2010. The

- impact of urbanization on current and future coastal precipitation: A case study for houston. *Environ. Plan. B Plan. Des.* 37, 284–304. doi:10.1068/b34102t
- Sienz, F., Schneidereit, A., Blender, R., Fraedrich, K., Lunkeit, F., 2010. Extreme value statistics for North Atlantic cyclones. *Tellus A* 62, 347–360. doi:10.1111/j.1600-0870.2010.00449.x
- Sillmann, J., Kharin, V. V., Zhang, X., Zwiers, F.W., Bronaugh, D., 2013. Climate extremes indices in the CMIP5 multimodel ensemble: Part 1. Model evaluation in the present climate. *J. Geophys. Res. Atmos.* 118, 1716–1733. doi:10.1002/jgrd.50203
- Sisternans, P., Nieuwenhuis, O., 2004. Holland Coast (the Netherlands). *Erosion Case Study* 31, 1–17.
- Sluijter, R., Leenaers, H., Camarasa, M., 2011. *De Bosatlas van het klimaat*. Noordhoff uitgevers.
- Sluiter, R., 2014. Product Description KNMI14 Daily Grids, KNMI Technical report TR-346.
- Sluiter, R., 2012. Interpolation Methods for the Climate Atlas. KNMI Tech. Rapp. TR-335, R. Netherlands Meteorol. Institute, Bilt 1–71.
- Sluiter, R., 2009a. Interpolation Methods for Climate Data Literature Review, KNMI, De Bilt, official website.
- Sluiter, R., 2009b. Interpolation methods for climate data: a literature review. KNMI, R&D Information, Obs. Technol. ... 1–28.
- Smits, I., Wijngaard, J.B., Versteeg, R.P., Kok, M., 2004. Statistiek van extreme neerslag in Nederland. *STOWA Rapp. Utr.*
- Stallins, J.A., Carpenter, J., Bentley, M.L., Ashley, W.S., Mulholland, J.A., 2013. Weekend-weekday aerosols and geographic variability in cloud-to-ground lightning for the urban region of Atlanta, Georgia, USA. *Reg. Environ. Chang.* 13, 137–151. doi:10.1007/s10113-012-0327-0
- Steenefeld, G.J., Koopmans, S., Heusinkveld, B.G., Van Hove, L.W.A., Holtslag, a. a M., 2011. Quantifying urban heat island effects and human comfort for cities of variable size and urban morphology in the Netherlands. *J. Geophys. Res. Atmos.* 116, 1–14. doi:10.1029/2011JD015988
- Steenefeld, G.J., Koopmans, S., van Hove, L.W.A., Holtslag, A.A.M., 2010. Urban Heat Island Effects and Human Comfort in a Mild Cfb Climate: Exploring Long Term Observations by Hobby Meteorologists in The Netherlands, in: 9th Symposium on the Urban Environment, Amer Meteorological Society, 2-6 August 2010, Keystone, Colorado, USA. p. paper-1.
- Stewart, I.D., Oke, T.R., 2012. Local climate zones for urban temperature studies. *Bull. Am. Meteorol. Soc.* 93, 1879–1900. doi:10.1175/BAMS-D-11-00019.1
- Stjern, C.W., 2011. Weekly cycles in precipitation and other meteorological variables in a polluted region of Europe. *Atmos. Chem. Phys.* 11, 4095–

4104. doi:10.5194/acp-11-4095-2011
- Stolk, A., 1989. Zandsysteem kust: een morfologische karakterisering. Rijkswaterstaat (RWS), Ministerie van Verkeer en Waterstaat.
- Stone, B., Vargo, J., Habeeb, D., 2012. Managing climate change in cities: Will climate action plans work? *Landsc. Urban Plan.* 107, 263–271. doi:10.1016/j.landurbplan.2012.05.014
- Stull, R., 2017. *Practical Meteorology: An Algebra-based Survey of Atmospheric Science*. The University of British Columbia, Vancouver, Canada.
- Stull, R.B., 2011. *An introduction to boundary layer meteorology*. Univ. of British Columbia.
- Sun, X., Ren, G., Ren, Z., Shen, Z., 孙秀宝, 任国玉, 任芝花, 沈志超, 2013. Effects of Wind-Induced Errors on Winter Snowfall and Its Trends. *Clim. Environ. Res.* 18, 178–186. doi:10.3878/j.issn.1006-9585.2012.11133
- Suomi, J., Hjort, J., Käyhkö, J., 2012. Effects of scale on modelling the urban heat island in Turku, SW Finland. *Clim. Res.* 55, 105–118. doi:10.3354/cr01123
- Tank, A.K., n.d. High resolution observations for climate change monitoring of extremes, Triennial Scientific Report 2007-2009.
- Tao, W.K., Chen, J.P., Li, Z., Wang, C., Zhang, C., 2012. Impact of aerosols on convective clouds and precipitation. *Rev. Geophys.* 50. doi:10.1029/2011RG000369
- Ter Maat, H.W., Moors, E.J., Hutjes, R.W. a., Holtslag, a. a. M., Dolman, a. J., 2013. Exploring the Impact of Land Cover and Topography on Rainfall Maxima in the Netherlands. *J. Hydrometeorol.* 14, 524–542. doi:10.1175/JHM-D-12-036.1
- Theeuwes, N.E., Steeneveld, G.-J., Ronda, R.J., Holtslag, A.A.M., 2016. A diagnostic equation for the daily maximum urban heat island effect for cities in northwestern Europe. *Int. J. Climatol.* doi:10.1002/joc.4717
- Theil, H., 1950. A rank-invariant method of linear and polynomial regression analysis. I. *Nederl. Akad. Wetensch., Proc.* 53, 386–392. doi:10.1007/978-94-011-2546-8
- Thielen, J., Wobrock, W., Gadian, A., Mestayer, P.G., 2000. The possible influence of urban surfaces on rainfall development: a sensitivity study in 2D in the meso- g -scale. *Atmos. Res.* 54, 15–39.
- Tian, Y.E., Xu, Y., Booiij, M.J., Zhang, Q., Lin, S., 2011. Trends in precipitation extremes and long-term memory of runoff records in Zhejiang , east China 227–232.
- Tippett, L.H.C., 1925. On the extreme individuals and the range of samples taken from a normal population. *Biometrika* 364–387.
- Trenberth, K.E., Smith, L., Qian, T., Dai, A., Fasullo, J., 2007. Estimates of the Global Water Budget and Its Annual Cycle Using Observational and Model Data. *J. Hydrometeorol.* 8, 758–769. doi:10.1175/JHM600.1
- Trusilova, K., Jung, M., Churkina, G., 2009. On climate impacts of a potential

- expansion of urban land in Europe. *J. Appl. Meteorol. Climatol.* 48, 1971–1980. doi:10.1175/2009JAMC2108.1
- Trusilova, K., Jung, M., Churkina, G., Karsten, U., Heimann, M., Claussen, M., 2008. Urbanization impacts on the climate in Europe: Numerical experiments by the PSU-NCAR mesoscale model (MM5). *J. Appl. Meteorol. Climatol.* 47, 1442–1455. doi:10.1175/2007JAMC1624.1
- Unger, J., 2004. Intra-urban relationship between surface geometry and urban heat island: review and new approach. *Clim. Res.* 27, 253–264. doi:10.3354/cr027253
- United Nations, 2015. Department of Economic and Social Affairs, population division. *World Urban. Prospect. 2014 Revis. (ST/ESA/SER.A/366)*.
- van den Besselaar, E.J.M., Klein Tank, A.M.G., Buishand, T.A., 2012. Trends in European precipitation extremes over 1951–2010. *Int. J. Climatol.* 2689, n/a–n/a. doi:10.1002/joc.3619
- van den Hurk, B., Siegmund, P., Tank, A.K., Eds., 2014. *KNMI'14: Climate Change scenarios for the 21st Century - A Netherlands perspective* 115.
- van Haren, R., van Oldenborgh, G.J., Lenderink, G., Collins, M., Hazeleger, W., 2013. SST and circulation trend biases cause an underestimation of European precipitation trends. *Clim. Dyn.* 40, 1–20.
- van Hove, B., Steeneveld, G.-J., Jacobs, C.M.J., ter Maat, H.W., Heusinkveld, B.G., Moors, E.J., Holtslag, A.A.M., 2010. Modelling and observing urban climate in the Netherlands. *Alterra*.
- Van Hove, L.W.A., Jacobs, C.M.J., Heusinkveld, B.G., Elbers, J.A., van Driel, B.L., Holtslag, A.A.M., 2015. Temporal and spatial variability of urban heat island and thermal comfort within the Rotterdam agglomeration. *Build. Environ.* 83, 91–103. doi:10.1016/j.buildenv.2014.08.029
- Van Hove, L.W.A., Steeneveld, G.J., Jacobs, C.M.J., Heusinkveld, B.G., Elbers, J. a, Moors, E.J., Holtslag, a a M., 2011. Exploring the Urban Heat Island Intensity of Dutch cities. *Clim. Sci. Urban Des.* 1–60. doi:ISSN 1566-7197
- van Luijtelea, H., Gastkemper, H.G., Beenen, A.S., 2008. Heavier Rainfall Due to Climate Change.
- Van Minnen, J., Ligtoet, W., van Bree, L., de Hollander, G., Visser, H., van der Schrier, G., Bessembinder, J., van Oldenborgh, G.J., Prozny, T., Sluijter, R., 2013. The effects of climate change in the Netherlands: 2012. PBL Netherlands Environmental Assessment Agency.
- Van Montfort, M.A.J., Witter, J. V., 1986. The Generalized Pareto distribution applied to rainfall depths. *Hydrol. Sci. J.* 31, 151–162. doi:10.1080/02626668609491037
- von Storch, H., 1995. Misuses of Statistical Analysis in Climate Research. *Anal. Clim. Var. SE - 2* 11–26. doi:10.1007/978-3-662-03167-4_2
- Wang, J., Zhang, X., 2008. Downscaling and projection of winter extreme daily precipitation over North America. *J. Clim.* 21, 923–937. doi:10.1175/2007JCLI1671.1
- Wasko, C., Sharma, A., 2014. Quantile regression for investigating scaling of

- extreme precipitation with temperature. *Water Resour. Res.* 50, 3608–3614. doi:10.1002/2013WR015194
- Wentz, F.J., Ricciardulli, L., Hilburn, K., Mears, C., 2007. How much more rain will global warming bring? *Science* (80-.). 317, 233–235. doi:10.1126/science.1140746
- Westra, S., Alexander, L. V., Zwiers, F.W., 2013. Global increasing trends in annual maximum daily precipitation. *J. Clim.* 26, 3904–3918. doi:10.1175/JCLI-D-12-00502.1
- Westra, S., Fowler, H.J., Evans, J.P., Alexander, L. V., Berg, P., Johnson, F., Kendon, E.J., Lenderink, G., Roberts, N.M., 2014. Future changes to the intensity and frequency of short-duration extreme rainfall. *Rev. Geophys.* 52, 522–555. doi:10.1002/2014RG000464
- Wiacek, A., Taylor, J.R., Strong, K., Saari, R., Kerzenmacher, T.E., Jones, N.B., Griffith, D.W.T., 2007. Ground-based solar absorption FTIR spectroscopy: Characterization of retrievals and first results from a novel optical design instrument at a new NDACC complementary station. *J. Atmos. Ocean. Technol.* 24, 432–448. doi:10.1175/JTECH1962.1
- Wijngaard, J.B., Kok, M., Smits, I., Talsma, M., 2005. Nieuwe statistiek voor extreme neerslag. *H2O* 6, 35–37.
- Wilks, D.S., 1993. Comparison of three-parameter probability distributions for representing annual extreme and partial duration precipitation series. *Water Resour. Res.* 29, 3543–3549.
- Willems, P., 2013. Multidecadal oscillatory behaviour of rainfall extremes in Europe. *Clim. Change* 120, 931–944. doi:10.1007/s10584-013-0837-x
- Willems, P., 2013a. Adjustment of extreme rainfall statistics accounting for multidecadal climate oscillations. *J. Hydrol.* 490, 126–133. doi:10.1016/j.jhydrol.2013.03.034
- Willems, P., 2013b. Revision of urban drainage design rules after assessment of climate change impacts on precipitation extremes at Uccle, Belgium. *J. Hydrol.* 496, 166–177. doi:10.1016/j.jhydrol.2013.05.037
- Willems, P., Arnbjerg-Nielsen, K., Olsson, J., Nguyen, V.T.V., 2012. Climate change impact assessment on urban rainfall extremes and urban drainage: Methods and shortcomings. *Atmos. Res.* 103, 106–118. doi:10.1016/j.atmosres.2011.04.003
- Willems, P., Olsson, J., Arnbjerg-Nielsen, K., Beecham, S., Pathirana, A., Gregersen, I.B. and, Madsen, H., 2012. Impacts of climate change on rainfall extremes and urban drainage systems. IWA publishing.
- Willett, K.M., Jones, P.D., Gillett, N.P., Thorne, P.W., 2008. Recent changes in surface humidity: Development of the HadCRUH dataset. *J. Clim.* 21, 5364–5383. doi:10.1175/2008JCLI2274.1
- Witter, J. V., 1984. Heterogeneity of Dutch rainfall.
- WMO, 2007. Guide to the Global Observing System. Report No. 488. WMO-No. 488 170. doi:ISBN 92-63-13488-3
- Wolters, D., Brandsma, T., 2012. Estimating the Urban Heat Island in

- Residential Areas in the Netherlands Using Observations by Weather Amateurs. *J. Appl. Meteorol. Climatol.* 51, 711–721. doi:10.1175/JAMC-D-11-0135.1
- World Urbanization Prospects The 2014 Revision, n.d.
- Yang, P., Ren, G., Hou, W., Liu, W., 2013. Spatial and diurnal characteristics of summer rainfall over Beijing Municipality based on a high-density AWS dataset. *Int. J. Climatol.* 33, 2769–2780. doi:10.1002/joc.3622
- Yang, P., Ren, G., Yan, P., 2017. Evidence for a strong association of short-duration intense rainfall with urbanization in the Beijing urban area. *J. Clim.* 30, 5851–5870. doi:10.1175/JCLI-D-16-0671.1
- Yue, S., PILON, P., PHINNEY, B., 2003. Canadian streamflow trend detection: impacts of serial and cross-correlation. *Hydrol. Sci. J.* 48, 51–63. doi:10.1623/hysj.48.1.51.43478
- Yue, S., Pilon, P., Phinney, B., Cavadias, G., 2002. The influence of autocorrelation on the ability to detect trend in hydrological series. *Hydrol. Process.* 16, 1807–1829. doi:10.1002/hyp.1095
- Zhang, C.L., Chen, F., Miao, S.G., Li, Q.C., Xia, X.A., Xuan, C.Y., 2009. Impacts of urban expansion and future green planting on summer precipitation in the Beijing metropolitan area. *J. Geophys. Res.* 114, D02116. doi:10.1029/2008JD010328
- Zhang, X., Aguilar, E., Sensoy, S., Melkonyan, H., Tagiyeva, U., Ahmed, N., Kutaladze, N., Rahimzadeh, F., Taghipour, A., Hantosh, T.H., Albert, P., Semawi, M., Karam Ali, M., Said Al-Shabibi, M.H., Al-Oulan, Z., Zatar, T., Al Dean Khelet, I., Hamoud, S., Sagir, R., Demircan, M., Eken, M., Adiguzel, M., Alexander, L., Peterson, T.C., Wallis, T., 2005. Trends in Middle East climate extreme indices from 1950 to 2003. *J. Geophys. Res.* 110, D22104. doi:10.1029/2005JD006181
- Zhang, X., Wan, H., Zwiers, F.W., Hegerl, G.C., Min, S.K., 2013. Attributing intensification of precipitation extremes to human influence. *Geophys. Res. Lett.* 40, 5252–5257. doi:10.1002/grl.51010
- Zhang, X., Wang, J., Zwiers, F.W., Groisman, P.Y., 2010. The influence of large-scale climate variability on winter maximum daily precipitation over North America. *J. Clim.* 23, 2902–2915. doi:10.1175/2010JCLI3249.1
- Zhang, X., Yang, F., 2004. RCLimDex (1.0) user manual. *Clim. Res. Branch Environ. Canada* 22, 1–23.
- Zhang, X., Zwiers, F.W., Hegerl, G.C., Lambert, F.H., Gillett, N.P., Solomon, S., Stott, P.A., Nozawa, T., 2007. Detection of human influence on twentieth-century precipitation trends. *Nature* 448, 461–465. doi:10.1038/nature06025
- Zhou, B., Rybski, D., Kropp, J.P., 2013. On the statistics of urban heat island intensity. *Geophys. Res. Lett.* 40, 5486–5491. doi:10.1002/2013GL057320
- Zolina, O., Simmer, C., Kapala, A., Bachner, S., Gulev, S., Maechel, H., 2008. Seasonally dependent changes of precipitation extremes over Germany

Bibliography

- since 1950 from a very dense observational network. *J. Geophys. Res. Atmos.* 113, 1–17. doi:10.1029/2007JD008393
- Zondervan, J.G., 1978. Modelling urban run-off A quasilinear approach.
- Zwiers, F.W., Alexander, L. V, Hegerl, G.C., Knutson, T.R., Kossin, J.P., Naveau, P., Nicholls, N., Schär, C., Seneviratne, S.I., Zhang, X., 2013. Climate Extremes: Challenges in Estimating and Understanding Recent Changes in the Frequency and Intensity of Extreme Climate and Weather Events 339–389. doi:10.1007/978-94-007-6692-1

Summary

The detection of changes in weather is important for the preparedness of societies for extreme events due to climate and urbanisation. Knowledge of the behaviour of extreme events is needed for many practical problems, as most infrastructures were designed with the assumption of a stationary climate (i.e., constant properties over time) and are sensitive to extreme weather events such as extreme precipitation. Precipitation extremes affect runoff volumes, infrastructures, aquatic ecosystems and species and, most notably, human life. Current trends in extreme precipitation due to, for example, climate and urbanisation, could violate the time-invariant assumptions for design criteria, which might lead to more uncertainty in return level estimations and a consequential increase in the failure probability of infrastructures. Although variations in meteorological parameters are widely accepted, stationary assumptions are commonly used to design infrastructure. This study aims to add to the knowledge of changes in precipitation and the nonstationary behaviour of precipitation due to climate and urbanisation.

The main objective of this research was to understand and quantify the effects of urbanisation and climate change on precipitation in the Netherlands. Consideration was given to the impacts of urbanisation on precipitation extremes via the comparison of observations over urban and non-urban areas using trend detection and attribution analysis approaches. The EVT offers statistical properties for the distribution of extremes in sufficiently large time series and further provides a probabilistic distribution of extreme events for quantifying the return levels of a given return period. In this respect, the block maxima approach was applied to characterize the behaviour of extreme precipitation, and the probability of the maxima was determined for each block. The GEV function fitted to the obtained maxima of blocks, and subsequently, the return levels for different return periods were estimated. A common challenge in nonstationary distributions is the selection of suitable covariates to explain variations, here variations in extreme precipitation. Therefore, seasonal models based on the sinusoidal pattern of precipitation occurrences and the correlation of these occurrences with other climatological parameters were studied. Although the nonstationary estimations had less uncertainty than the stationary estimations, some uncertainty remained due to the influences of other forcing factors and spatial dependencies.

The study attempted to characterize and attribute the seasonal variation of daily extreme precipitation events in the Netherlands (Chapter 2). Statistical models for extreme values were used to fit daily rainfall maxima for all months during the period of 1961-2014 using data from 231 rain gauges distributed across the country. The climatological spatial variability of extreme precipitation was illustrated on a daily basis. A harmonic model for all monthly

maxima was adopted instead of individual models. The fitted distributions show the inaccuracy of stationary assumptions for estimating return levels. The nonstationary model estimated parameters with less uncertainty and with smaller CIs than the stationary model, thus permitting a more accurate representation of extreme precipitation in the Netherlands. The spatial pattern of the annual mean location and scale of the GEV parameters was compatible with the coastal land cover (such as the wooded and heathland areas of the Veluwe region of Gelderland province) and orography (in the southeast of the country). The regional differences for the location parameter peaked over the west coast, especially over the central west coast during the summer half-year (between June and November), while the centre and east of the country had the highest regional differences during the winter half-year (between December and May). The scale parameter peaked in the centre of the country during the summer and was highest in the east in the early summer and along the west coast in the spring. The spatial distribution of the extreme event probability clearly reflects regional differences in the Netherlands.

In Chapter 3, index analysis performed on the precipitation data for one 54-year period and two independent multi-decadal periods displayed positive signals for the frequency and intensity of extreme events. An analysis of extreme precipitation trends for each index revealed the existence of spatial differences in the number and magnitude of extreme events over the Netherlands. The increases in extreme precipitation were high in comparison to the increases in annual total precipitation. Significant differences were found between an earlier multi-decadal period and a recent multi-decadal period in the Netherlands. The differences in the monthly maximum daily precipitation amounts and trends between the two multi-decadal periods were reflected by higher precipitation values in the late summer and autumn. The significant changes in different indices indicate that severe precipitation events were not distributed homogeneously across the study area. The possible effects of land use on extreme precipitation were assessed by quantifying the differences between urban and rural rain gauge stations using a spatial gridding method. The data from all the categorized stations show that urban areas receive more intense extreme precipitation than rural areas, but this discrepancy is rarely significant and depends on the investigated region. Relative to other areas in the Netherlands, urban areas in the western populated regions of the country exhibit prominent urban land use influences on extreme precipitation patterns. Five years of basic weather observations (2011-2015) from the automatic and amateur networks received much attention during an analysis of urban effects on meteorological parameters, with a focus on temperature and precipitation (Chapter 4). The hourly analysis indicates that the UHI effect is a nocturnal phenomenon in the Netherlands. The role of UHIs was more prominent after sunset, when the effect had a magnitude of over 2°C. The seasonal analysis revealed that the UHI occurred in all seasons during the year, not only during

summer. However, the UHI intensities in summer were higher than those in other seasons. The significant linear relationship between UHI intensity and population density suggest that a highly dense population influences the UHI intensity. Although there was no clear relationship between precipitation and other basic meteorological parameters, the hourly precipitation increased up to 7% more in urban areas than in rural areas. Furthermore, the precipitation difference between urban and rural areas was the highest after sunrise in the morning. The maximum precipitation occurrences were more likely to be greater in the urban stations than in the paired rural stations. The distribution of hourly precipitation showed the highest location parameter value for August (with an 11% increment in urban areas). In addition, a distinct seasonal cycle for the precipitation based on the UHI demonstrated the maximum UHI and precipitation that occurred in summer. Faster warming occurred in spring, and quicker cooling occurred in autumn. The findings indicate a distinct seasonal cycle for temperature and precipitation in Dutch residential areas and are in agreement with results obtained by amateur weather stations and the scientific literature.

The scaling of extreme precipitation with temperature was performed using the statistical quantile regression and binning methods described in Chapter 5. Positive 3-7% scaling rates at most stations were found between extreme precipitation and dew point and air temperature from 1985 to 2014 throughout the country. The stationary model was improved by modelling the nonstationary behaviour of extreme precipitation associated with the dew point and atmospheric air temperatures, as well as the NAO index. A higher precipitation for urban than for non-urban areas was found by considering the land cover upwind from the stations. The return levels for the monthly maximum daily precipitation were estimated to be 5-7% higher in urban areas than in non-urban areas in August. Likewise, the IDF curves were improved by nonstationary estimations associated with the dew point and atmospheric air temperatures of urban and non-urban areas. The results showed a higher frequency and intensity of extreme precipitation events in urban areas than in non-urban areas for short durations. The study concluded that nonstationary models refine IDF curves and should be used for analysing extreme precipitation by considering the probable covariates due to external forces (such as large-scale modes, circulation types and temperature changes). This study raises the need for a better estimation of changes in the frequency and intensity of extreme precipitation and the acceptance of nonstationary behaviour in the context of urbanisation and climate variabilities. Overall, although the effects of urban areas on extreme precipitation in the Netherlands seems not to be statistically significant, a consistent picture regarding the sign (i.e. positive) was presented throughout this study. While the differences are not very large they are persistent and could be important. It should be noted that for drawing firm conclusion, new observations in the case study with

Summary

similar local conditions (e.g., some measurements in rural areas and a few in the urban-influenced neighbours and others far away) are needed to better quantify the instrumental errors and uncertainties.

Samenvatting

De voorspelling van veranderingen in het weer is belangrijk voor de paraatheid van de samenleving voor extreme weersomstandigheden, veroorzaakt door het veranderende klimaat. Verstedelijking en uitbreiding van urbane gebieden en het verharde oppervlak, wordt ook meer en meer genoemd als factor bij veranderende neerslagpatronen en karakteristieken.

Kennis van het gedrag van extreme gebeurtenissen in stedelijk gebied is noodzakelijk bij vele praktische hydrologische problemen, aangezien de huidige technische ontwerpen van stedelijke water infrastructuur in NL, nog steeds gebaseerd zijn op een normaal en niet-veranderlijk of stationair klimaat. Vele huidige infrastructuur blijkt echter gevoelig voor extreme neerslag en de daarmee verbandhoudende klimaatsverandering.

Huidige waarnemingen en tendenzen in extreme neerslag stellen de veronderstelling van een niet-veranderlijk klimaat bij het ontwerpen van water infrastructuren in grote vraag. Grotere onzekerheden in de herhalingsfrequentie van extreem weer zijn nu aan de orde.

Deze studie heeft tot doel bij te dragen aan de kennisopbouw over de huidige waargenomen veranderingen in extreme neerslag en het niet-stationaire gedrag van het weer boven NL. Hierbij werd de combinatie van een veranderend klimaat, landgebruik en verstedelijking nader onderzocht.

Het hoofddoel van deze studie was het kwantitief bepalen van de invloeden van verstedelijking en klimaatprocessen op extreme neerslag in Nederland. Dit is uitgevoerd door lange tijdseries van neerslag waarnemingen te vergeleken tussen landelijke en stedelijke gebieden in NL, en middels statistische analyses tot uitspraken te komen. Hierbij werd o.a. gebruik gemaakt van de extreme waarde kanstheorie. Het toepassen van de gegeneralizeerde extreme waarde of GEV-kansverdeling of distributie op niet stationaire data was hier een van de uitdagingen.

De studie (Hoofdstuk 2) heeft ook geprobeerd om de seizoens- en de landelijke variaties in extreme neerslagen toe te wijzen aan veranderlijken zoals landgebruik, hoogteligging and ligging t.o.v. de zee. De klimatologische middellange termijn (30 - 60 jaar) variatie van extreme neerslag in NL kon aangetoond worden. Duidelijk werd ook dat niet-stationaire model veronderstellingen nodig zijn bij de analyse en interpretatie van neerslag gegevens. Niettegenstaande er geen duidelijke relatie tussen neerslag en andere meteorologische variabelen kon gevonden worden, werd neerslag intensiteiten (1-uur waarnemingen) tot 7% hoger gevonden in stedelijk gebied ten opzichte van de groene zone, ie. bos-, natuur- en landbouwgebieden. Met

name in de maand augustus kan deze toename in extreme neerslag intensiteit tot 11% bedragen (1-uur meetinterval).

In het 3de hoofdstuk werd een index-analyse uitgevoerd op een 54-jaar neerslag serie om naast de herhaalfrequenties ook de neerslag intensiteiten van extreme buien beter te kwantificeren. Hierbij konden ook regionale verschillen aangetoond worden. De significantie van de veranderingen was ook niet homogeen verdeeld over NI en regionale verschillen duidelijk aantoonbaar.

In Hoofdstuk 4 werd een reeks originele waarnemingen (2011-2015) van weer amateurs, verspreid over heel Nederland meegenomen in de analyse. Dit om het aantal waarnemingen in urbane en peri-urbane gebieden te kunnen uitbreiden. Deze waarnemingen werden initieel onderworpen aan een betrouwbaarheidsanalyse. Door combinatie van de KNMI en deze gegevens kon het "UHI - Urban Heat Island" fenomeen aangetoond worden in een aantal stedelijke gebieden. Het stedelijk hitte eiland effect was het meest waarneembaar na zonsondergang, maar kan soms tot +2°C bedragen.

In Hoofdstuk 5 werden de oorzaken en de voorspelbaarheid van extreme neerslag verder onderzocht. Hierbij werd de relatie van extreme neerslag met luchttemperaturen (op grond niveau i.e. 1.5 - 2-m), en in de lagere atmosfeer (850 hPa) maar ook met een regionale middellange termijn klimaat-index verder onderzocht. De combinatie van lucht- en dauwpunt temperaturen op deze twee hoogtes met de variatie van de NAO ("Nord Atlantic Oscillation"), een graadmeter met een bepaalde voorspelbaarheid van het regionale weer en neerslag op middellange termijn (i.e. 3 tot 6-maanden) voor Noordwest en Zuid Europa, leek nuttige informatie in te houden voor het voorspellen van extreme neerslag in NL.

Nog een praktische conclusie van deze studie is de aanbeveling om het niet-stationaire gedrag van weer en klimaat, en de huidige kennis over de causale verbanden tussen extreme neerslag en klimaat beter mee te nemen bij de ontwerpcriteria van water infrastructuur in stedelijk gebied. Een toename in extreme (uur) neerslag intensiteiten lijkt reeds een feit in verschillende regio's in Nederland.

Biography

Vahid Rahimpour was born on 7th July 1981 in Tehran, Iran. He studied civil/ water engineering at the Azad University- Central branch of Tehran. His B.Sc. project focused on the evaluation of dam construction impacts on the downstream environment. His M.Sc. research was focused on water resources management and decision support system (DSS) for Tehran water supply system. After graduation, he started his professional career in collaboration with engineering consultancy on the design and supervision of various water-related projects. In 2013, he was awarded the European Commission, Erasmus Mundus Scholarship to pursue his doctoral research at water resource department of the Faculty of Geo-Information Science and Earth Observation (ITC), University of Twente, which resulted in this thesis and the following publications:



Scientific publications:

- Rahimpour, V., Zeng, Y., Mannaerts, C.M., Su, Z., 2018. Response of extreme precipitation over the Netherlands to urbanization. Under review: *Journal of Applied Meteorology and Climatology*
- Rahimpour, V., Zeng, Y., Mannaerts, C.M., Su, Z., 2018. Urban impact on air temperature and precipitation over the Netherlands 75, 95–109.
doi:<https://doi.org/10.3354/cr01512>
- Rahimpour, V., Zeng, Y., Mannaerts, C.M., Su, Z., 2017. Detecting the effect of urban land use on extreme precipitation in the Netherlands. *Weather Clim. Extrem.* 17, 36–46. doi:10.1016/j.wace.2017.07.003
- Rahimpour, V., Zeng, Y., Mannaerts, C.M., Su, Z., 2016a. Attributing seasonal variation of daily extreme precipitation events across The Netherlands. *Weather Clim. Extrem.* 14, 56–66.
doi:10.1016/j.wace.2016.11.003
- Rahimpour, V., Zeng, Y., Mannaerts, C.M., Su, Z., 2016b. Land Cover Effects on Extreme Precipitation in the Netherlands, in: *Living Planet Symposium*. p. 175.